A DYNAMICAL STUDY OF THE 1958-59 STRATOSPHERIC POLAR VORTEX

by

Byron W. Boville

A thesis submitted to the Faculty of Graduate Studies and Research in partial fulfillment of the requirements for the degree of Doctor of Philosophy.

Department of Meteorology,
McGill University,
Montreal.

March, 1961

PREFACE

This thesis is presented in partial fulfillment of the requirements for the Ph.D. degree in Meteorology at McGill University.

The winter stratosphere is characterized by a strong, cold circumpolar vortex with temperatures varying from about -55C in mid-latitudes to about -80C near the pole. Observed winds in the centre of the current usually lie in the 100kt to 200kt range and the current is marked by very large-scale deformations. An intense warming wave spreads across the Arctic in the late winter (the time varies from mid-January to mid-March) and the major strength of the vortex decays rapidly with this so-called final warming.

The dynamical character of this vortex has been largely unknown. What are the sources and distributions of its kinetic and potential energies? Do moving or baroclinically unstable perturbations exist? What are the nature of the large-scale deformations and the final warming phenomenon? What effect do these have on ozone concentrations?

In an effort to provide some answers to these questions the author has made an intensive investigation of the 1958-59 winter, using Fourier techniques. The project was carried out within the Arctic Meteorology Research Group under the direction of Professor F.K. Hare. Other members of the Group who contributed to the project were Miss C.V. Wilson and Miss K. Allington who collaborated in the synoptic and ozone studies, Mr. Andre Castonguay, meteorological

technician, Miss Ann Garrard, cartographer and Mrs. Pamela Barfield, typist. The numerical work was made possible through extensive use of McGill's IBM-650 computer and the efficient programming of Miss M.A. MacFarlane.

The analytical work received help from Mr. J.M. Leaver and the staff of the Central Analysis Office. The author wishes to acknowledge continuous encouragement and support for his studies from the Director of the Meteorological Branch, Department of Transport and his research staff.

TABLE OF CONTENTS

		Page
Preface		ii
List of figures		vi
List of mathematical symbols		xi
List of Appendices		xiv
Abstract		xv
1.	Introduction	1
1.1	The Problem	1
1.2	The Data	2
1.3	The Upper Air Charts	7
2.	The Mean Flow of the Stratosphere	13
2.1	The Polar Easterlies	13
2.2	The Krakatoa Easterlies	16
2.3	The Polar-Night Westerlies	20
2.4	The Upper Stratospheric Westerlies	21
3.	Physical Problems	24
3.1	The Radiation Budgets	24
3.2	Ozone	30
4.	Synoptic Answers	46
4.1	The Aleutian Stratospheric Anticyclone	46
4.2	Baroclinic Waves	57
4.3	The Final Warming	60
5.	Dynamical Problems	67
5.1	Absolute Angular Momentum	67

Table of Contents (continued) Page

5.2 Energy 78

5.3 Waves 87

6. Quantitative Dynamical Analysis 93

6.1 The Fourier Series Approach 93

6.2 Kinetic Energy 99

6.3 Momentum 105

6.4 Heat Transport 109

6.5 Energy Conversions 114

7. Discussion 125

7.1 Conclusions 125

7.2 Status of the Problem 127

References 128

Appendices 134

LIST OF FIGURES

Fig.		Page
1.	Solar radiation corrections applied at stations to four radiosonde types selected from Teweles and Finger (1960).	5
2.	Approximate areas of sunlight and darkness for radiosonde balloons in the middle stratosphere.	9
3.	Observed stratospheric temperatures at Resolute, N. W. T., July, 1958 to June, 1959. The dashed line is a smoothed representation of the top of the radiosonde ascents.	10
4.	Schematic meridional cross sections showing the main wind currents. Isotachs in kt and temperatures in ^{o}C. Inserts are relative angular momentum per unit volume (10^{5} cgs). Heavy solid lines are temperature maxima and heavy broken lines are temperature minima.	14
5.	Daily variations of the 25-mb geopotential height difference between 65N and 80N on the 150W meridian, June, 1958 - May, 1959.	15
6.	25-mb chart for June 24, 1958, a typical summer chart.	18
7.	Temperatures and winds in the middle stratosphere at Balboa, Canal Zone, every fifth day, July, 1958 to June, 1959.	19
8.	Reconstructed winds (m sec^{-1}) and temperatures (^{o}C) 20 km to 100 km from Murgatroyd (1957).	23
9.	The temperature profile and infra-red cooling from Plass (1956) together with the solar heating curve from Pressman (1955).	26

Fig.		Page
10.	Radiation computations from Murgatroyd and Goody (1958).	27
11.	Selected radiation computations for the 60N-70N latitude belt a_1, a_2 - Ohring, April and October; H_2O, CO_2, O_3 b_1, b_2 - Goody, summer and winter; CO_2, O_3, O_2 c_1, c_2 - Brooks, April and July; CO_2, O_3.	29
12.	Vertical time-section of observed temperatures at Bitburg, Germany for February, 1959.	33
13.	Time sections of observed total ozone and 30-mb temperatures at Lerwick, Oxford (Camborne) and Rome.	34
14.	30-mb charts for January 2 and 17, 1960.	36
15.	Time section of observed total ozone and 30-mb temperatures at Moosonee, Ontario, January, 1960.	37
16.	The vertical distribution of ozone, microns per mb, for standard Umkehr curves I and III and the potential temperatures for an isothermal stratosphere at -63C and -53C.	39
17.	Observed values of total ozone (microns) together with tentative isolines for September 25 and November 24, 1958.	44
18.	25-mb chart for January 1, 1958, a typical mid-winter chart.	47
19.	Daily 25-mb temperatures for Fairbanks, Alaska; Resolute, N.W.T.; and Lerwick, U.K.; October, 1958 - March, 1959.	49

Fig.		Page
20.	Spectrum analyses of the observed temperatures at Resolute, N. W. T. and Lerwick, U.K. through the 1958-59 season showing temperature variance as a function of period.	51
21.	Fourier analysis of 25-mb and 500-mb heights showing reduction of variance by wave number. Inserts are the positions of the eccentric troughs, wave number one.	53
22.	Observed temperature and geopotential height data for St. Paul Island, October, 1958.	55
23.	Adiabatic vertical motions and temperatures at 25 mb at Fairbanks and St. Paul Island during October, 1958.	56
24.	Isochrones of identifiable waves on 25-mb charts, winter, 1959.	58
25.	The 25-mb space mean and quasi-vorticity ($Z - \overline{Z}$) fields for January 12, 13, 14, 15, 1959, (units - hnds of ft).	59
26.	The departure of the 25-mb space mean charts from the monthly mean, January, 1959. (units - hnds of ft).	61
27.	Time profiles of the temperatures at Keflavik, Iceland for January, 1959. The 500-mb profile has been inverted for comparison with the stratospheric profiles.	62
28.	Isochrones of the final-warmings, based on 100-mb temperature data, for the 1956-57, 1957-58 and 1958-59 winters.	65
29.	Schematic representation of zonal rings and polar caps.	68
30.	Schematic mean meridional circulations.	72

Fig.		Page
31.	Schematic tilted trough momentum transfer.	75
32.	Tropospheric energy components of the general circulation.	81
33.	Reconstructed temperature profiles for typical winter conditions.	83
34.	Schematic representation of Fleagle's stream surface of maximum slope.	88
35.	Perturbation growth rates as a function of wave number and latitude for an isothermal lapse rate and a meridional temperature gradient of 1 degree C per lat. deg. (after Fleagle, 1957).	90
36.	The amplitudes and longitudinal trough positions of wave number one at 500 mb and 25 mb shown as consecutive vectors for the 36 charts at five-day intervals, October, 1958 - March, 1959.	98
37.	Isoline representation of the amplitudes of wave number two at 500 mb, 100 mb and 25 mb based on the charts at five-day intervals, October, 1958 - March, 1959.	100
38.	The total kinetic energy 40N to 80N at 500 mb, 100 mb and 25 mb based on the 36 charts, October, 1958 - March, 1959 (10^{15} joule mb^{-1}).	102
39.	The average kinetic energy, October, 1958 - March, 1959 as a function of wave number at 500 mb, 100 mb and 25 mb. (10^{15} joule mb^{-1}).	103

Fig. Page

40. The relative angular momentum for the polar cap north of 50N; October, 1958 to March, 1959 at 500 mb, 100 mb and 25 mb. (10^{21} joule sec mb^{-1}). 107

41. Isolines of geostrophic heat transport across latitude circles at 25 mb, October, 1958 - March, 1959. (10^{12} joule mb^{-1} sec^{-1}). 112

42. The average heat transport at 25 mb as a function of wave number. (10^{11} joule mb^{-1} sec^{-1}). 113

43. The average eddy potential to eddy kinetic energy conversion at 25 mb for January, 1959 as a function of wave number. (10^{10} joule mb^{-1} sec^{-1}). 118

44. 25-mb energy components for the month of January, 1959. Rectangular boxes - energy.....10^{16} joule Diamond boxes - energy conversion....10^{10} joule sec^{-1}. 123

A-1, 2, 3, 4, 5, 6, 24, 28, 29, 30. Selected 25-mb charts from an atlas series at five-day intervals, October, 1958 to March, 1959. Appended.

List of Mathematical symbols

a ..... radius of the earth

a_n, b_n, c_n ..... Fourier amplitude, temperature

A_n, B_n, C_n ..... Fourier amplitude, geopotential height

C ..... energy conversion process

E ..... kinetic energy per unit volume (5.2 - 1)

e, sub-fix ..... eddy component

g ..... acceleration of gravity

G ..... energy generating process

g, sub-fix ..... geostrophic

H, H_T ..... heat, heat transport

K ..... kinetic energy

K_r ..... relative angular velocity of the air

L ..... coriolis parameter, $2(\Omega + K_r)\sin\phi$

m ..... zonal wave number

m ..... last significant wave (6.1)

M, M_T ..... angular momentum, momentum transport

n ..... Fourier wave number

N ..... number of points

P ..... pressure, probability (6. 1)

AIP ..... available potential energy

q, Q ..... non-adiabatic heat addition

q ..... number of waves tested (6. 1)

r ..... number of cases (6. 1)

R ..... gas constant for dry air

R ..... distance from earth's axis, $a \cos \phi$

S_z ..... stability parameter, $\frac{1}{\theta} \frac{\partial \theta}{\partial Z}$

T ..... temperature

U_z ..... baroclinic parameter, $\partial U / \partial Z$

U ..... speed of basic zonal current

u, v, w ..... velocity components, dx/dt, dy/dt, dw/dt

x, y, z ..... eastward, northward and vertical coordinates

Z ..... geopotential height

z, sub-fix ..... zonal component

α ..... specific volume

$\bar{\alpha}^2$ ..... $= \frac{1}{a^2} \left(\frac{m^2 - \sin^2 \phi}{\cos^2 \phi} + \nu^2 \right)$ (4.3)

α, β, γ ..... computed Fourier amplitudes (6.1)

β ..... Rossby parameter $= -\frac{1}{a} \frac{\partial L}{\partial \phi}$

γ ..... coefficient of piezotropy, $d\rho / dP$ (4.3)

δ ..... angle between stream surface and horizontal

Δ ..... finite increment

θ ..... potential temperature

θ_n ..... phase angle

ν ..... meridional wave number

λ ..... longitude

ρ ..... density

σ_R, σ_i ..... frequency, Real and imaginary

σ ..... ozone amount (3.2)

σ^2 ..... variance (6.1)

τ ..... torque

ϕ ..... latitude

ψ ..... ozone mixing ratio

ω ..... dP/dt; vertical motion re pressure coordinate

Ω ..... angular velocity of the earth

List of Appendices

Appendix A: Thirty-six 25-mb charts, one for every fifth day, for the period October, 1958 to March, 1959. These charts show the characteristic changes in the horizontal circulation of the middle stratosphere in relation to the polar-night vortex.

Abstract

The circulation of the stratosphere and its relation to the troposphere is presented for the six-month period October, 1958 to March, 1959. The study is based mainly on circumpolar analyses at five-day intervals at the 500-mb, 100-mb and 25-mb levels, supported by numerous space and time sections. Fourier analysis of the circumpolar charts is used to compute energies and energy exchanges after the manner of Lorenz (1955) and unstable wave characteristics following the linear theory of Fleagle (1957). The polar-night middle stratosphere is found to be baroclinically unstable in mid-winter, otherwise the energy exchanges appear to be ascribable to forced perturbations.

1. INTRODUCTION

1.1 The Problem

During recent years the advent of higher level radiosonde and rocket information has focused more attention on meteorological processes in the middle stratosphere. Since Scherhag's (1952) report on the explosive stratospheric warming various authors have provided material on that phenomenon. Godson and Lee (1958) demonstrated the jet stream character of the flow. Craig and Hering (1959) illustrated the large scale of the horizontal and vertical motions and confirmed a dynamic origin (subsidence) for the major temperature change. These and similar studies have continued to add to the increasing knowledge of the structure of stratosphere, but have been unable to come to grips with the energetics of the problem because of inadequate observational material.

The stratospheric analysis project of McGill University, through its daily cross sections and synoptic charts, (up to the 25-mb level) has shown the feasibility of an intensive dynamic study of the middle stratosphere. The author launched such an investigation of the region following two complementary lines of attack.

(i) A synoptic study, using the daily charts and cross sections supported by numerous time sections to make full use of all available information, to define the major changes and perturbation systems of the 1958-1959 year.

(ii) A hemispheric general circulation study, utilizing machine techniques, to attempt a definition of the energetics of the middle stratosphere and its relation to the energetics of the troposphere. It is believed that this is a first attempt to define the energetics of the middle stratospheric-tropospheric regions by wave number analysis.

The author has attempted to include only those parts of the project in which he carried out most of the investigation. However, complete separation is not possible and the author is grateful to the many members of the Arctic Meteorology Research Group who collaborated with him, in particular to Professor F.K. Hare who conceived and directed the project; to Miss M.A. MacFarlane who did the programming for the McGill IBM 650 computer; to Miss K. Allington and Miss C.V. Wilson who collaborated in the ozone and synoptic studies; to Mr. Andre Castonguay as meteorological technician; and to Miss Ann Garrard for drafting the diagrams.

1.2 The Data

The basic data used in this study are drawn from the world-wide radiosonde networks with most stations having two ascents per day. The observed variables used are the pressure, P, the temperature, T, and the horizontal wind vector, **V**; the latter is available at most stations through the use of RDF (or in some cases radar) equipment.

The accuracy of the airborne instruments is usually given as $P \pm 3$ mb

and $T \pm 0.5^{o}C$. In upper air work pressure is generally an independent variable, and the dependent variable is the derived geopotential height, Z, which is computed using the hydrostatic approximation in the form:

$$Z = \frac{R}{g} \int_{P}^{P_o} T \; d\ln P$$

At any particular level the accuracy of Z depends on the amount of systematic error in T[1] and P. The accuracy is clearly a function of P and it is usually considered that the standard error has the following approximate values

500 mb $\pm$ 50 ft; 100 mb $\pm$ 125 ft;

50 mb $\pm$ 200 ft; 25 mb $\pm$ 300 ft; 10 mb $\pm$ 500 ft.

These figures are confirmed by synoptic experience for most networks in the troposphere. At stratospheric levels up to 25 mb they appear reasonable for a fairly homogeneous[2] network in the dark part of the hemisphere; they are not realistic for non-homogeneous networks in sunlit areas. Investigations by Teweles (1960) suggest that exposure and ventilation become critical sources for temperature errors in the stratosphere. This type of systematic error was clearly evident on the McGill daily synoptic charts and a study showed that at 25 mb the sunlit

---

[1] In height computation T should be the virtual temperature, but in the stratosphere the difference is of no consequence.

[2] homogeneous with regard to instrument type.

areas had temperatures averaging 3°C warmer and geopotential heights 400 ft higher than in the dark areas. The correction required is largely a function of instrument type and solar elevation angle, information available at the observing site. Station corrections ranging up to 10 to 20° C are applied, as shown by several examples in fig.1. However, in many cases they do not appear to be sufficient: the Japanese, American and German areas all showed the +3°C effect at 25 mb, and only the U.K. data at 30 mb appeared to be adequately reduced.

The correction is also complicated by pressure errors. In regions where the temperature decreases with height the pressure and radiation temperature errors will tend to compensate each other, but where temperature increases with height they tend to be additive. In the presence of a 5 mb pressure error an additional temperature error of 1 to 2°C at 25 mb may be incurred solely because of the radiation effect. Since pressure errors are likely to be random in the horizontal (from station to station) this adds an incoherent error field to the charts in the sunlit regions.

The wind reports contain various instrumental errors, such as target hunting, but the main limitations in the stratosphere are due to range and elevation angle. The standard vector errors following Meunch (1958) are approximately:

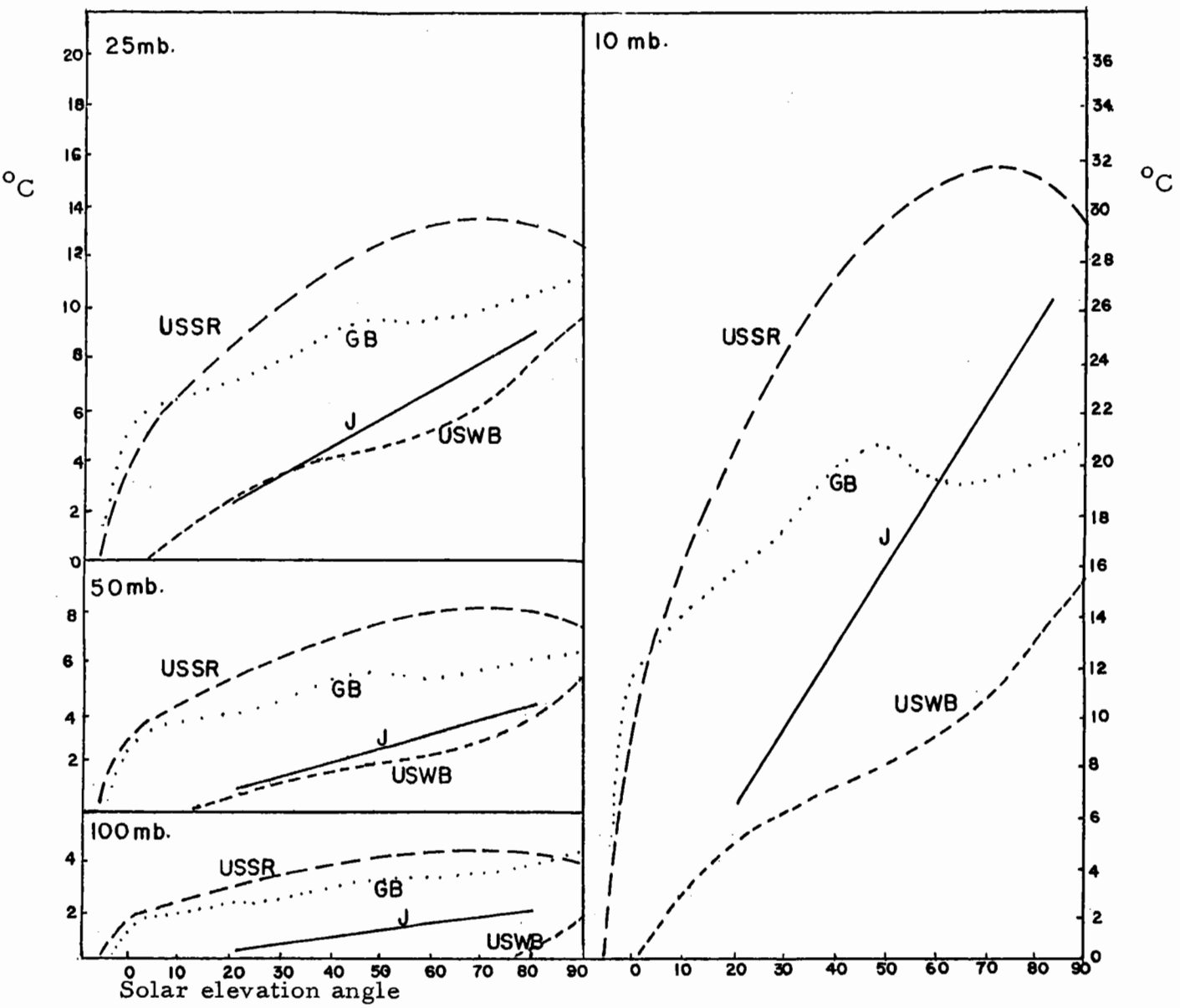

Fig.1. Solar radiation corrections applied at stations to four radiosonde types selected from Teweles and Finger (1960).

Table 1.

Rawinsonde, approximate vector errors, kt.

	troposphere	lower and middle stratosphere	upper stratosphere
strong winds	1 - 5	5 - 10	10 - 30
light winds	1 - 5		

In summer the wind reversal in the stratosphere favours high elevation angles and reliable wind reports are generally available to above 25 mb. In winter the trend for increasing westerlies with height acts in the reverse sense. Fortunately the winter stratospheric jet stream is usually well separated from the main tropospheric ones, so that with good wind equipment a fair number of ascents reach into the middle stratosphere, Orvig (1959). In the upper parts of such ascents range and elevation angles become critical, hence direction and average speeds are probably meaningful, but vertical shears are not, i.e. indications of maxima or minima in the vertical are likely to be spurious.

Investigations of the middle stratosphere are largely dependent on the number of ascents reaching into the layer. Over North America the proportion is very high and even in the polar-night area, where cold and dark drastically reduce the number of successful ascents, there are sufficient for reliable analyses. This favourable area can be expanded

to Japan, on the west, and to Iceland, Germany and the Mediterranean, on the east, and the coverage is still fairly adequate. Over the remainder of the hemisphere practically no ascents reach 25 mb. Over China many ascents reach 60-50 mb making vertical extrapolation feasible, and a similar situation prevails in eastern Siberia. Over the remainder of the U.S.S.R. there are very few reports above 100 mb.

1.3 The Upper Air Charts

The daily chart series at the 200-mb, 100-mb and 25-mb levels and the cross sections plotted by the Central Analysis Office and analyzed by members of the Arctic Meteorology Research Group were of great use in providing material and continuity. However, the higher level charts were effectively limited by data coverage to the North American area. In order to achieve hemispheric specification the 100-mb and 25-mb charts were completely plotted every fifth day. Because of the difficulties involved, and in order to achieve consistency, the analyses were done by the author. The main data source was the 'Northern Hemisphere Data Tabulations' of the U.S. Weather Bureau. Additional information was obtained from national bulletins, and supplementary Asiatic data were supplied by the Arctic Forecast Team in Edmonton.

The daily hemispheric (0000Z) 500-mb charts available at the Central Analysis Office were used as the tropospheric analyses. On the project days these 500-mb maps were checked for consistency over

Europe and Asia with the 'Täglicher Wetterbericht' Amtsblatt des Deutschen Wetterdienstes. The maps were all drawn on hemispheric 1:20 m polar stereographic charts true at 60N, an adequate scale for this type of upper air analysis.

The 100-mb data were considered adequate for direct isotherm and contour analysis in all areas. The analysis was performed over the 500-mb chart to provide consistency in error and hydrostatic checks, but differential analysis for that layer was not considered appropriate.

At 25 mb data problems were critical in most areas and procedures had to be varied. For good data areas ascents terminating between 50 and 25 mb were utilized through a plot of the terminal temperature. For poor data areas all data above 100 mb were plotted. Over Russia all available data for the five day period centered on the chart were checked and any data above 100 mb were plotted for extrapolation. In addition time sections of the 12-hour temperature data for a large number of stations gave a comprehensive check in height and time. (see for example the Resolute section, fig. 3).

The sunlight radiation problem requires an outline of the area to be affected (see fig. 2). The important line is that separating balloons in darkness from those in sunlight at the analysis level. Simple geometry (neglecting refraction) shows that sunrise at a height Z is given by the solar elevation angle, d, where $d = \cos^{-1}\left(\frac{a}{a + Z}\right)$. Expansion of this

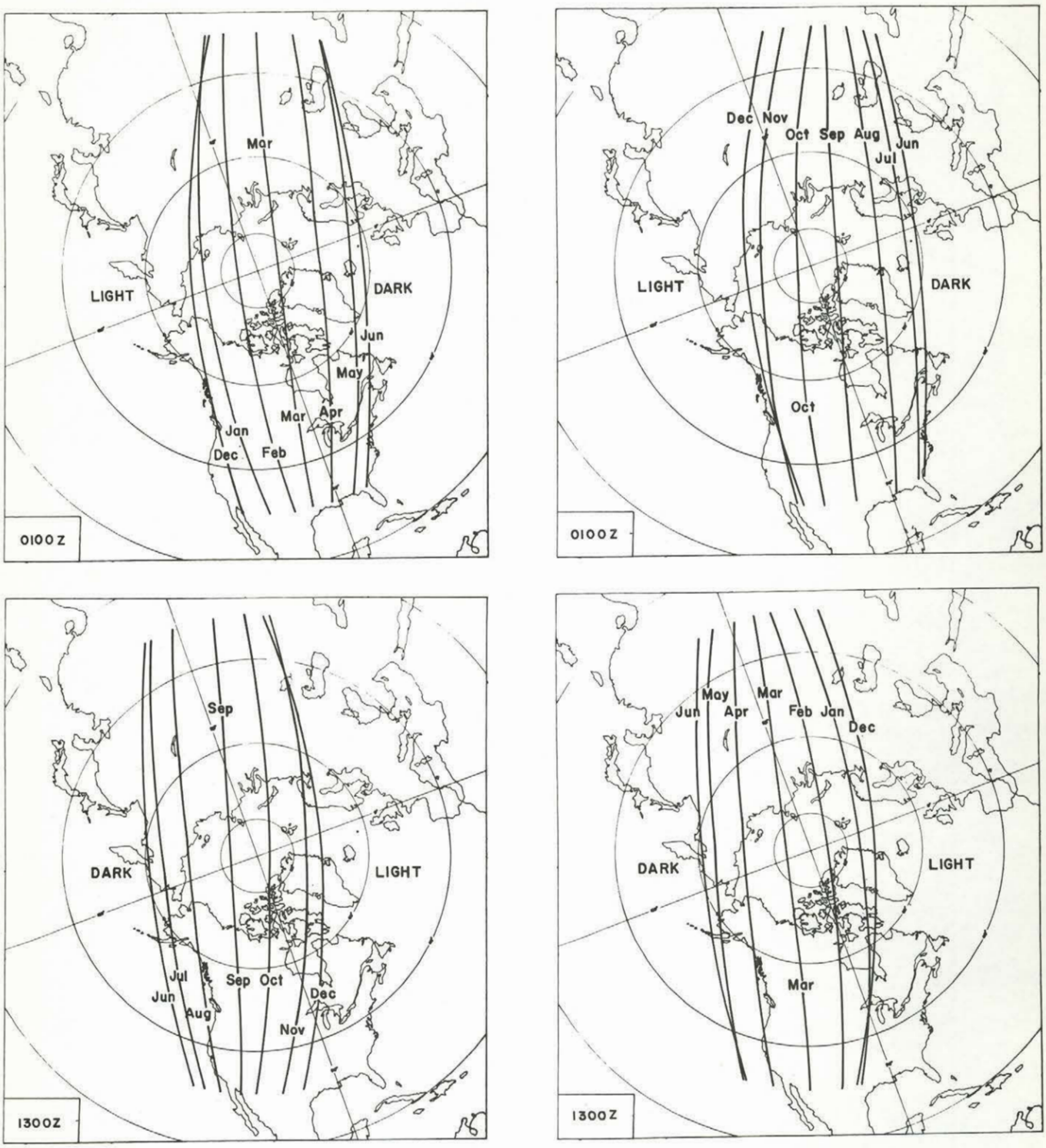

Fig. 2. Approximate areas of sunlight and darkness for radiosonde balloons in the middle stratosphere.

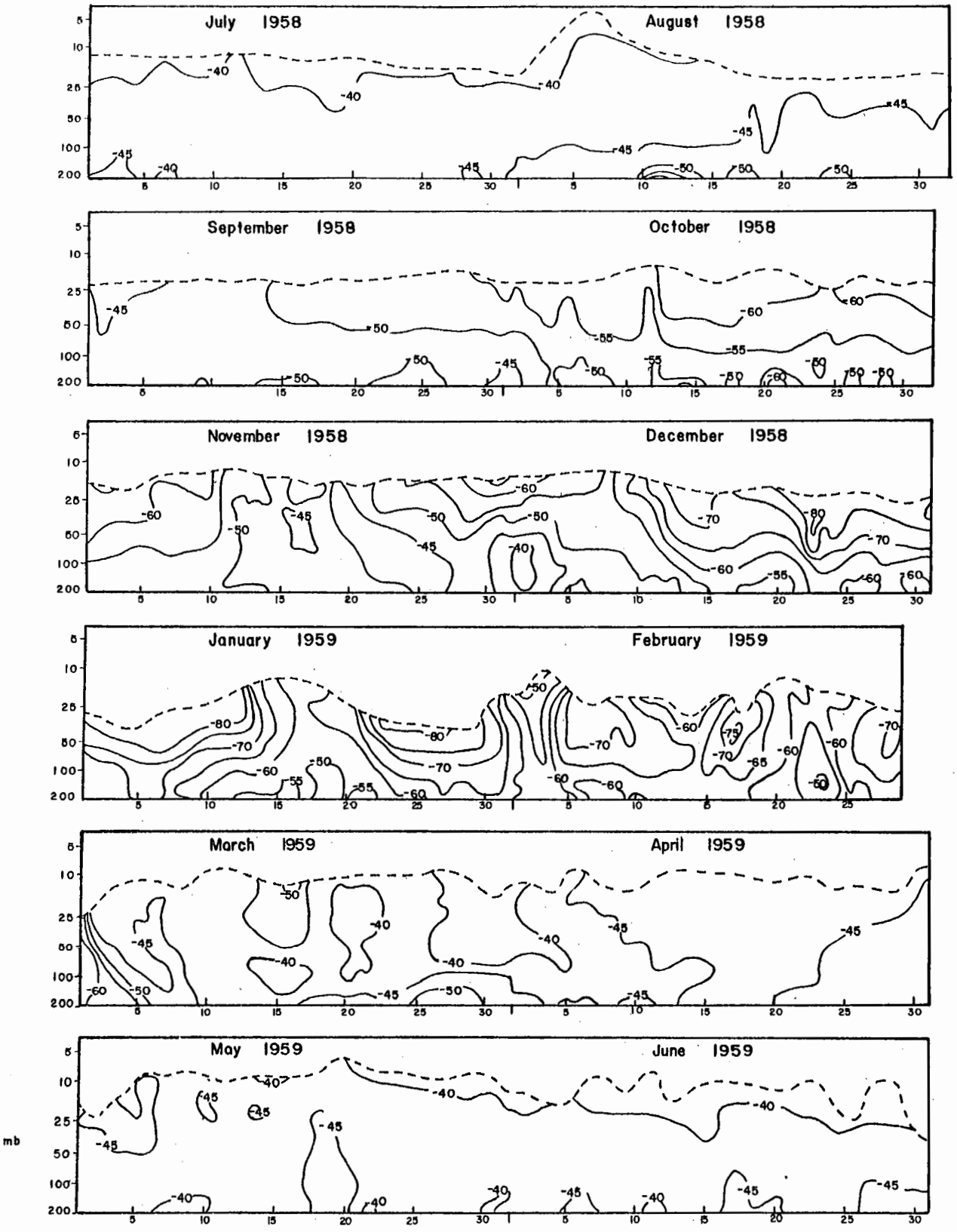

Fig. 3. Observed stratospheric temperatures at Resolute, N. W. T., July, 1958 to June, 1959. The dashed line is a smoothed representation of the top of the radiosonde ascents.

in a power series yields to a first approximation

$$-d \text{ (degrees)} = \sqrt{Z} \text{ (km)}$$

A check against accurate polar-night boundary figures (provided by the Research Division of the Canadian Meteorological Branch) based on ray tracing techniques indicates that the above is a reasonable approximation. Sunrise and sunset in the lower and middle stratosphere are then defined by solar elevations of -4 to -6 degrees. It may be noted that a variation of time of release of radiosondes by 20 minutes alters the sun line by 5 longitude degrees; hence for analysis purposes great accuracy in the definition of the sunrise (sunset) line is meaningless. For convenience the solar elevation angle was assumed to be -6 degrees, which is the same as civil twilight, and is available in standard astronomical tables. It is further assumed that balloons are released at the synoptic hour minus 30 minutes and take 90 minutes to reach the middle stratosphere, i.e. at 0100 and 1300 GMT. The lines plotted on fig. 2 are thus civil twilight at 0100 and 1300 GMT on the 21st day of each month and are interpreted as sunrise and sunset lines at 25 mb for the 0000 and 1200 GMT synoptic charts. The lines are, in any case, objectively determined, so that allowance can be made for any deviations from the assumed conditions.

In the sunlit part of the hemisphere both the 0000Z and 1200Z data at 25 mb were plotted for each station. In most cases this gave a direct comparison of dark and sunlit observations on the same instrument type

and permitted fairly objective radiation corrections.

At the 25-mb level temperature, being a directly observed variable and containing the least systematic error, was analyzed first on a hemispheric basis, using both time and space continuity and appropriate radiation corrections. The geopotential height was then computed for all partial ascents and the analyzed 100-mb and 25-mb temperatures served as controls. The contour lines were then drawn directly on the basis of the observed and computed heights (and winds). The analyses for the winter months were independently checked by 100-25 mb differential analysis. Since the best data have a standard error of $\pm$ 300 ft at 25 mb it was not considered sound to draw contours at less than 400 ft intervals. The 25-mb analyses are considered to be independently reliable and accurate on the planetary scale except for the Russian sector. In that area they are undoubtedly biased towards lower-level dependence, although fair control is imposed by data in adjacent areas.

2. THE MEAN FLOW OF THE STRATOSPHERE

The mean flow of the stratosphere can be conveniently divided into four main systems; (1) the polar easterlies, (2) the Krakatoa easterlies, (3) the polar-night westerlies, and (4) the upper stratospheric westerlies. These currents are shown on fig. 4.

2.1 The Polar Easterlies

The course of the polar easterlies at 25 mb during the 1958-1959 year is shown clearly by fig. 5. The current was consistently in the range 10 to 20 kt in June and July. It dropped slowly from 10 kt in early August and ended on August 28. The current was re-established on April 3, 1959 and was in the summer 10 to 20 kt range by the end of May. This accords with Hare's (1960a) description of the summer circulation, and it is apparent that such a current extending from early April to late August is a regular feature of the general circulation.

It has been suggested that the polar easterlies are merely a northward extension of the main stratospheric easterlies and that the apparent separation at 25 mb is due to the upward extension of the middle latitude core of the Ferrel westerlies. Fig. 4 would seem to indicate such a construction. In addition, radiation computions of recent years (fig. 11) show a deficit in polar latitudes in summer requiring some dynamical heating mechanism.

There are several points that suggest that the above arguments may

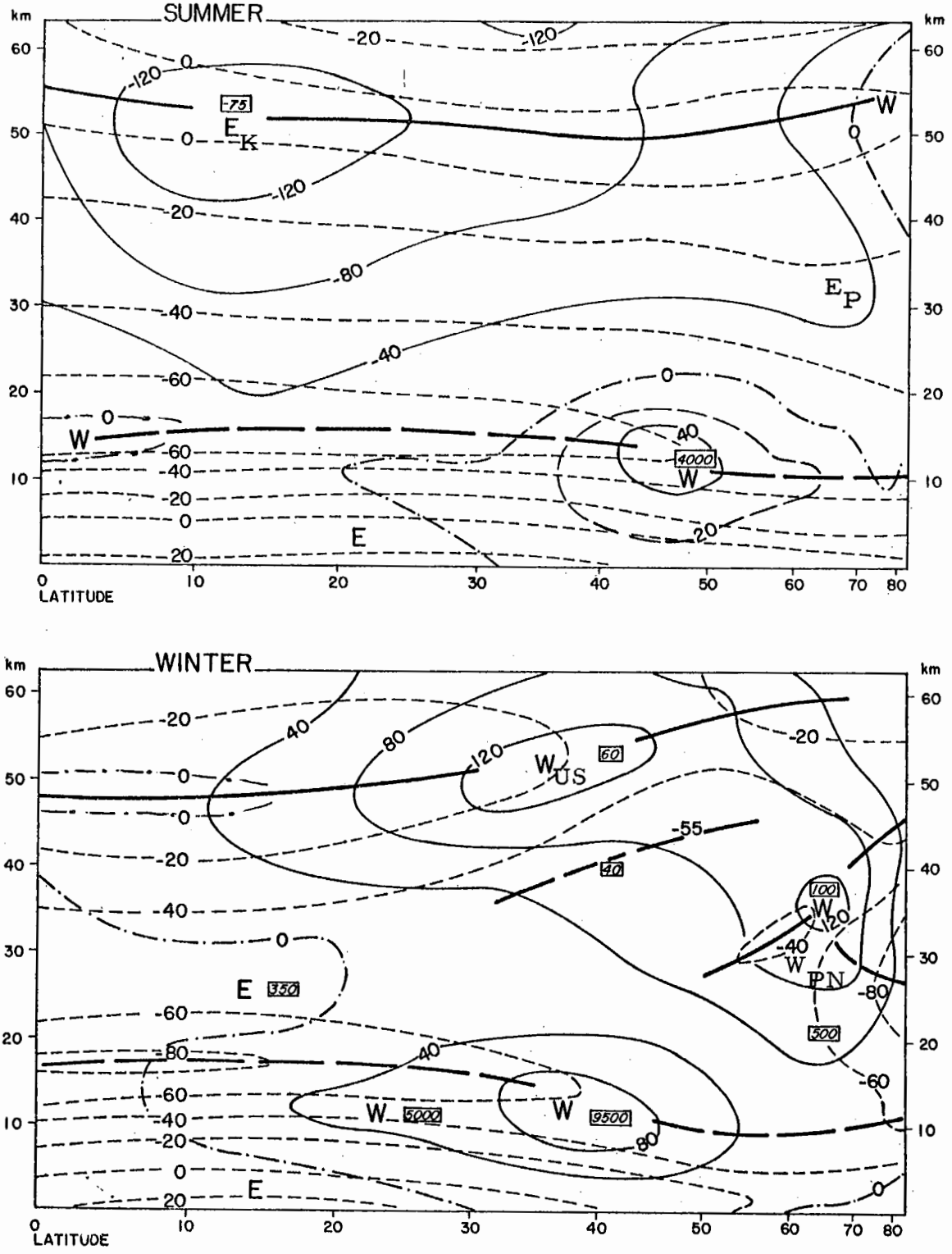

Fig. 4. Schematic meridional cross sections showing the main wind currents. Isotachs in kt and temperatures in °C. Inserts are relative angular momentum per unit volume (10^5 cgs). Heavy solid lines are temperature maxima and heavy broken lines are temperature minima.

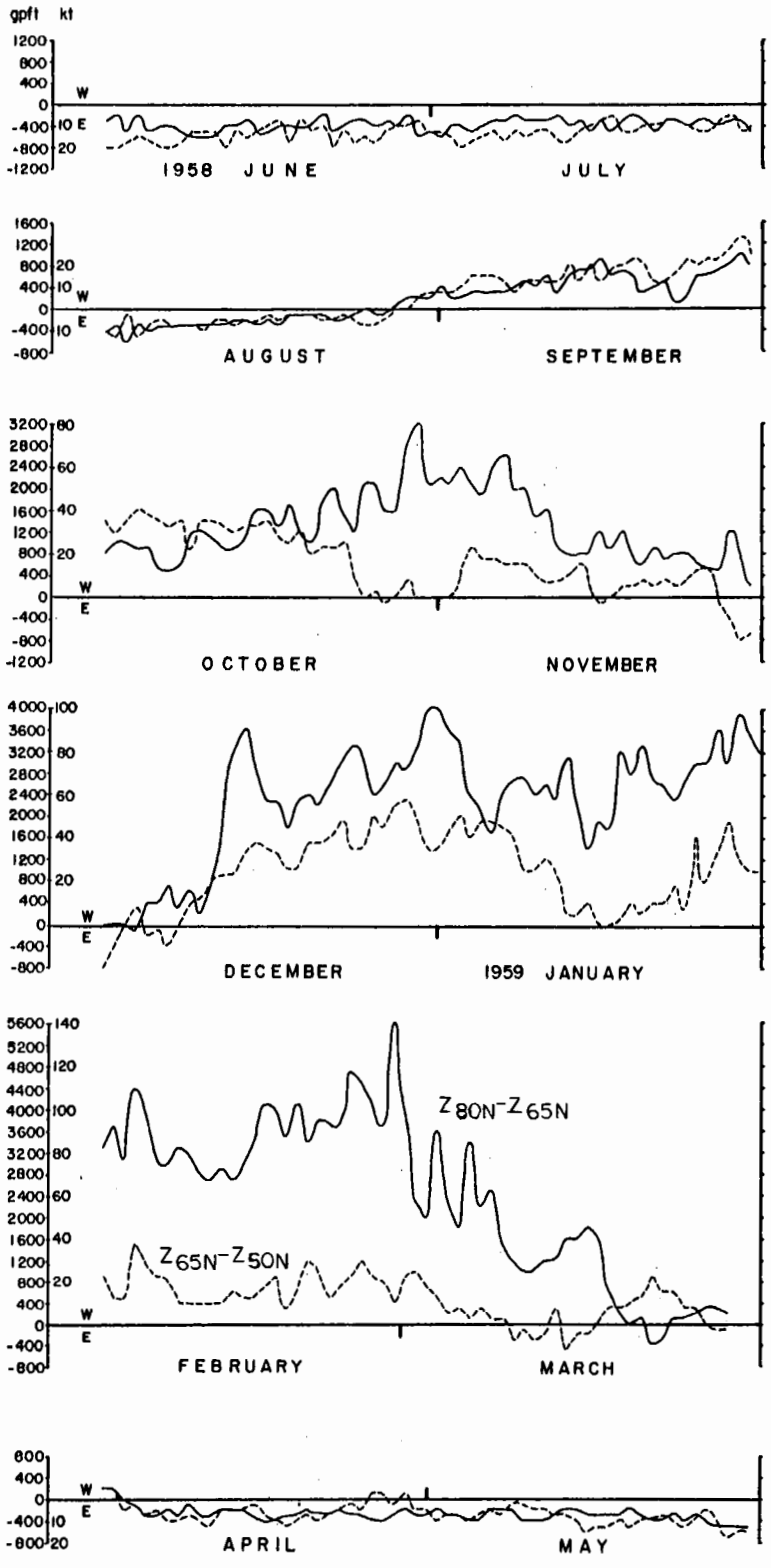

Fig.5. Daily variations of the 25-mb geopotential height difference between 50N and 80N on the 150W meridian, June, 1958 - May, 1959.

not be valid. There is as yet no concrete evidence for significant eddies in the polar easterlies that could achieve a northward heat transport against the gradient. The other possible mechanism would be a mean meridional circulation with subsidence at high latitudes. However, momentum considerations according to section 5.1, would then require an upward transfer of westerly angular momentum into the Arctic stratosphere, which is inconsistent with the maintenance of an easterly current. It would thus appear that the polar regions in summer must be very close to radiative equilibrium, and that the equilibrium temperatures are higher at the more northerly latitudes. The summer polar easterlies, then, are probably a consequence of the latitudinal distribution of equilibrium temperatures in the vicinity of the maximum ozone concentration in the vertical. As such it appears sound to consider the current as a (physical) entity.

2.2 The Krakatoa Easterlies

After the great Krakatoa volcanic eruption in August, 1883, the ash cloud in the stratosphere circled the earth three times from east to west whilst diffusing laterally about five degrees each time (Lettau 1951). In November the cloud was observed to spread rapidly north-eastward from North America into Europe, thereafter covering the entire hemisphere. Thus over 75 years ago direct evidence was at hand for the existence of the summer stratospheric easterlies, and for the eccentric development

in the polar-night westerlies during the fall season.

The structure and variability of the tropical stratospheric circulation has been described by McCreary (1959) on the basis of high level wind observations in the Pacific. The summer structure was similar to that shown in fig. 4, with a fairly steady easterly current having core speeds in the 100 to 150 kt range at 12 degrees N near the stratopause[1]. The winter circulation was light and variable. The variability noted by McCreary was primarily interannual with little short-period change.

The typical summer map (fig. 6, June 24, 1958) shows the hemispheric extent of the lower part of the Krakatoa easterlies at 25 mb with all tropical stations reporting easterly winds in the 50 to 80 kt range. The persistent nature of the summer circulation is shown by the time section for Balboa, fig. 7. That section and the daily 80 W meridional cross sections failed to confirm the day to day steadiness in the tropical circulation found by McCreary. Large changes do occur on occasions as a result of interaction with the polar-night westerlies. In particular when sharp troughs break off and move southward across the southern United States and the Caribbean quite large space and time vector wind changes are observed. The apparent absence of such short period changes in McCreary's results is probably due to the insulation of the Pacific area

---

[1]Stratopause - in this paper - the temperature maximum near 50 km.

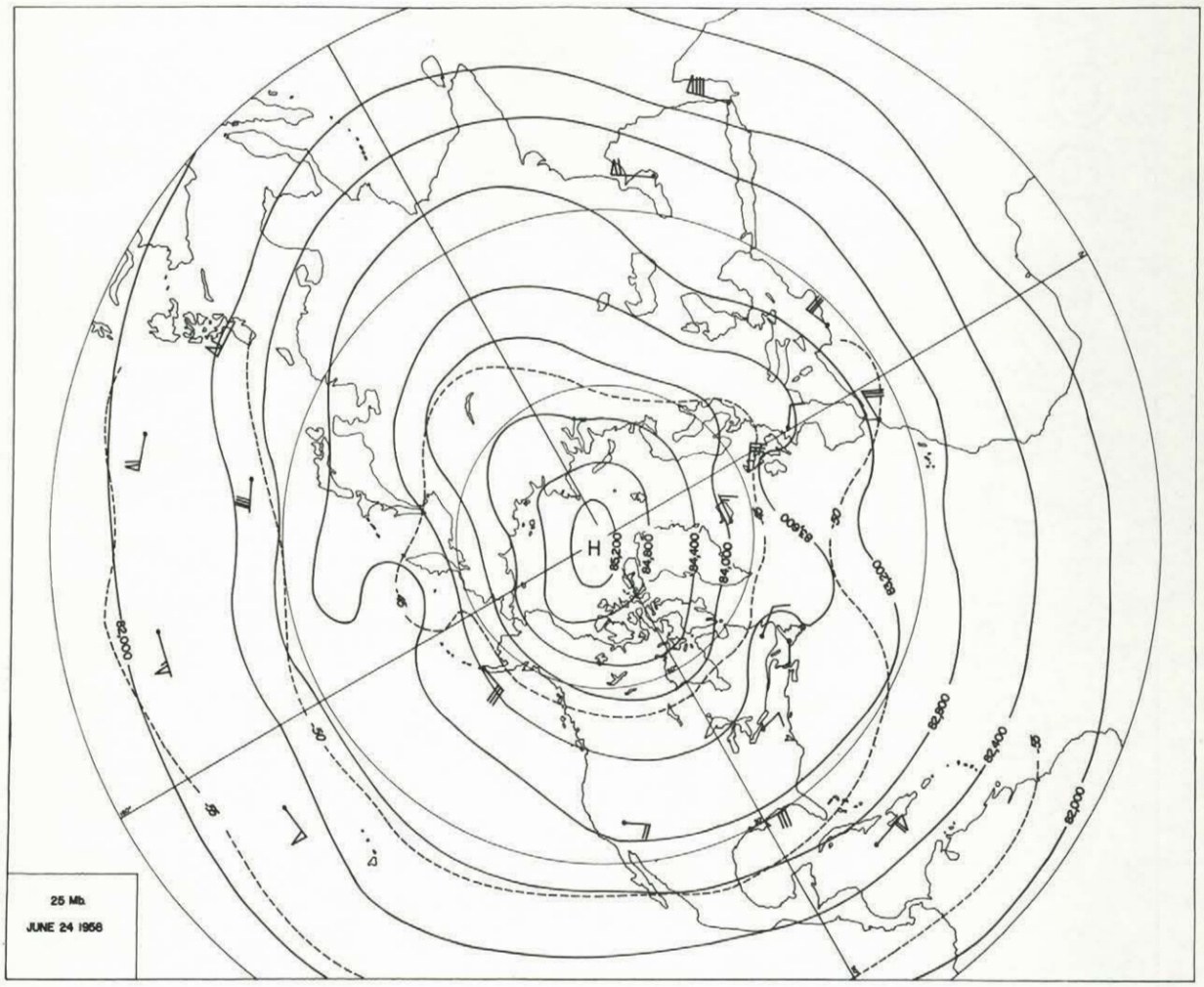

Fig. 6. 25-mb chart for June 24, 1958, a typical summer chart.

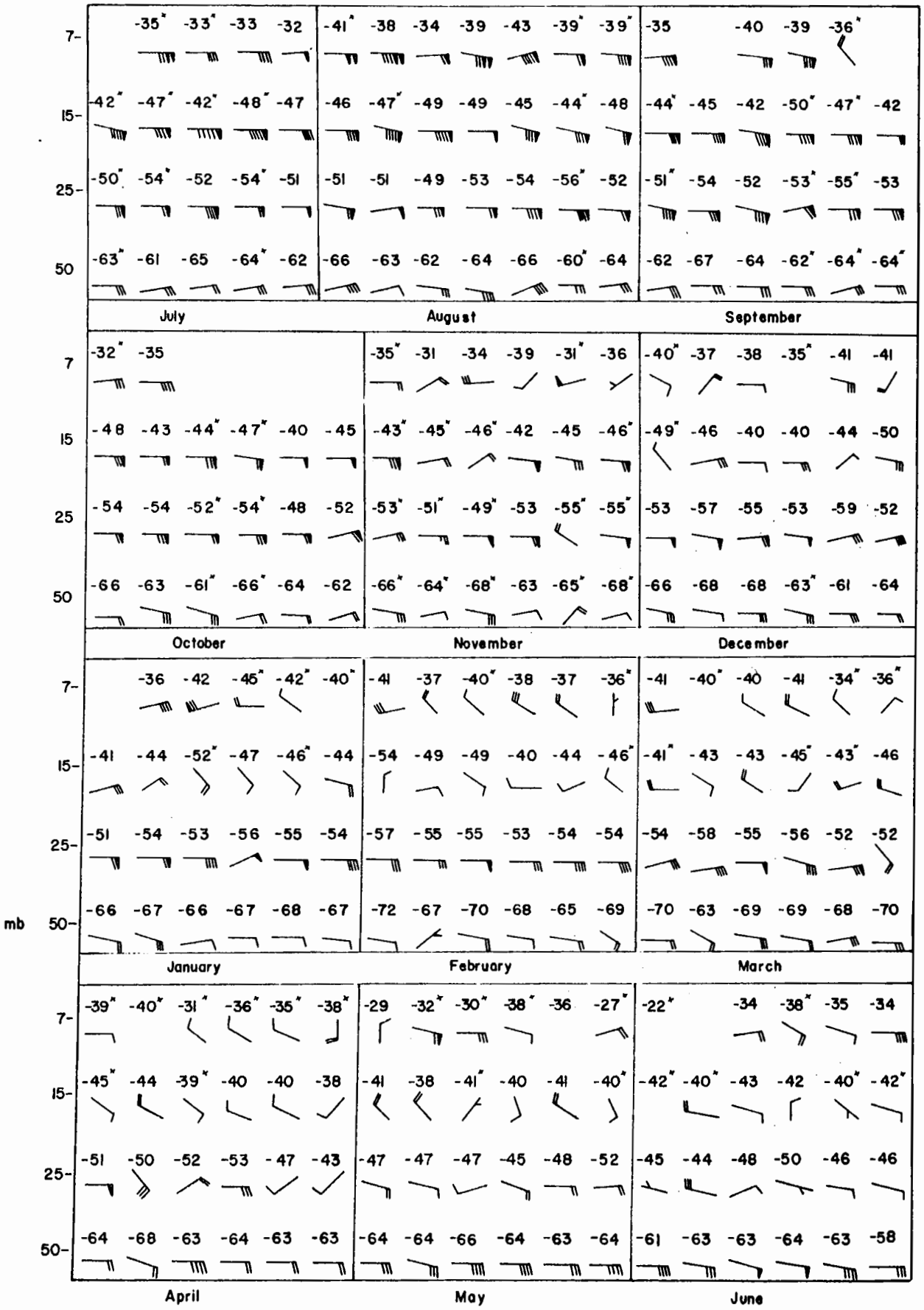

Fig. 7. Temperatures and winds in the middle stratosphere at Balboa, Canal Zone, every fifth day, July, 1958 to June, 1959.

from the shorter polar-night variations by the Aleutian anticyclone. The dependence of the tropical variations on the polar westerlies suggested by McCreary is supported by this study.

The above results, together with the relative angular momentum computations shown on fig. 40, form the basis for the following highly tentative hypothesis. The polar-night and upper stratospheric westerlies are a consequence of radiative imbalance; the stratospheric easterlies are a counter current required to satisfy the angular momentum balance, and hence occur where the geostrophic thermal wind requirements are at a minimum, i.e. in the tropics.

2.3 The Polar-Night Westerlies

The polar-night westerlies have been described by Hare (1960) on the basis of upper wind and temperature statistics and the map series of the Arctic Meteorology Research Group. A compilation of 100-mb 10-day running mean temperature for available Arctic stations by Godson (1958) confirms the existence of the polar-night vortex each year. Although the data show great inter-annual variability in the behaviour of the vortex, they indicate that the 1958-1959 winter can be considered as representative of the dominant type.

The behaviour of the westerlies on a daily basis in the region of highest wind speed is shown by the 150 W height gradients on fig. 5. The relative angular momentum computations for hemispheric zones (fig. 40)

show that these height gradients are indicative of the vortex trends. From a nil circulation in late August the westerly flow increased to 20 to 30 kt in early October. The increasing westerly trend over the Pacific was interrupted by the formation of the Aleutian anticyclone in mid-October, but to the north the flow increased to near 80 kt in late October. The excursion of the anticyclone into the Arctic regions in November almost destroyed the westerlies, and the flow remained sluggish well into December. The circumpolar westerlies were re-established abruptly on December 13-14th by strong cyclonic development over the Canadian Arctic, with the northern Alaskan winds increasing from near zero to 90 kt in 48 hours. Thereafter, the vortex remained strong with the Arctic flow oscillating locally in major wave activity between 40 and 120 kt. In late February the zonal flow increased to a maximum of 140 kt to be followed by the final warming on March 1-4. At that time the westerlies decreased abruptly from 140 to 60 kt as the vortex centre moved out of the Arctic basin into Siberia. The vortex then gradually weakened, to be replaced by the summer easterlies in April.

2.4 The Upper Stratospheric Westerlies

The most comprehensive survey of the higher level wind and temperature structure has been given by Murgatroyd (1957) for the layer 20 to 100 km. Measurements in the upper stratosphere have been mostly by smoke drift from shells and rockets, anomalous sound propagation and

more recently by radar using chaff or falling spheres ejected from rockets. These methods are expensive and complex: hence the data are sparse and difficult to interpret. Since only a few of the newer rocket data have been published little can be added to Murgatroyd's picture. Thus, as in fig. 8, the winter tendency is for a circumpolar belt of strong west winds covering most of the hemisphere and centred in lower - mid-latitudes and near the stratopause. The detailed structure or variability of the belt is not known. Some comments on the relation of this belt to the polar-night westerlies are offered in section 5.2.

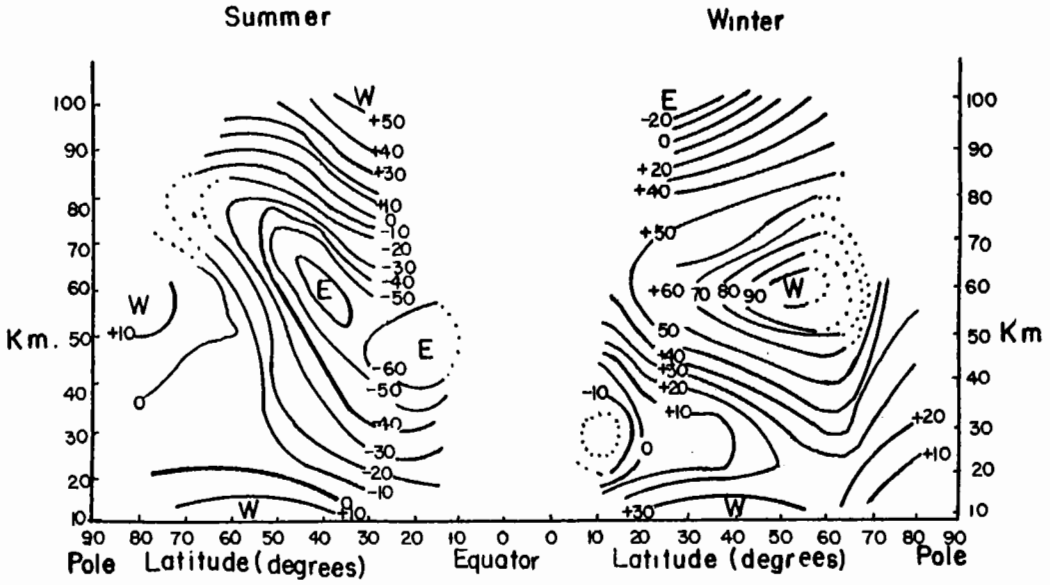

Fig. 8. Reconstructed winds (m sec^{-1}) and temperatures (^{o}C) 20 km to 100 km from Murgatroyd (1957).

3. PHYSICAL PROBLEMS

The problems in the stratosphere can be restricted by considering only those relevant to large scale thermodynamic energy processes. The water vapour distribution is still an open question, but is generally considered to be of minor importance in stratospheric energy processes. The discussion may then be limited to the general radiation budget and the ozone distribution.

3.1 The Radiation Budget

Several comprehensive reports on radiation computations in the stratosphere using numerical integration methods have appeared in the past few years. The radiative changes due to solar heating of ozone computed by Pressman (1955) and the infra-red cooling of carbon dioxide by Plass (1956) were followed by the budgets for the lower and middle stratosphere by Ohring (1958) and Brooks (1958) and for the middle and upper stratosphere and the mesosphere by Murgatroyd and Goody (1958). The validity of the budgets depends mainly on the absorption coefficients, the gas concentrations, the integregation techniques and the temperature structure. Although there have been advances in all these it appears that the budgets, like most stratospheric computations, should be used with reservations and may usefully be considered in the light of their dynamical implications.

The temperature profile used by Plass, together with his results for

the infra-red cooling by CO_2 and $CO_2 + O_3$ are shown on fig. 9. The ozone heating figures for lower mid-latitudes in summer from Pressman have been added to illustrate the approximate balance of the two computations.

Ohring divided the stratosphere into two layers, one from the tropopause to 21 km and the second from 21 to 55 km. The budgets are based on absorption by ozone, carbon dioxide and water vapour. For the entire stratosphere he finds that the Arctic regions have a deficit of 0.5 to 1.0°C per day and the tropical regions an excess of about the same amount. The 21 to 55 km layer has an excess of about 0.5°C per day in the tropics at all seasons whereas the Arctic has an excess (about 0.5°C per day) in summer only with a deficit of about 1°C per day in winter. The stratospheric layer below 21 km has a small deficit at all seasons. Brooks examined the carbon dioxide cooling in more detail than Ohring and on the available evidence found general agreement with Ohring's results.

Murgatroyd and Goody presented monthly diagrams for solar absorption due mainly to ozone in the stratosphere and mesosphere, and molecular oxygen above the mesopause. Their infra-red cooling rates due to the 15μ CO_2 and the 9.6μ O_3 bands were only for summer and winter, as they used the available temperature cross sections of Murgatroyd (1957). Their complete results for summer and winter are given as fig. 10. These show a slight deficit in the middle stratosphere at all seasons, with a maximum of 1 to 2°C per day in winter. The upper

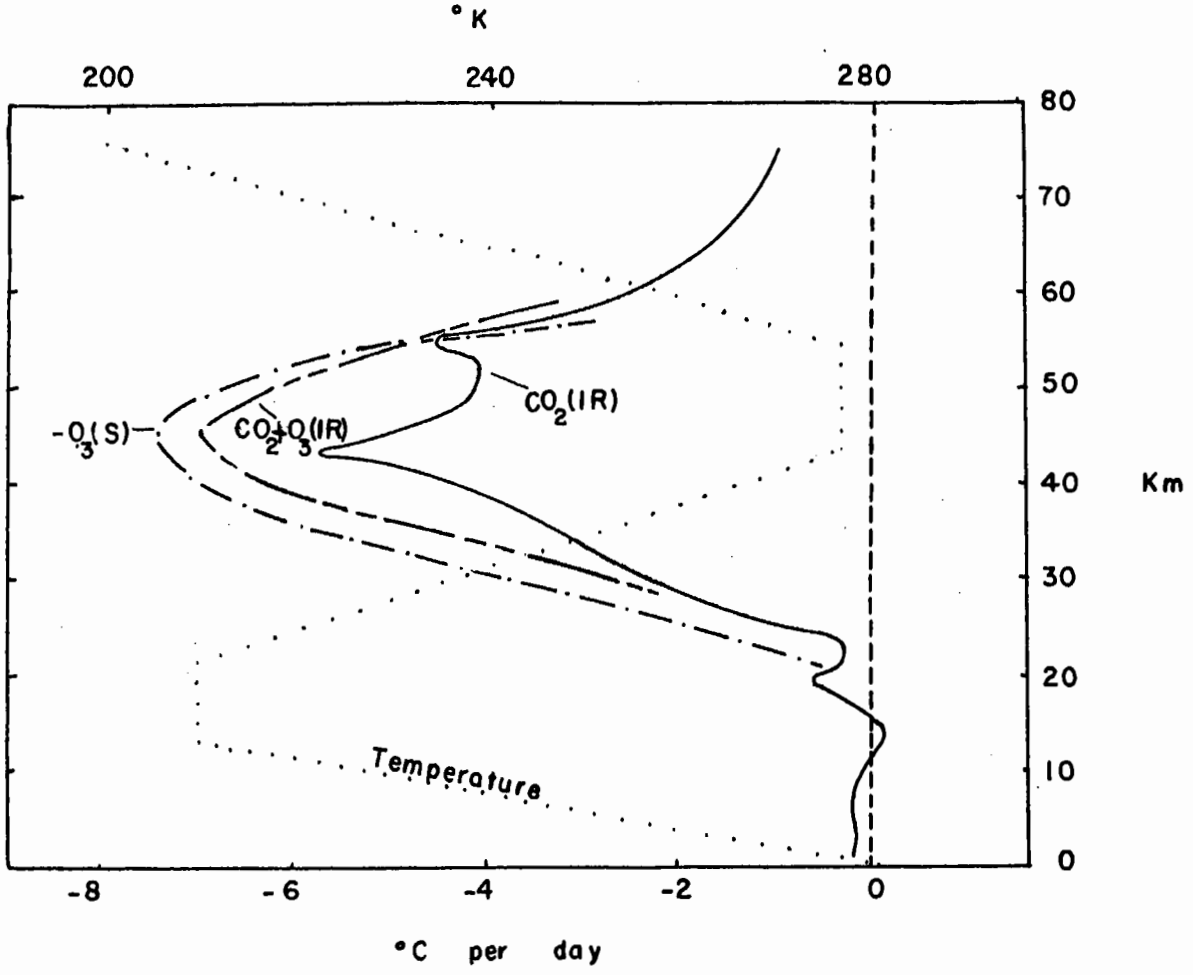

Fig. 9. The temperature profile and infra-red cooling from Plass (1956) together with the solar heating curve from Pressman (1955).

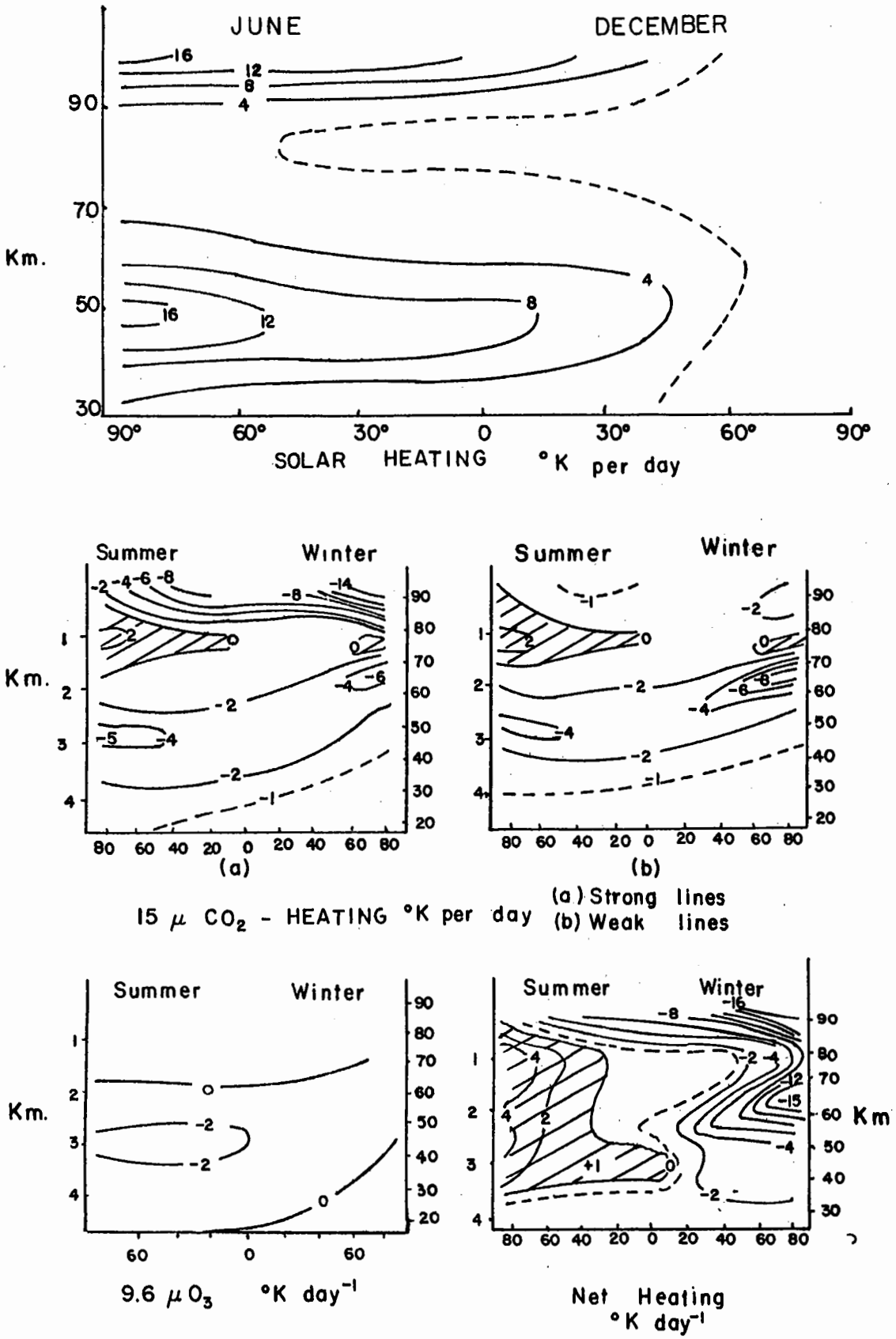

Fig. 10. Radiation computations from Murgatroyd and Goody (1958).

stratosphere and mesosphere have a summer excess of 2 to 4°C per day at higher latitudes and a winter deficit at all levels, with a maximum deficit of 15° C per day at the stratopause in the polar dark region.

A number of computations for the 60-70 N belt are shown together on fig. 11. At levels where the results overlap the agreement is quite good. All estimates agree that below about 30 km the stratospheric radiative changes are small with a deficit (1°C per day or less) at all latitudes and seasons. The winter deficit in the Arctic regions is in agreement with dynamical factors, as the Arctic regions cool at an average of about 0.3°C per day in the presence of a northward eddy heat transport. A late spring-summer deficit is more difficult to reconcile, since this is a period of slowly rising temperatures with an apparent minimum of turbulent heat transfer. It seems more likely that the calculations are within computational error and that a balance or slight excess exists down to at least 20 km. This difference might arise from variations in the vertical distribution of ozone, or in the solar ultra-violet intensities. The excess shown for the upper stratosphere and the lower mesosphere is consistent with the summer warm phase. The winter cooling along the stratopause of up to 15°C per day shown by Murgatroyd and Goody appears to be excessive, and a dynamical process to achieve local thermal balance in that area is difficult to conceive. Assuming that the infra-red cooling rates are reliable to within several degrees per day for the given

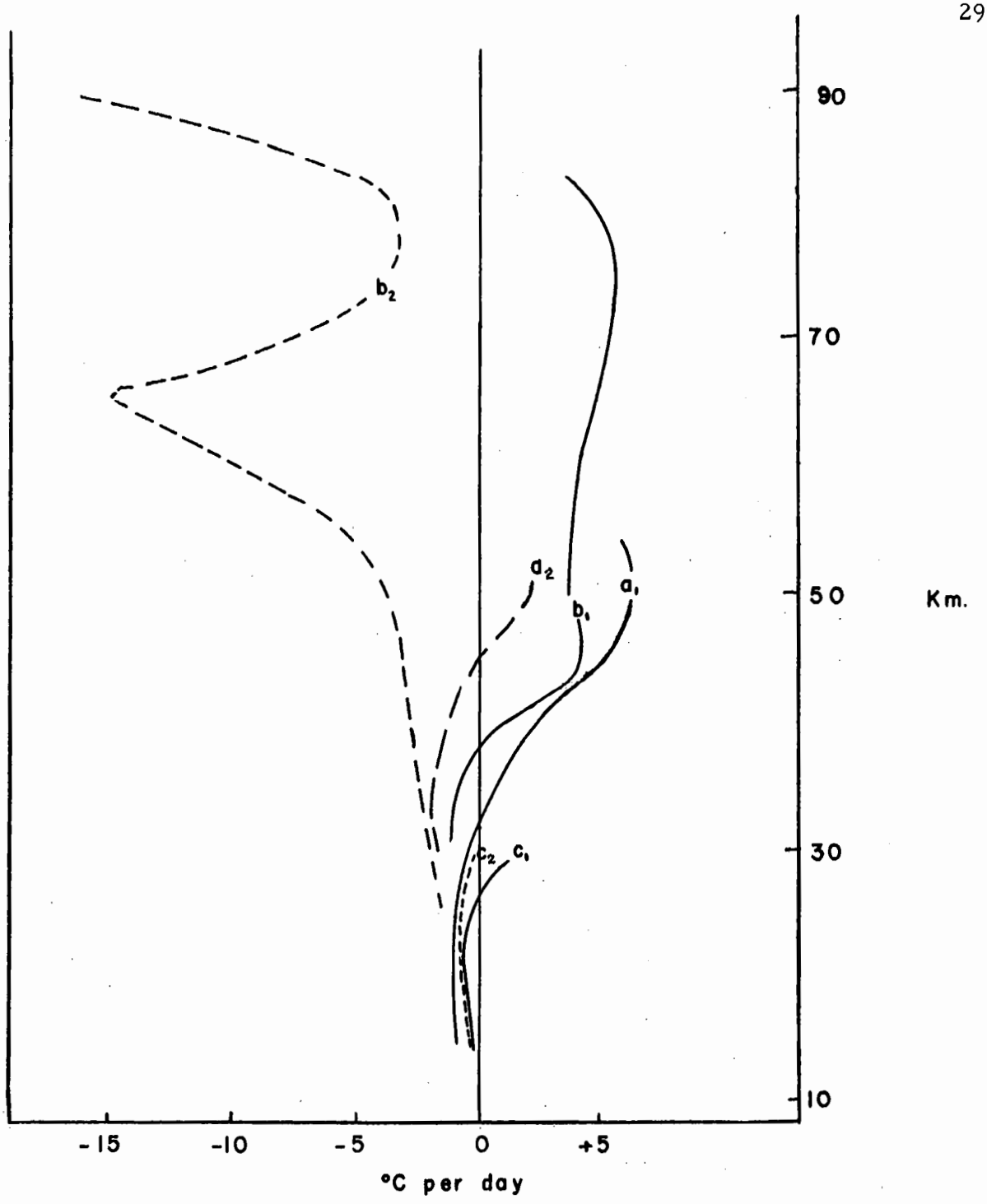

Fig. 11. Selected radiation computations for the 60N-70N latitude belt

a_1, a_2 - Ohring, April and October; H_2O, CO_2, O_3

b_1, b_2 - Goody, summer and winter; CO_2, O_3, O_2

c_1, c_2 - Brooks, April and July; CO_2, O_3.

temperature structure (this seems plausible from the balanced values of other seasons) it is likely that the temperature structure would relax to a more reasonable radiative value. A lower maximum value and a much flatter vertical temperature profile would be the probable result.

3.2 Ozone

The vertical thermal structure of the atmosphere appears to be determined primarily by its regions of strong absorption of solar radiation. Absorption in the far-ultra-violet by molecular oxygen contributes to high temperatures in the thermosphere, absorption in the ultra-violet band by ozone yields the temperature maximum near 50 km, and absorption in the visible and near-visible wave lengths at or near the earth's surface gives the surface maximum. Between the maxima lie the minima, the mesopause region at about 80 km and the tropopause region at about 13 km. Ozone may thus be considered the determining radiative constituent of the middle and upper stratosphere and because of its highly variable total concentration it has important implications for both radiative and circulation computations.

The ozone concentration above about 35 km is in photochemical equilibrium according to Craig (1950) the amount depending mainly on the solar ultra-violet intensity. Below 35 km the half life of ozone increases rapidly and it can be treated as quasi-conservative below 30 km. Ozone escaping into the troposphere is rapidly dispersed (and eventually destroyed

at the ground); hence concentrations are generally low below the tropopause. It follows then that changes in the total amount of ozone apart from ultra-violet effects will be due mainly to processes occuring between the tropopause and 35 km. A satisfactory dynamical mechanism for the relationship between total ozone variations and tropospheric weather systems was introduced by Reed (1950), who showed that the associated subsidence (or ascent) in the lower stratosphere should increase (or decrease) total ozone. By applying boundary conditions at the tropopause and 35 km Godson (1959b) showed that Reed's mechanism will be effective at all levels below the maximum of ozone mixing ratio in the vertical. The ozone-tropospheric perturbation effects have been well substantiated by Normand (1953). Wexler and Moreland (1958) suggested a connection between total ozone variations and the polar-night westerlies. More recently Godson (1960) has postulated a fundamental role for these westerlies in determining the seasonal and latitudinal distribution of total ozone. Allington, Boville, and Hare (1960) showed that large winter ozone changes at Edmonton and Moosonee could be related to travelling waves in the polar-night westerlies.

The large amplitude variations in total ozone resulting from active systems in the middle stratosphere will be shown by two case studies. The first occurred in the European sector in February, 1959 and the second over North America in January, 1960.

Case A: On February 17, 1959 (fig. A 28) the polar-night vortex was centred north of Greenland. A baroclinic trough over Greenland began to deepen and then moved south-eastward. By February 22 (fig. A 29) the thermal centre was closed off and centred over Northern Ireland, moving east-southeastward at a phase velocity of about six degrees longitude per day; on February 27 (fig. A 30) it was over the Black Sea. It produced 30-mb temperatures of -88C at Stornoway and -89C at Leuchars (Scotland). Even over the Black Sea, 30-mb temperatures fell below -70C. The time cross section for Bitburg, Germany, for February, 1959 (fig. 12) shows that the system's passage caused a profound cooling through most of the stratosphere, followed by a warming to normal values.

Very large total ozone changes occurred as the system passed. Fig. 13 gives time-sections for total ozone and 30-mb temperature at Lerwick, Oxford, and Rome, the temperature record on the Oxford section being for Camborne (Cornwall). At all three stations the records show (i) short-period fluctuations of amplitude up to 700 microns uncorrelated with 30-mb temperature; (ii) a very pronounced minimum associated with the passage of the stratospheric cold core on February 22nd at Lerwick, 23rd at Oxford, and 25th at Rome; (iii) a sharp recovery to more normal values in the rear of the core, followed at Lerwick only by a rise to very high values (5350 microns on March 6th,

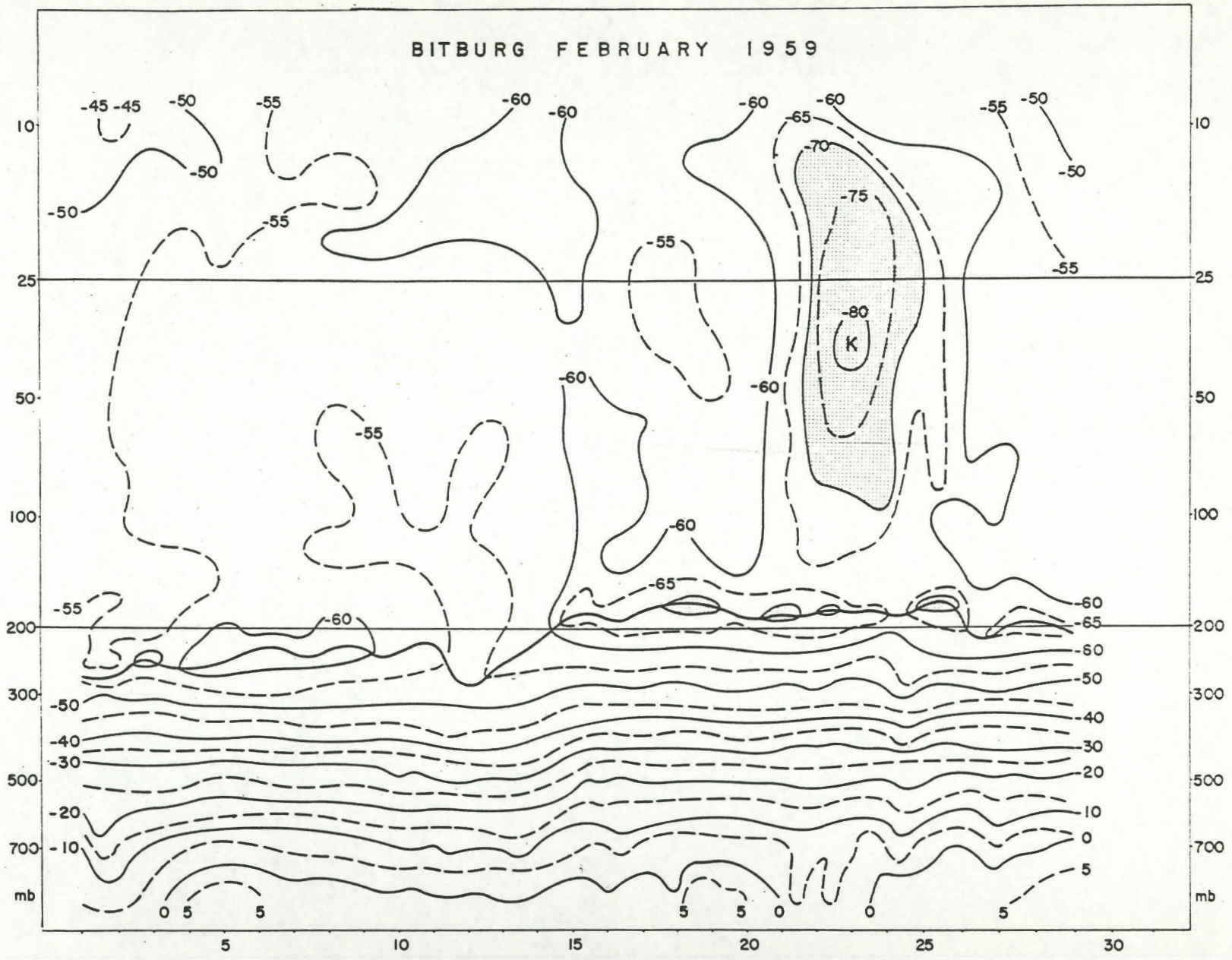

Fig. 12. Vertical time-section of observed temperatures

at Bitburg, Germany for February, 1959.

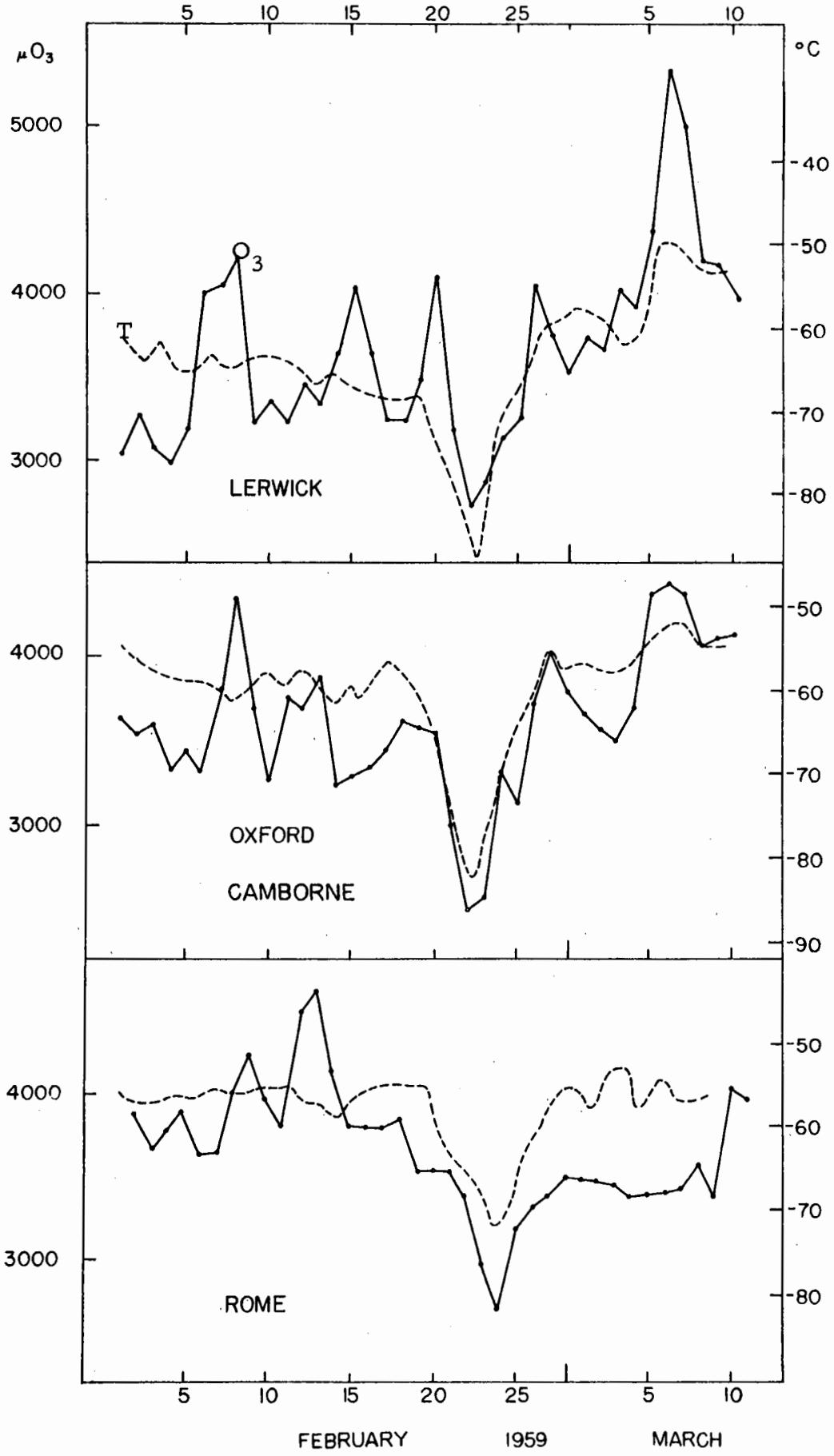

Fig. 13. Time sections of observed total ozone and 30-mb temperatures at Lerwick, Oxford (Camborne) and Rome.

associated with the final stratospheric warming).

The variations listed under (i) above are ascribed to travelling waves in the tropospheric (Ferrel) westerlies due to the Reed-Normand effect. Those under (ii), however, are of larger amplitude, and are connected with the dynamical effects of the stratospheric cold core. At all three stations the total ozone fell to well below 3000 microns. The total decrease can be estimated as about 700 microns at Lerwick and Rome and 1000 microns at Oxford (the last being about one-third of the amount prevailing before the approach of the cold core).

Case B: The second case developed in January, 1960 over North America. On January 2 (fig. 14) the middle stratospheric circulation had its normal aspect, with a warm high over Alaska and a cold trough east of Greenland. The second and third weeks of the month were marked, however, by (i) the warming and intensification of the Alaskan high (see fig. 14, Jan. 17) and (ii) the deepening of a cold trough across Hudson Bay, with the creation by January 10 of a closed cold vortex which moved southwest to Saskatchewan by January 17 and into the western plains of the United States by January 19. Thereafter, it filled up slowly. The centre of the stratospheric low passed northwest of Moosonee, Ontario, on January 12-13.

The consequences are shown in fig. 15, which presents a time-section of 30-mb temperatures and total ozone at Moosonee for January,

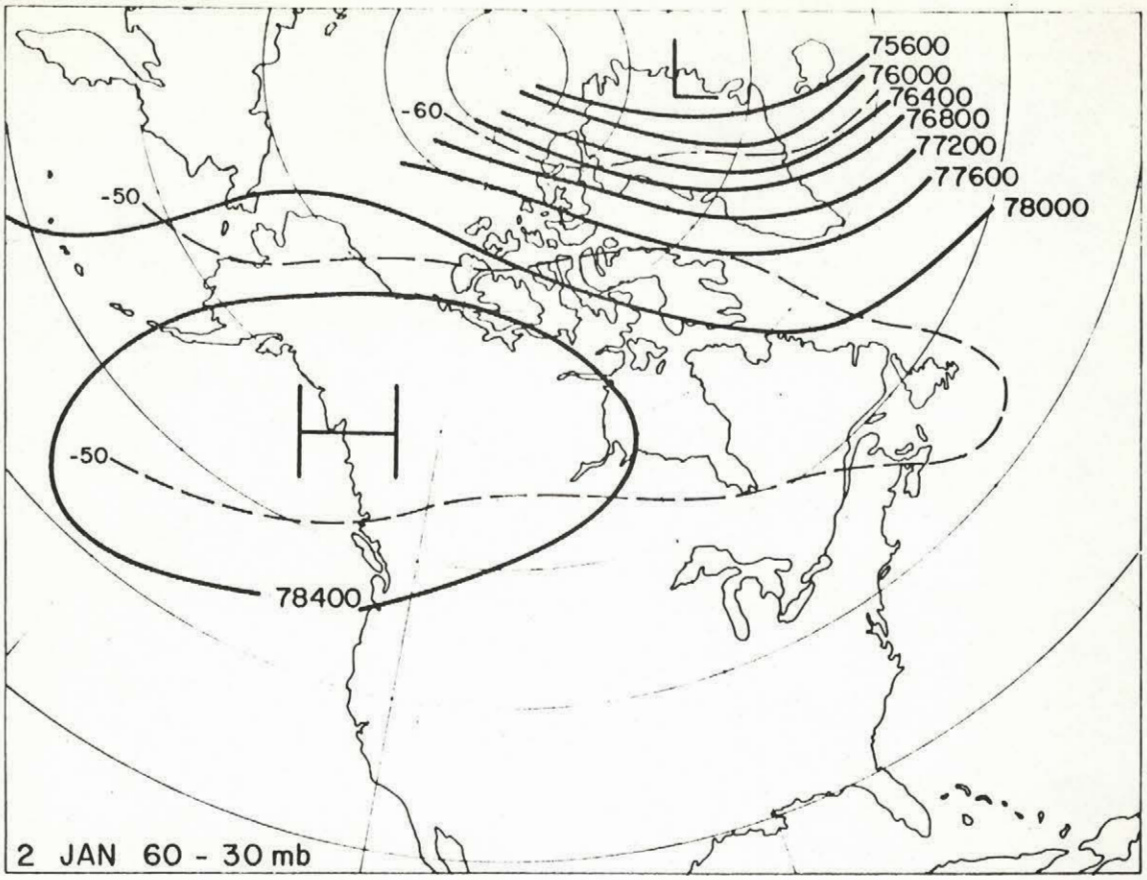

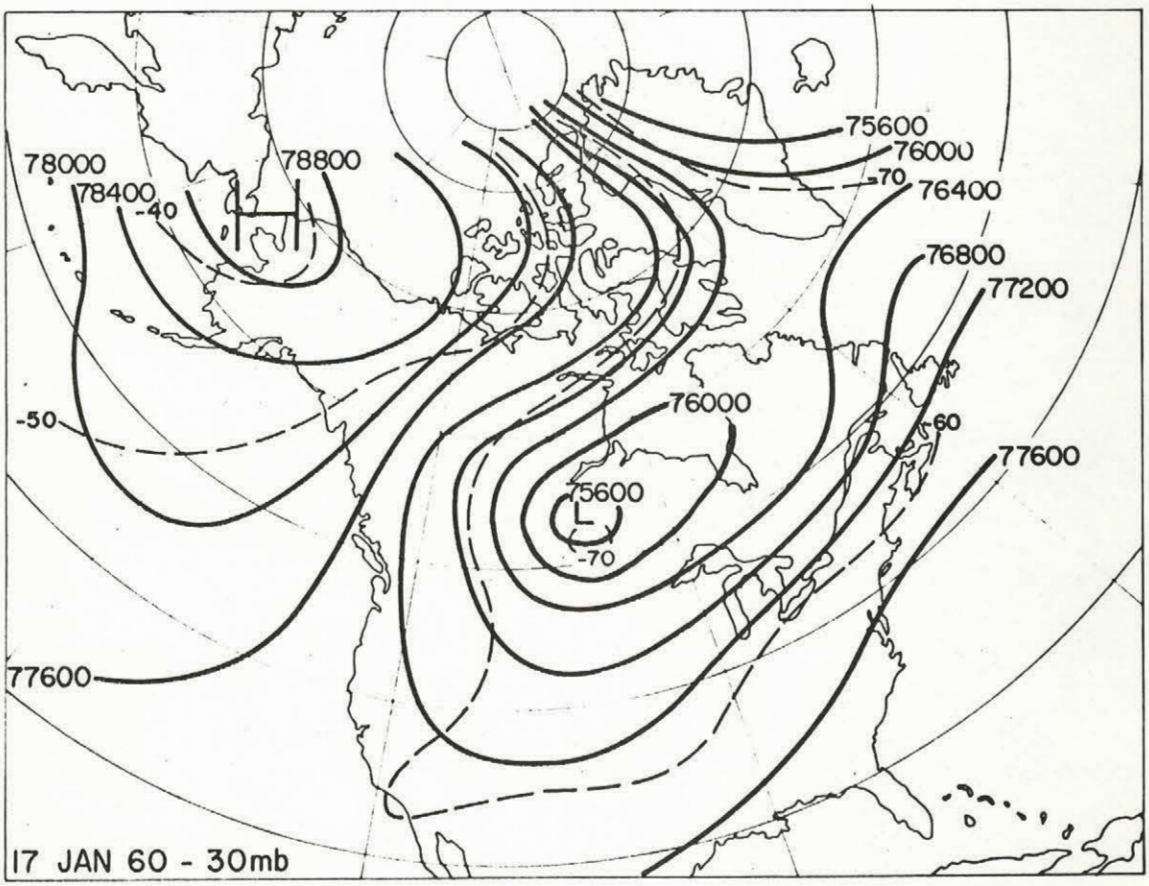

Fig. 14. 30-mb charts for January 2 and 17, 1960.

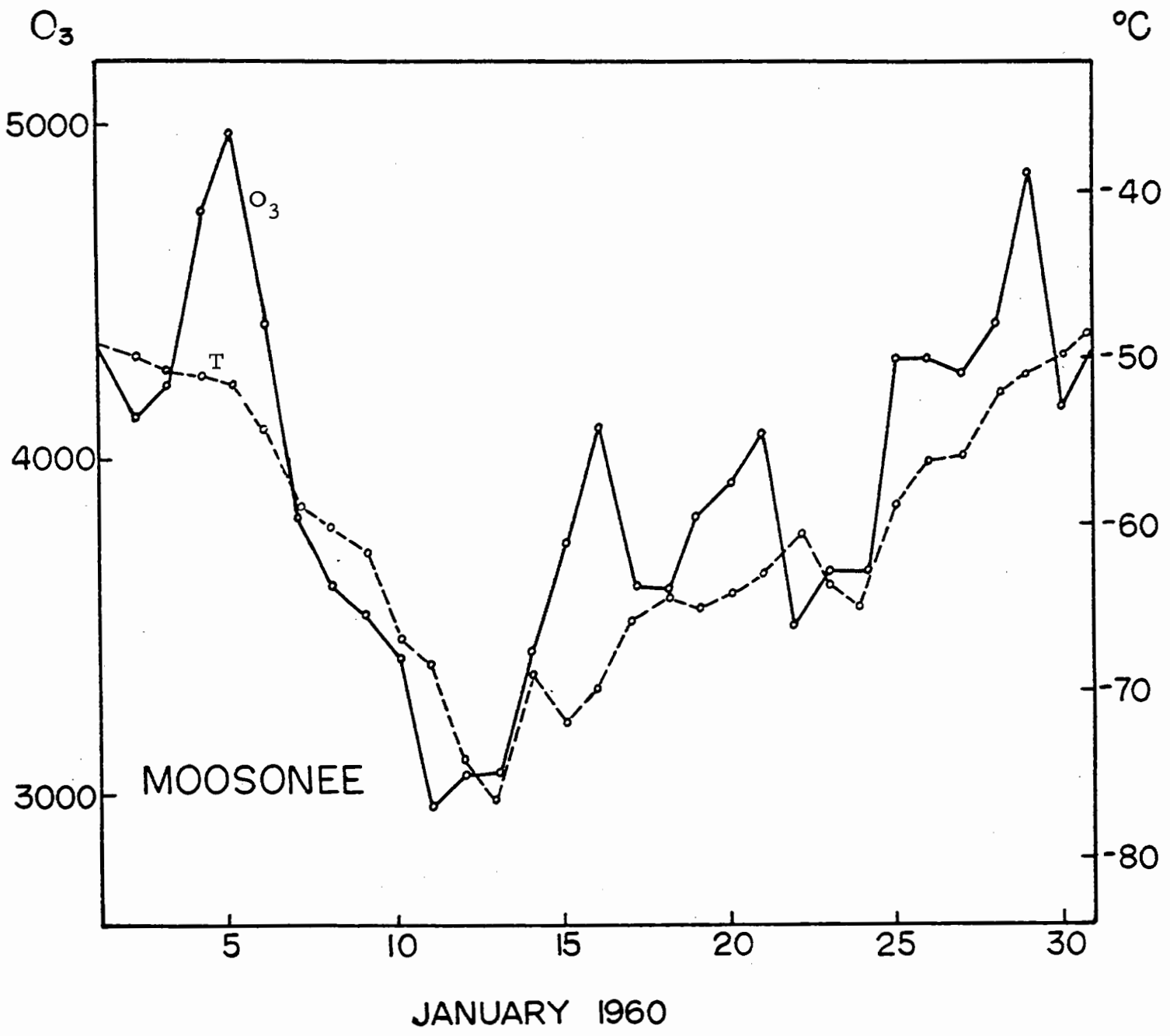

Fig. 15. Time section of observed total ozone and 30-mb temperature at Moosonee, Ontario, January, 1960.

1960. The approach of the cold low was accompanied by a progressive fall of total ozone, from about 4980 microns on January 5 to about 3000 microns on January 11-13, associated, as in Case A, with the dynamically induced temperature minimum. With the recovery of temperature after the low had passed away southwestward, ozone also recovered to a more characteristic value.

The above ozone-temperature correspondence has also been examined more objectively, the following method being used to separate the effects of the two stratospheric layers. Smoothed ozone mixing ratio curves were derived from the standard Umkehr distributions* and compared with the potential temperature profile for a winter isothermal stratosphere. It is apparent in fig. 16 that the profiles of the parameters can be matched very closely by the use of appropriate scaling factors. The factors clearly change considerably from the middle to the lower stratospheric regimes. In the absence of observed data the ozone mixing ratio was assigned the analytic form of potential temperature and it follows that

$$\psi = c\theta + b \qquad (3.2 - 1)$$

where ψ = ozone mixing ratio and θ = potential temperature. Thus

$$\psi = cTP^* + b \qquad (3.2 - 2)$$

where T = temperature and $P^* = \left(\frac{1000}{P}\right)^{0.277}$, and

$$\sigma = \int_{P_1}^{P_2} (cTP^* + b)\, dP \qquad (3.2 - 3)$$

* after Mateer (1960)

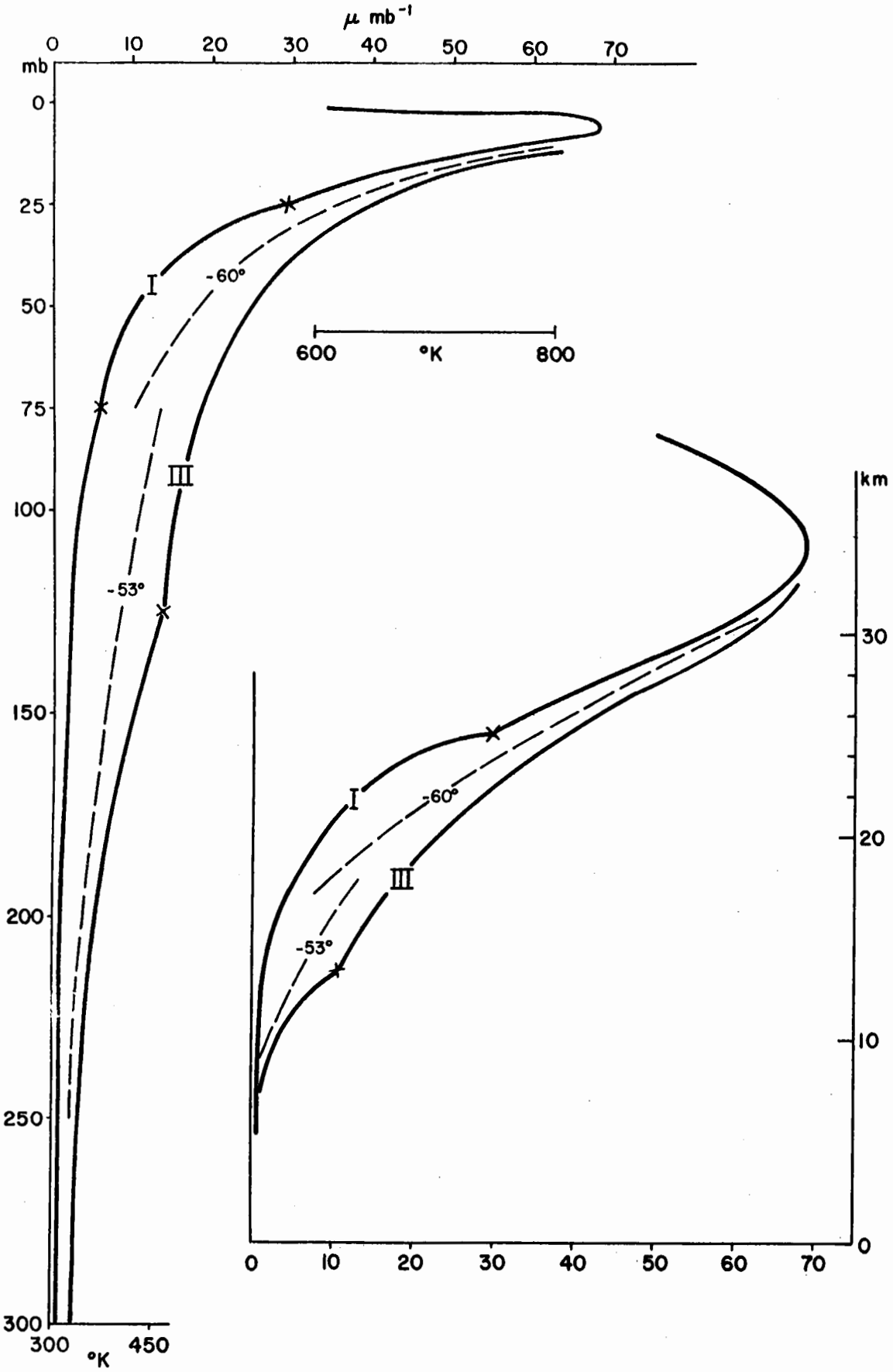

Fig. 16. The vertical distribution of ozone, microns per mb, for standard Umkehr curves I and III and the potential temperatures for an isothermal stratosphere at -60C and -53C.

where σ is the ozone amount between two pressure levels, P_1 and P_2. The integration of equation (3) becomes particularly simple for an isothermal lapse rate, in which case

$$\sigma = \left[1.404\, c\, TPP^{*} + b\, P\right]_{P_1}^{P_2} \qquad (3.2 - 4)$$

The coefficients in equation (4) were determined from the medium standard ozone curve for two layers, one set for the layer between 75 mb and 10 mb and another set for the layer between 250 mb and 75 mb. These were then applied to temperatures (adjusted to noon local time) at Moosonee for January, 1960 in the following manner: the 30-mb temperature was used for the upper layer and the 200-mb temperature for the lower layer, but the pressure at the base of the lower layer was allowed to vary with the tropopause. The computed ozone values were then correlated with the observed values. The upper layer (30 mb) and total ozone gave a linear correlation coefficient of r = 0.85. The lower layer (200 mb) gave a linear correlation coefficient of r = 0.42 and for a partial correlation coefficient the non-significant value of R = 0.23.

Discussion: The lower stratospheric effect appears to be negligible at Moosonee primarily because it is overshadowed by the larger activity in the middle stratosphere. It may also be noted that it is difficult to filter out disturbances whose periods are only two to three times the ozone reporting interval of twenty-four hours. The phasing of observation

times is particularly important at that lower limit of the time scale.

The middle stratospheric disturbances, generally having periods of over 10 days, will not suffer from the observational interval, and the phasing of data is not a problem. For these longer periods one would, however, expect non-adiabatic factors (radiative and chemical) to assume greater importance. The basis for the total ozone and 30-mb temperature correspondence in the polar night systems is the dominant role played by vertical motion in the presence of large vertical gradients. In addition, if (i) the basic horizontal distributions of the two parameters are similar or of a lower order of magnitude than the anomalies and (ii) non-adiabatic effects do not strongly alter the anomaly structure, then subsequent horizontal advection and vertical motions, regardless of how they combine, will tend to maintain anomaly correspondence.

It has already been demonstrated that dramatic changes in the middle stratospheric temperature patterns are accompanied by dramatic ozone changes. Some further speculation on the more general character of the above distributions will be carried out below. During the early autumn the middle stratosphere is essentially barotropic with no horizontal temperature contrasts (Hare, 1960b); thereafter, temperatures fall progressively in the polar regime, reaching the -70C mark at 30 mb in November and the -80C mark in December; at the same times average temperatures in middle latitudes at 30 mb are about -55C. The mean

latitudinal distribution of total ozone (Götz, 1951), appears to follow a similar pattern with amounts near 3000 μ and little gradient from mid-latitudes northward in the autumn. Thereafter, amounts fall in the polar regions to near 2000 μ in December, whereas in middle latitudes they remain constant or rise slowly. The hemispheric latitudinal distributions of the two variables are thus similar, and it remains to discuss the dominant anomalies superimposed on the zonal pattern.

The major asymmetric feature of the polar-night stratospheric circulation is the Aleutian warm anticyclone. This warm zone has been related by Boville (1960) to the great intensity and persistence of tropospheric cyclogenesis in the Aleutian area. During October 1958, associated with hemispheric-wide weather adjustments, there was intense cyclogenesis in that area. The vertical circulation associated with these events extended high into the less stable and slightly baroclinic middle stratosphere and created an anomalous warm centre with temperatures at 25 mb near the -40C mark over the Bering Sea, in contrast to temperatures near -65C at similar latitudes in the Atlantic sector. (Arcas rocket winds at Churchill, Manitoba, recently communicated by Dr. W.L. Godson of the Canadian Meteorological Branch suggest that a similar northwest thermal gradient reached up to near the stratopause in October, 1959). Unfortunately, ozone observations were not available to the author for the Alaskan area, and the effects could

not be examined in the warm zone source region. However, in November, 1958 the major part of the warm zone surged northeastward into the Arctic Islands at a time when lunar ozone observations were available from Resolute, N. W. T. The three observations on November 24, 25, and 26 showed values double the expected seasonal value and confirm the profound influence of the warm zones on the ozone distribution. These effects are shown schematically by the ozone distributions on fig. 17, the early autumn by the chart for September 25 and the warm zone effect by the one for November 24. The basis for these charts is described in the next paragraph. Similar phenomena do occur in the Atlantic cyclogenetic sector; however, activity there is not as conservative in position nor as consistently intense as the Pacific counterpart, and Atlantic warm stratospheric anticyclones appear to be infrequent.

Total ozone maps were plotted for the 1958-1959 year by the entry of five consecutive daily values for each station on a single chart: the centre day coincided with the dates of the 25-mb chart series. The similarity of the ozone distributions to the synoptic charts, along with the previously mentioned experiments, permitted the construction of ozone patterns on the following basis. The isotherms of the 200-mb chart (1200Z) and the 25-mb chart were each converted to total ozone increments using the potential temperature relationship of the previous section (equation 3.2 - 4). These derived ozone patterns were then

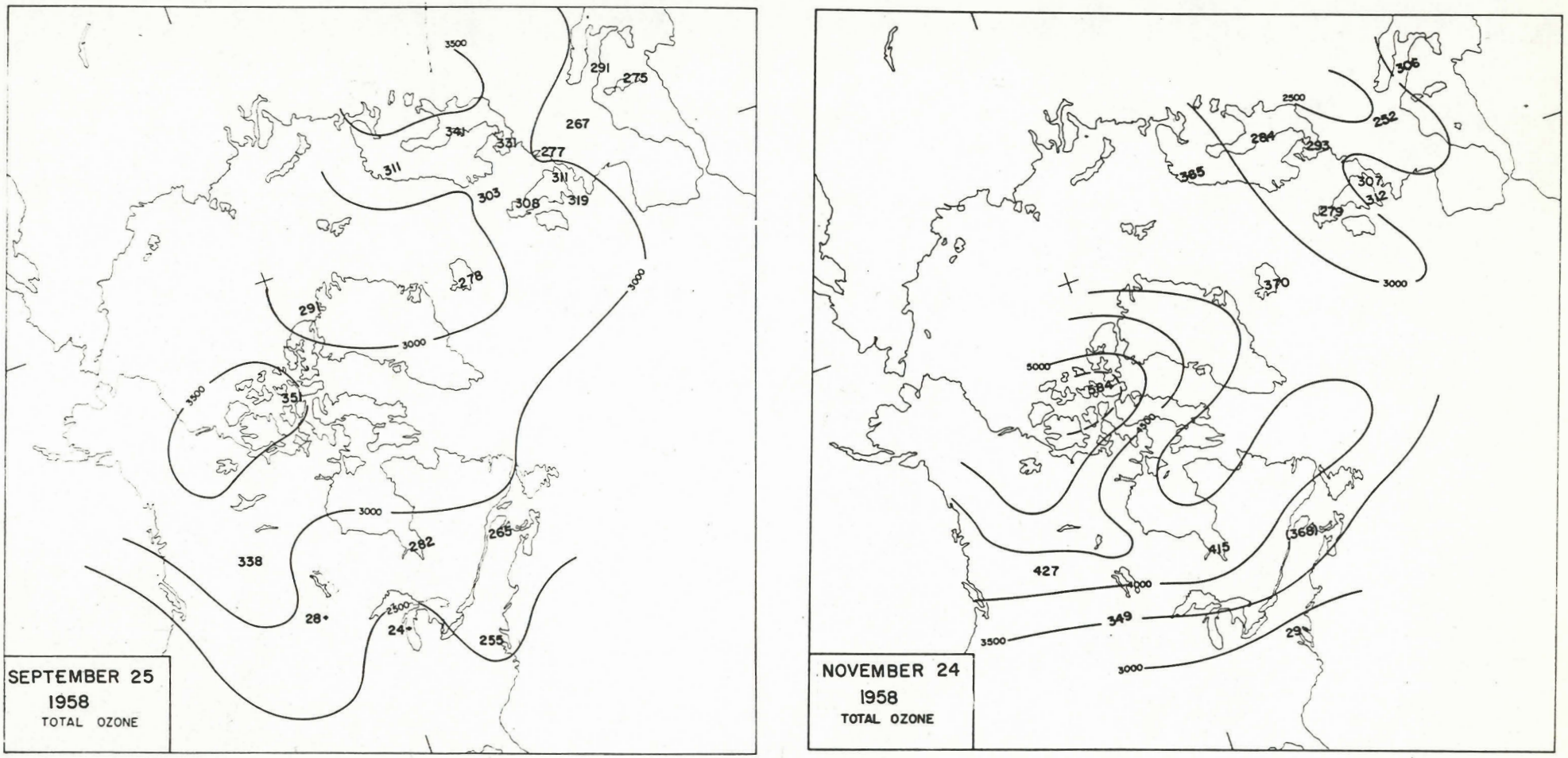

Fig. 17. Observed values of total ozone (microns) together with tentative isolines for September 25 and November 24, 1958.

superimposed on the plotted chart and relaxed subjectively to fit the observed data. The distribution lines on fig. 17 were drawn in that manner. Similar charts were drawn throughout the year, and these leave little doubt that all major anomalies of the polar-night vortex are accompanied by ozone anomalies.

The results of the foregoing cases would appear to justify the following conclusions:

(1) Total ozone in high latitudes in winter shows large variations ascribable to perturbations in the polar-night westerlies. Low ozone is associated with cold troughs and high ozone with warm ridges.

(2) The relation holds good for systems that break away from the polar-night vortex and move into lower latitudes. In such systems, the ozone variations due to their passage are large enough to be clearly visible even in the midst of tropospheric perturbation effects.

(3) The results favour the dynamics of the polar-night vortex as the major agent controlling the large-scale anomalies in the total ozone distributions of middle and high latitudes.

4. SYNOPTIC ANSWERS

It has long been clear that a purely deductive approach to the problem of atmospheric dynamics is out of the question. This fact arises from the extreme complexity of the circulation. The usual method is accordingly to define, measure and portray the dynamical structure of the atmosphere by empirical methods, including carefully-chosen case studies. It is the chief objective of dynamic meteorology to relate these results to established dynamical theory; in other words one tries to show the internal consistencies and relationships of the different scales of motion of this complicated mechanism with Newtonian dynamics. The relevant dynamical theory is reviewed in section 5. This part of the study will hence be concerned with an empirical view of the stratospheric circulation, through synoptic methods. The first section presents a study of the origin of the major winter circulation anomaly, the Aleutian stratospheric anticyclone, in the form in which it has been published (Boville, 1960). The other two sections present case studies of the wave activity and the final warmings.

4.1 The Aleutian Stratospheric Anticyclone

The chart for January 1, 1958, fig. 18, shows the characteristic features of the winter circulation. A diffuse high covers the tropical regions where winds are everywhere light and variable. The geopotential height at the equator is almost identical with the summer value whereas the height at the pole has dropped some 10,000 feet in association with the

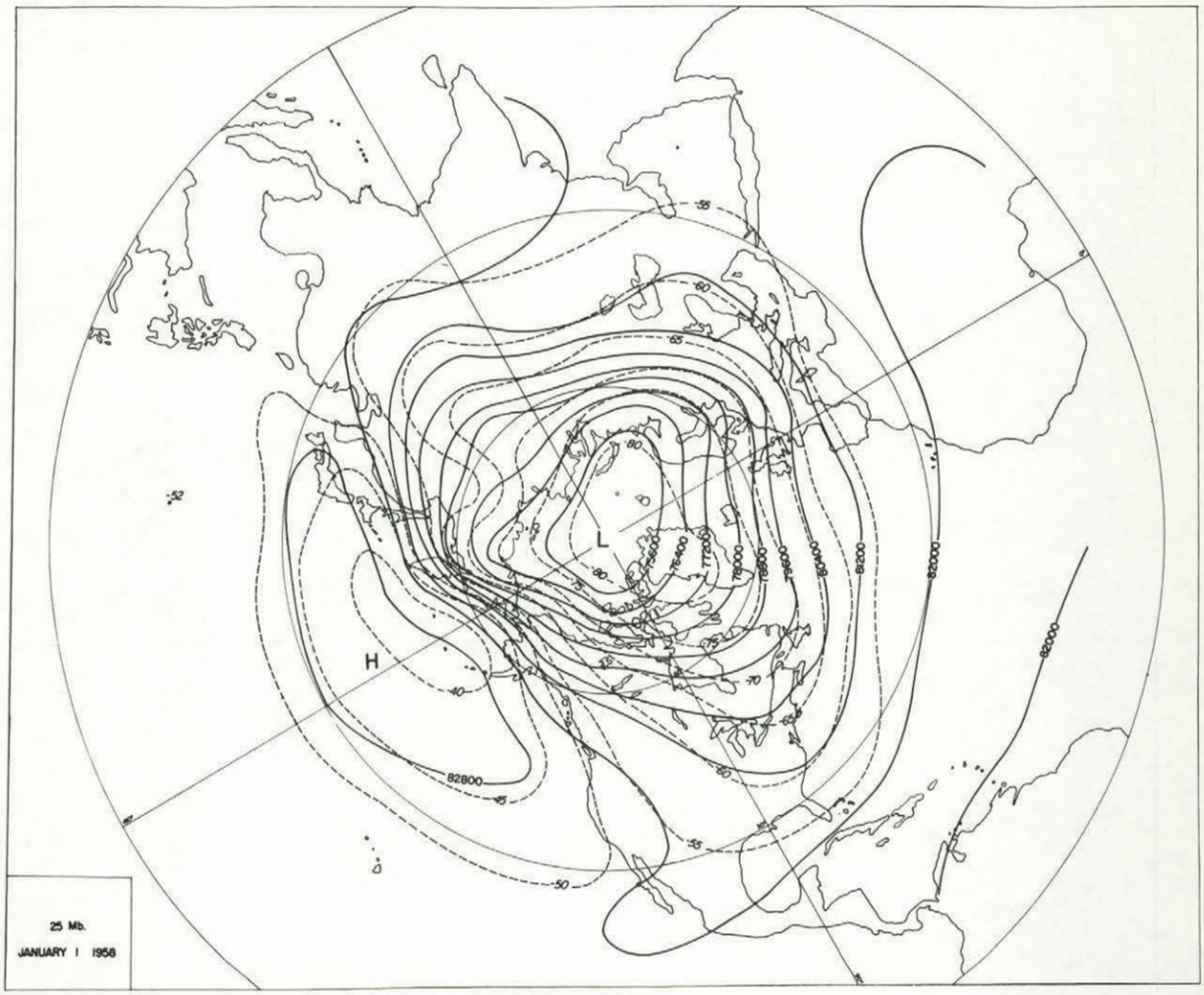

Fig. 18. 25-mb chart for January 1, 1958, a typical mid-winter chart.

intense polar vortex. Large scale waves are clearly present and the most striking asymmetry in the field is the large warm anticyclone over the north Pacific Ocean with an intense baroclinic zone over eastern Siberia and Alaska. A similar warm anticyclone was present throughout 1958-59 and studies by Godson (1959) using the available 100-mb temperatures over the past eighteen years suggest that it is a characteristic feature of at least six out of seven years. The study of the formation of this anticyclone is logically the first step in formulating the middle stratospheric dynamics.

Daily temperature values at 25 mb for October, 1958 through March, 1959 have been plotted as fig. 19, for Resolute and Lerwick. Fairbanks is included initially to show the locus of the October warming. During early October all three curves are similar, indicating the barotropic nature of the flow during the autumnal cooling. Subsequent to October 15th, Fairbanks and Lerwick curves diverge, whereas Resolute shows little change, pointing to motions on a very large geographic scale. Thereafter large scale waves are evident in the Resolute and Lerwick curves until the return to summer temperatures in March. During January and February, Resolute was near the path of the main stratospheric jet stream and its record shows a series of regular long period thermal waves. Lerwick, lying further downstream and to the south of the main polar night stream, shows a much more confused thermal pattern.

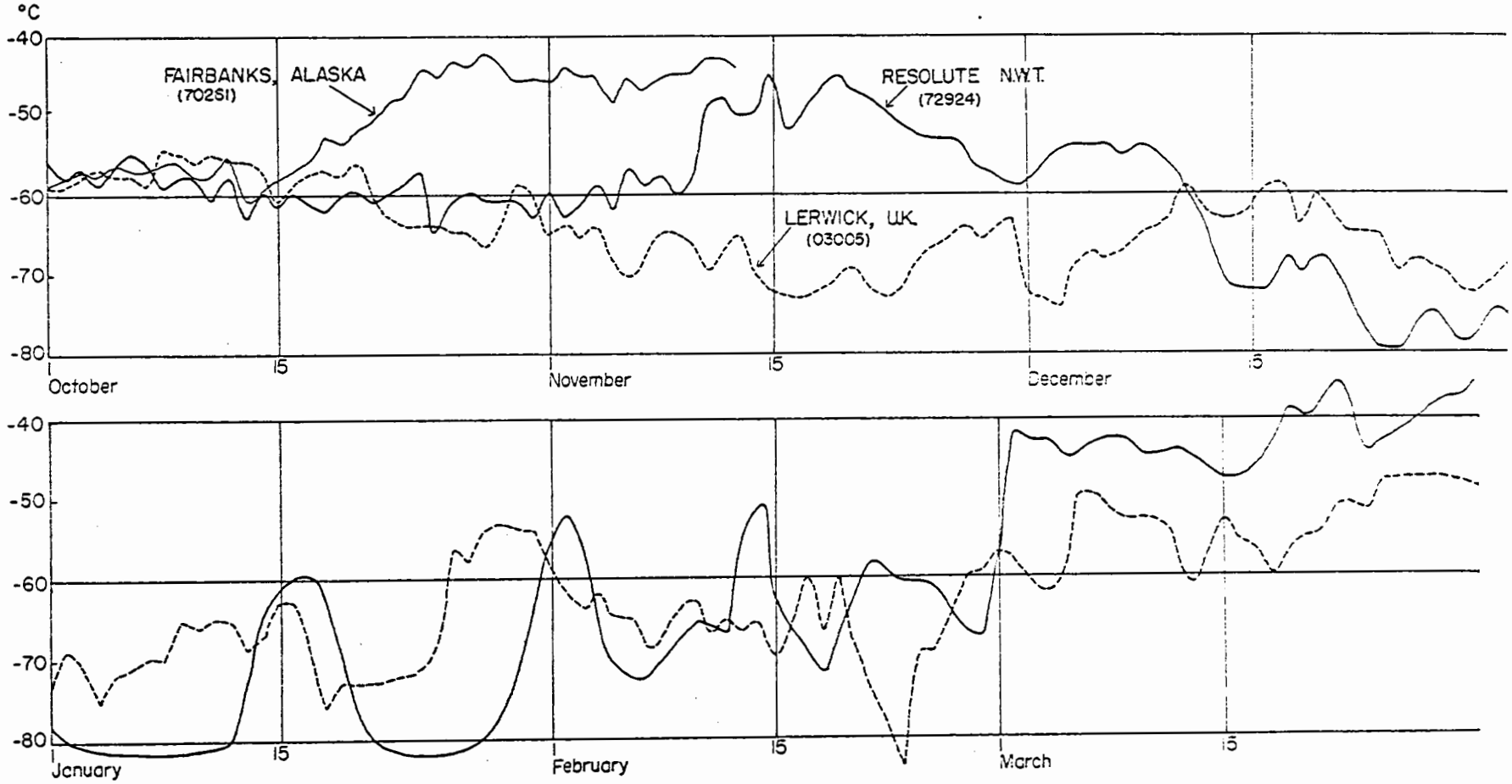

Fig. 19. Daily 25-mb temperatures for Fairbanks, Alaska; Resolute, N. W. T. and Lerwick, U. K.; October, 1958 - March, 1959.

Fig. 20, shows a spectrum analysis of the observed temperature data, using the coarse filter technique described by Cramer and Record (1955). The Resolute data show very different spectral characteristics for the troposphere and middle stratosphere. The 25-mb data has a strong seasonal shift, a second maximum in the 16-32 day range associated with the baroclinic waves, and a smaller short period temperature variance. There is little comparable in the 500-mb temperature variance, and little interdependence of the two wave regimes is indicated at that point. At Lerwick the two spectra are more similar and it is likely that away from the active polar night region the shorter waves of lower level Ferrel systems still possess some amplitude as high as 25 mb.

The analysis of the 25-mb height gradients from 65N to 80N at 150W during the main winter wave period gives average speeds of 70 kt in January and 90 kt in February. Daily cross-sections show mean core speeds at 25 mb of 140 kt with a half width of about 8 latitude degrees on the south side and 6 latitude degrees on the north side. The average temperature difference across the same band for January and February was 15C (1C per lat. deg.) the maximum value over the band was 30C, and the value increased to about 23C during wave development.

With respect to initiation of the Aleutian anticyclone the thermal regime indicates:-

1. There is not sufficient baroclinity at 25 mb in early October

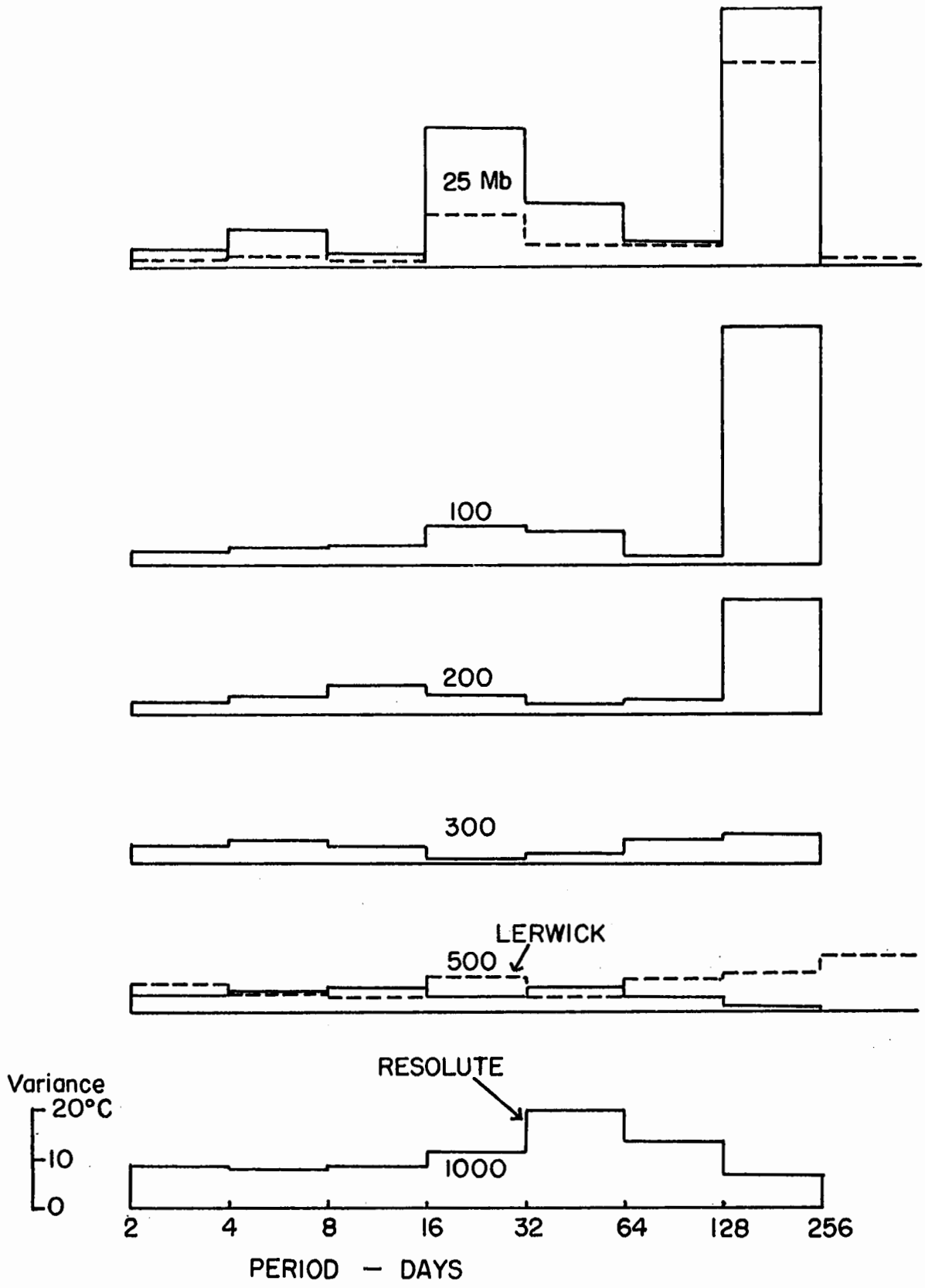

Fig. 20. Spectrum analyses of the observed temperatures at Resolute, N. W. T. and Lerwick, U. K. through the 1958-59 season showing temperature variance as a function of period.

to give rise to a large scale development. The origin of the anticyclogenesis should then be expected in the troposphere.

2. The very large scale of the phenomenon should make it readily evident from tropospheric analyses.

The 25-mb charts at 5 day intervals in October, 1958 (figs. A1-A6) show clearly the change from a weak poleward temperature gradient and a damped image of the tropospheric flow to the development of a strong thermal wave in the Kamchatka area and the establishment of anomalous warmth over the Bering Sea with its associated anticyclone.

A Fourier analysis of the geopotential heights at 60N for the 25-mb charts was compared with daily values available for 500 mb. Fig. 21, shows the comparison on a reduction of variance basis. There is a striking correspondence in the changes of wave number one. The eccentric trough at 500 mb was over western North America in early October, and shifted through a zonal phase in mid-October to eastern Asia in the second half of the month. The similar changes at 25 mb are consistent with warming at Fairbanks and cooling at Lerwick.

At sea-level these changes were associated with widespread weather adjustments (Ludlam, 1958). In the North Pacific there was little cyclonic activity prior to the fifteenth with a marked change to a series of 980 mb low pressure centres during the next two weeks.

The Stratospheric Warming: The strong cyclonic developments in

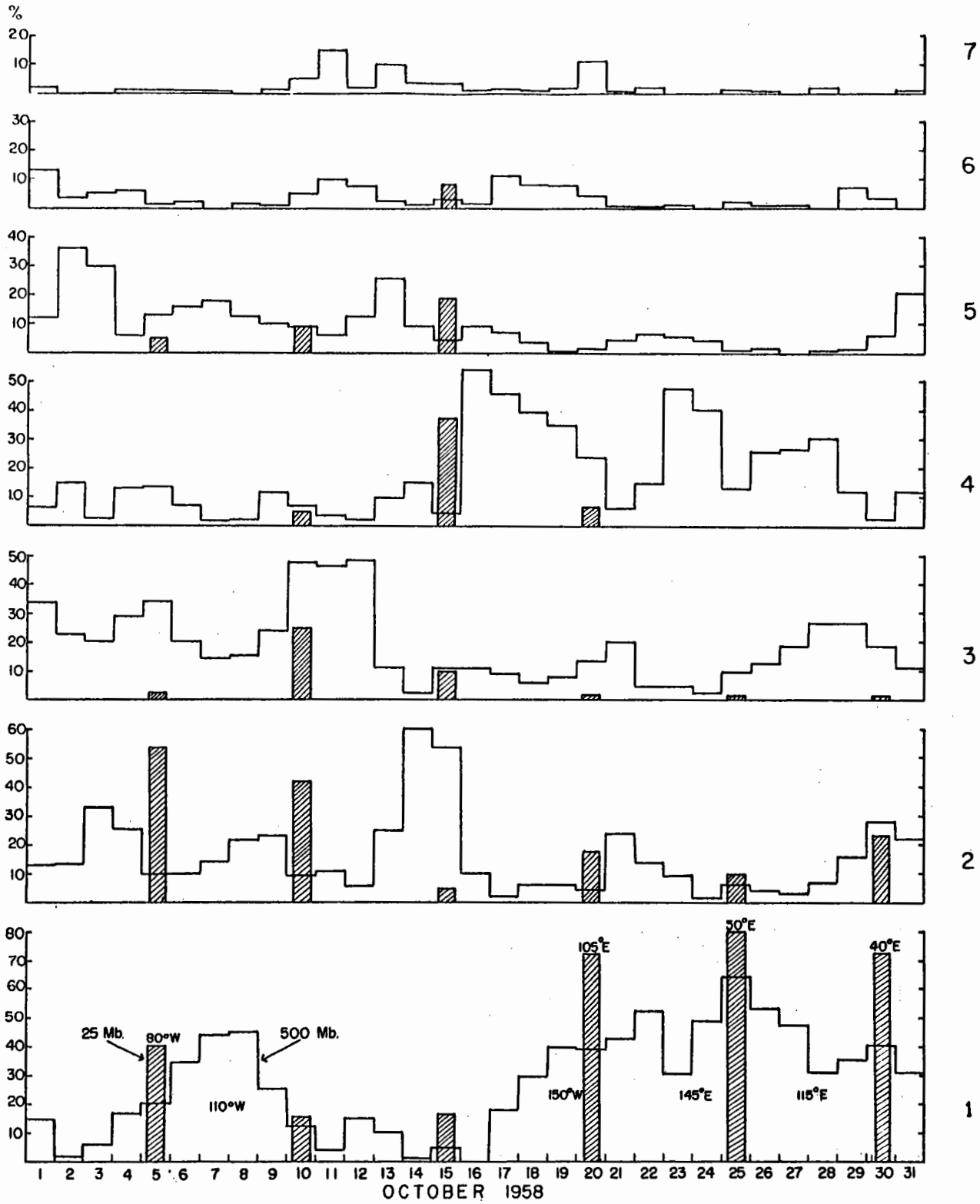

Fig. 21. Fourier analysis of 25-mb and 500-mb heights showing reduction of variance by wave number. Inserts are the positions of the eccentric troughs, wave number one.

the troposphere in the Kamchatka - Aleutian area were associated with strong compensating subsidence in the lower and middle stratosphere, creating a warm zone in that region. In fig. 22, the radiosonde data for St. Paul Island illustrate the changes. A series of minor changes culminated in a large amplitude system, with tropical air lifting the 500 mb temperature to --13C on the fourteenth and the next system dropping the 500 mb temperature to -41C on the twentieth. The initial change is strongly reflected at both 100 mb and 25 mb, but thereafter there is progressive warming at both levels and little sign of the lower level changes at 25 mb. These temperature rises were clearly the effect of subsidence, which was strongest at 100 mb and decreased upwards raising temperatures and thickness well above previous levels.

Vertical motions were computed adiabatically at St. Paul Island and Fairbanks and are shown together with the temperature curves in fig. 23. At St. Paul Island the temperature rise is accompanied by prolonged subsidence. On the other hand the warming at Fairbanks is associated largely with ascent. This indicates that warm zones in the middle stratosphere are likely to have subsidence only in the originating region and elsewhere the usual partnership of warm advection and ascent prevails.

It is concluded that the stratospheric warming which was localized in the Aleutian area developed in a baroclinically stable stratosphere in response to vertical circulations associated with large scale tropospheric changes and

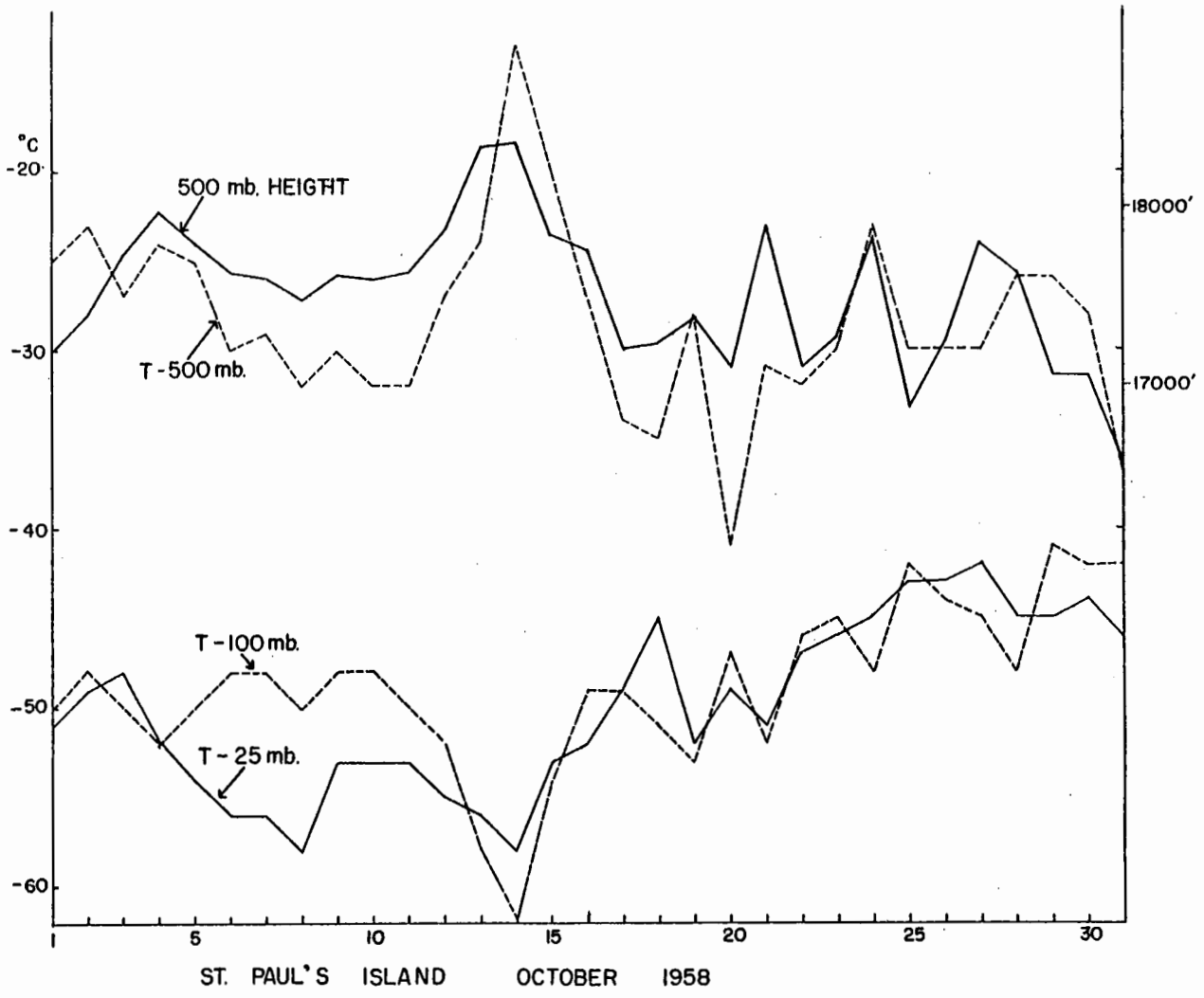

Fig. 22. Observed temperature and geopotential height data for St. Paul Island, October, 1958.

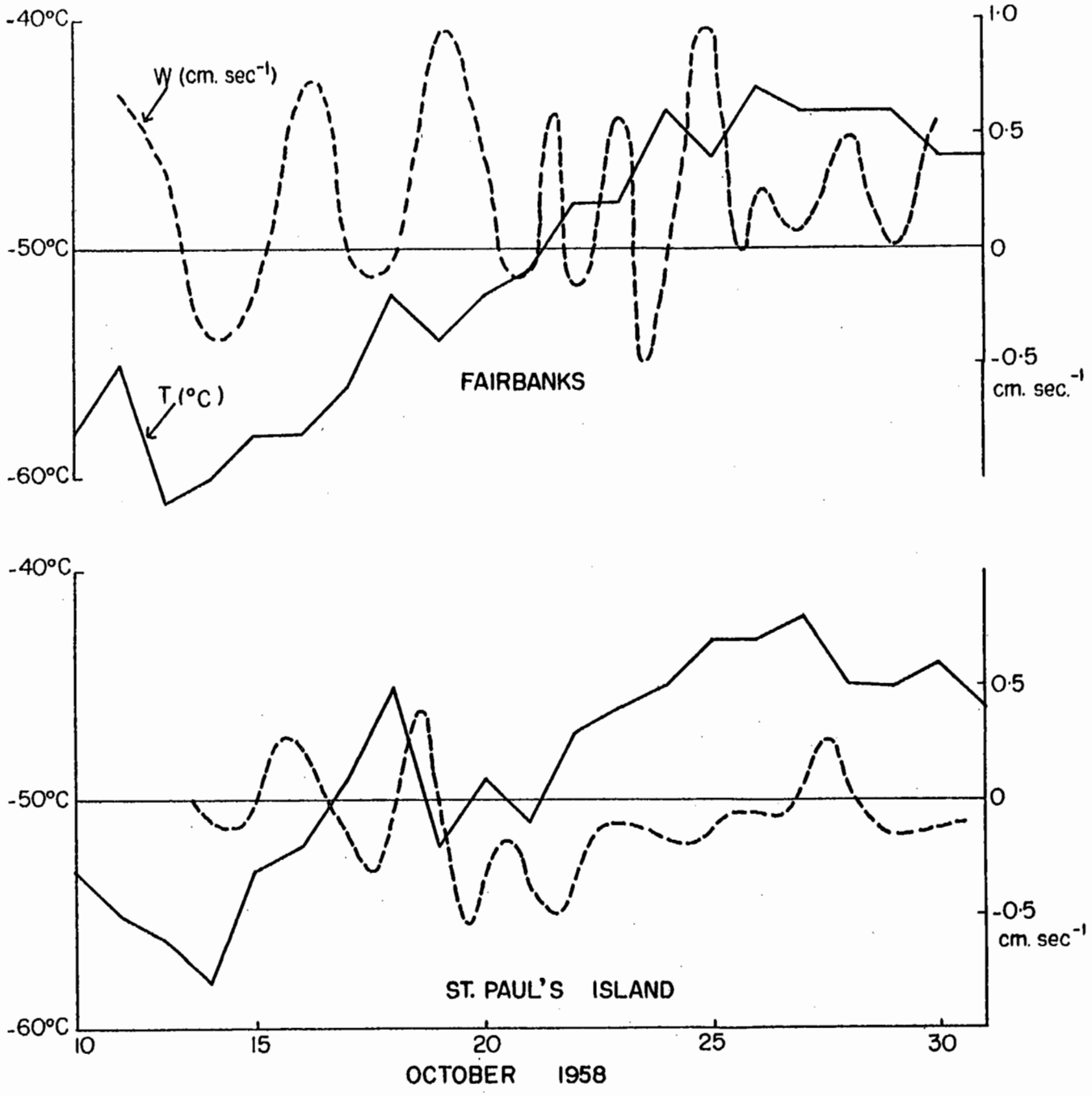

Fig. 23. Adiabatic vertical motions and temperatures at 25 mb at Fairbanks and St. Paul Island during October, 1958.

sea-level cyclogenesis.

4.2 Baroclinic Waves

A synoptic approach was required in order to make full use of the available data to identify wave activity and structure at 25 mb. Temperature, being the observed element, was the natural choice for a detailed study. Hence complete time sections of the twice daily temperature data were plotted for nearly all stations in the Alaskan, Canadian and northern North Atlantic sectors. An attempt was then made to identify characteristic temperature points from station to station, and thereby to plot the shape and speed of each wave throughout the winter. This did not prove an easy task, and it was possible to trace with confidence only waves with amplitudes of about 20°C or more. However the data showed beyond reasonable doubt coherent progressive waves at 25 mb. The three waves which were most readily identified and followed are shown on fig. 24.

These waves have also been tracked on the daily 25 mb charts. A vorticity analysis of the mid-January wave which went through most of its development in a satisfactory data region over North America has been performed to show the wave structure. The analysis was performed at various grid distances using the operational technique outlined by Boville and Kwizak (1959). Fig. 25, shows the quasi-vorticity $(Z - \bar{Z})$ field for January 12, 13, 14, 15 using a grid distance of 10 latitude degrees. The cyclonic centre of 500 ft. moved east-south-east off the Alaskan ridge and

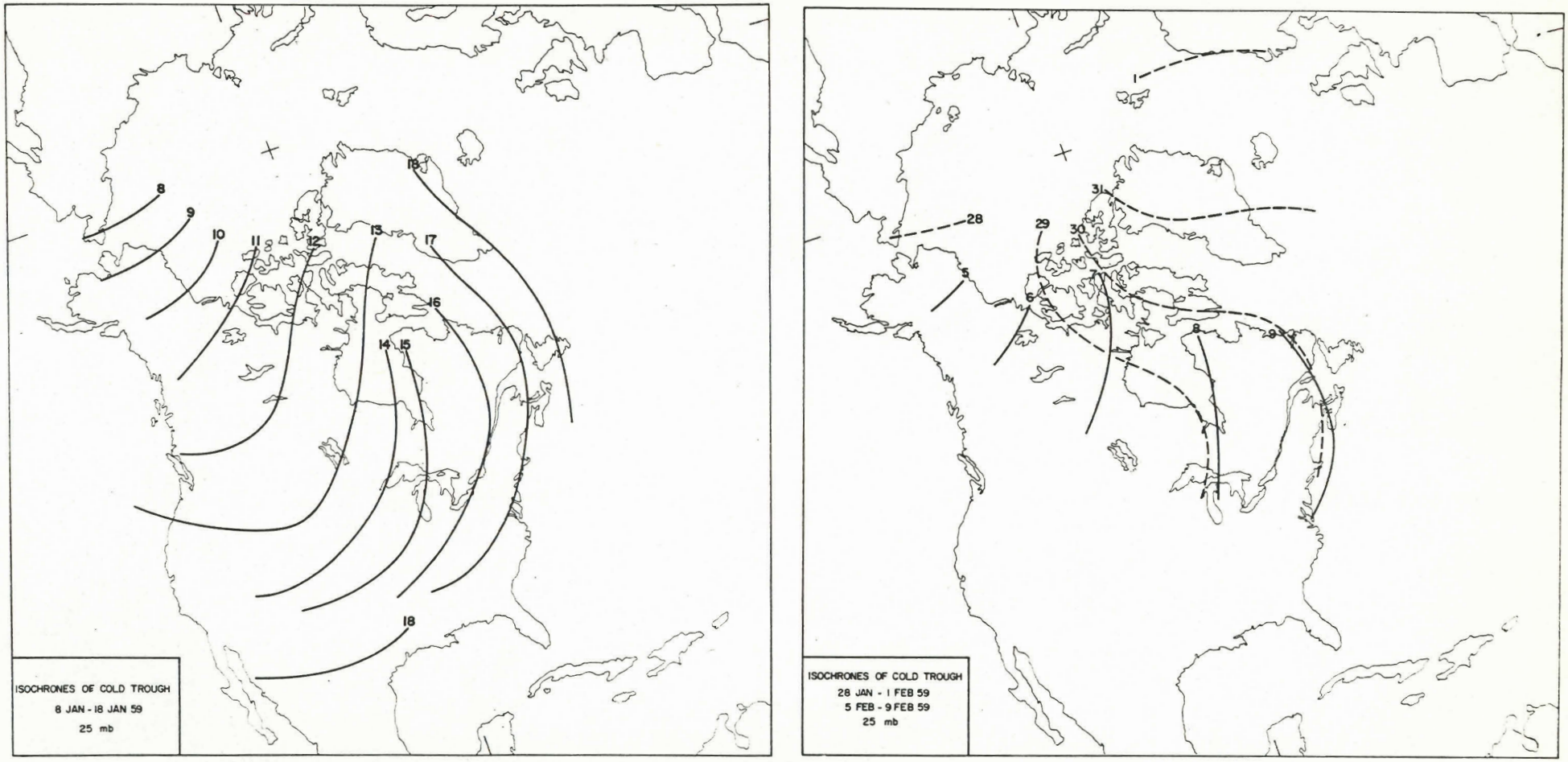

Fig. 24. Isochrones of identifiable waves on 25-mb charts, winter, 1959.

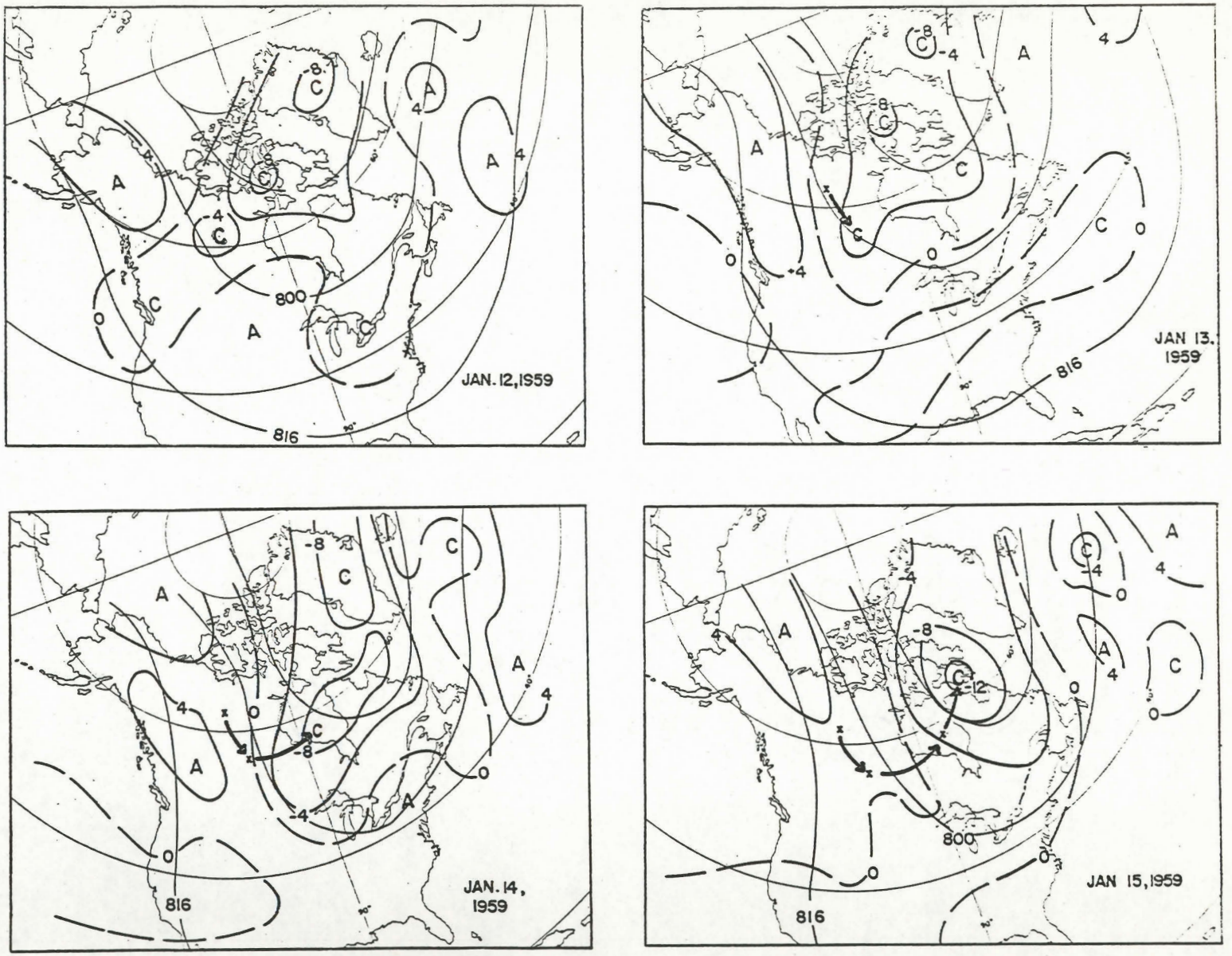

Fig. 25. The 25-mb space mean and quasi-vorticity ($Z - \bar{Z}$) fields for January 12, 13, 14, 15, 1959, (units - hnds. of ft.).

intensified to 1300 ft. as it recurved northward into the main trough area near Baffin Bay. The centre moved at a speed of about 30 kt in a current whose mean speed was about 80 kt. This type of development is quite typical of tropospheric baroclinic disturbances that develop over Canada. Fig. 26, shows the departure of each space mean 25-mb chart from the monthly mean showing that very large scale changes were taking place at the same time as the shorter wave changes. These charts thus provide clear evidence of wave activity and the non-linear interaction of different wave scales.

A vertical display of time profiles of the temperatures at Keflavik, Iceland for January, 1959 are shown in fig. 27. The 500-mb profile has been inverted to show more clearly the tropospheric correspondence. The 500-mb and 200-mb curves appear to march independently of the 25-mb and 10-mb curves through most of the month with a more-or-less neutral curve at 100-mb. In late January, however, there is apparent resonant interaction and large amplitude in-phase changes take place at all levels.

4.3 The final warming

By the use of ten-day running mean temperatures at 100 mb Godson (1958) has shown that the cold core of the polar-night vortex is characteristically eliminated each year by a marked warming wave which spreads over most of the inner Arctic in a period of two to three weeks. Detailed examination of the data and charts at higher levels indicate that, although the phenomenon is quite complex, there is a characteristic termination of the major strength of the circumpolar

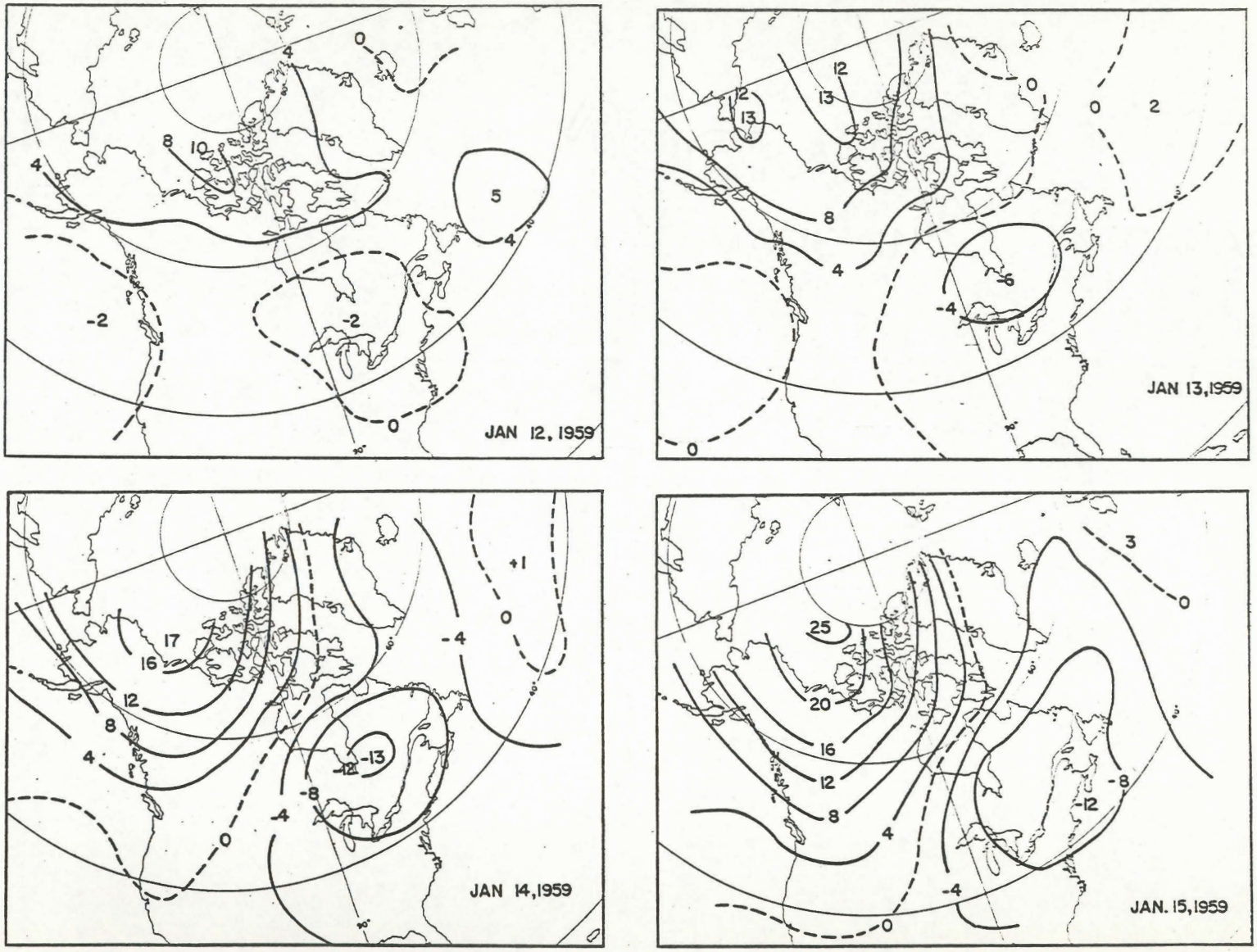

Fig. 26. The departure of the 25-mb space mean charts from the monthly mean, January, 1959. (units - hnds. of ft.).

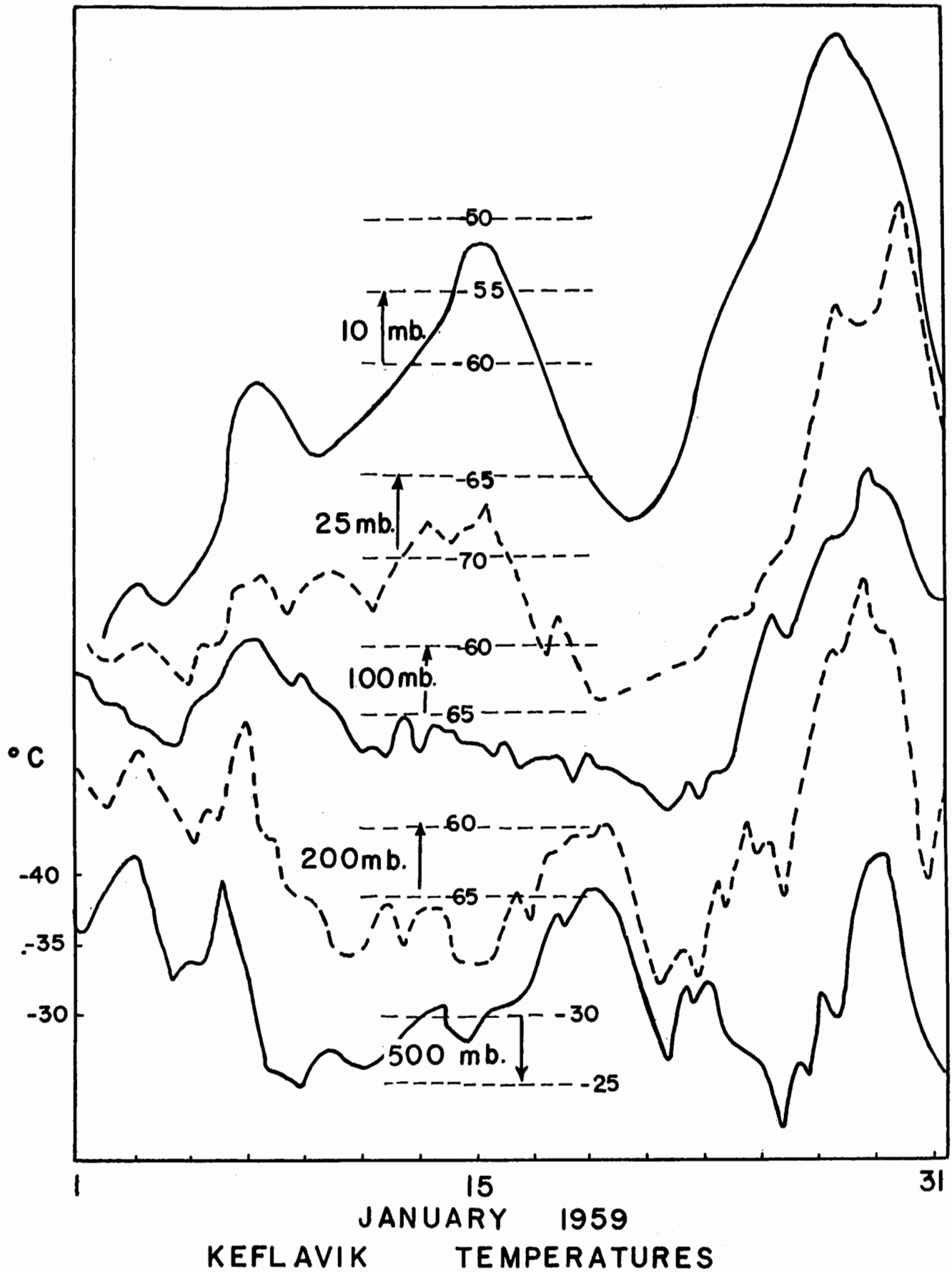

Fig. 27. Time profiles of the temperatures at Keflavik, Iceland for January, 1959. The 500-mb profile has been inverted for comparison with the stratospheric profiles.

vortex in a short period. Julian (1959) found a relationship between the time of decay of the westerlies and subsequent sea-level pressure rises over the Arctic basin, indicating a stratospheric-tropospheric coupling (but without suggesting any mechanism).

The available evidence shows that these warmings start from either the Aleutian area or the western North Atlantic, i.e., from either of the main areas of persistent intense sea-level cyclogenesis and deep lows. This factor strongly suggests that the linking mechanism may be similar to that proposed for the origin of the Aleutian anticyclone in the fall. Similar detailed case studies for other winters have not been carried out, but the form of the warmings in three winters is presented to illustrate the possibilities. The isochrones of the final warmings were based primarily on the graphs of 10-day running mean temperatures at selected stations kindly provided by Dr. Godson and supported by additional computations and daily maps. The day identified was the minimum or floor on the temperature profile preceding the rise.

The monthly mean sea-level pressure anomalies from "Die Grosswetterlagen Mitteleuropas" Amtsblatt des Deutschen Wetterdienstes have been used to define the areas of persistent cyclonic activity.

The 1956-57 winter: (fig. 28a) had the main warm belt over Eastern Siberia, but the major warming wave over the western hemisphere started in late January from the secondary warm zone over the western North Atlantic. This secondary warm zone was evident at all stratospheric levels. The warming moved north-eastward into the Norwegian Sea and

spread westward across Greenland and the Canadian Arctic where it merged with another warming, spreading out of the Siberian - Alaskan area. The January sea-level pressure anomaly shows an average 15-mb below normal centre (a mean 980-mb low) off the south-east coast of Greenland whereas the Gulf of Alaska had an 18-mb above normal centre with above normal values almost to Kamchatka. The major cyclonic activity thus appears to have been in the North Atlantic where the major warming originated. The February, 1957 anomalies after the warming show a complete reversal to above normal pressures, the phenomenon noted by Julian.

The 1957-58 winter: (fig. 28b) had a vortex collapse in the second half of January but the progress differed from the previous winter. The warm belt was present in the Aleutian - Alaskan area but a warm area in the Atlantic was completely absent. The warming spread out from the Aleutian warm belt covering the Arctic in about ten days. A strong warming did take place at high levels (25 to 10 mb) over eastern North America and the Atlantic in late January, but it did not penetrate down to the 100-mb level. Assuming dynamic control this latter high-level warming may well have been a down-stream effect from the strong ridge development over Alaska. The January, 1958 pressure anomalies correspond to these changes. The North Atlantic had a broad positive pressure anomaly and the Gulf of Alaska had an 18-mb below normal anomaly. Following the final warming February, 1958 shows above normal values over most of the Arctic basin.

The 1958-59 collapse: (fig. 28c) did not come until late February

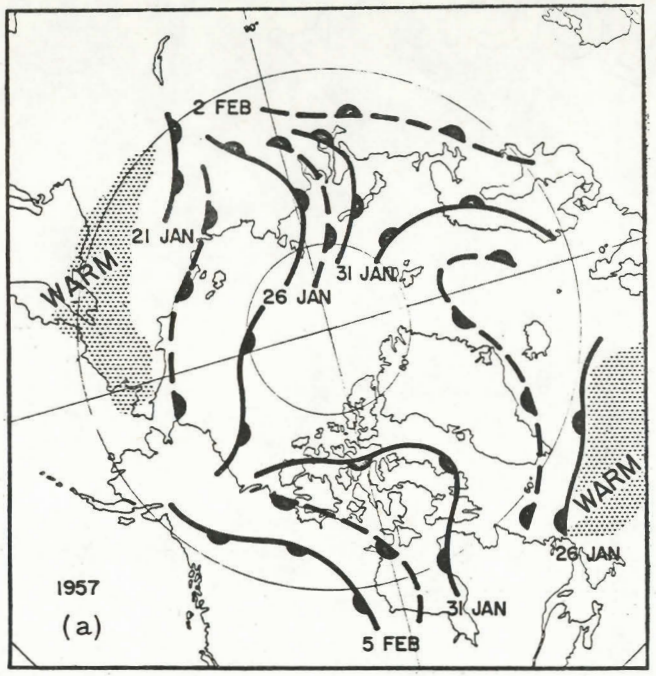

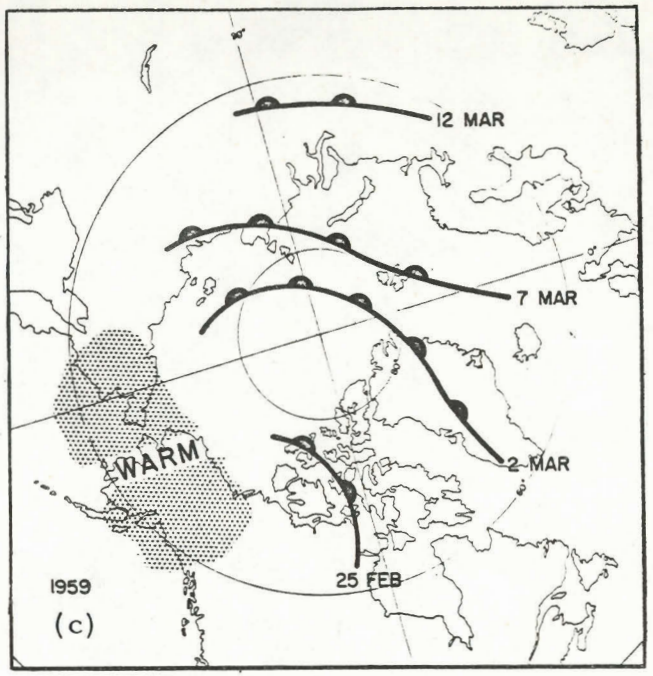

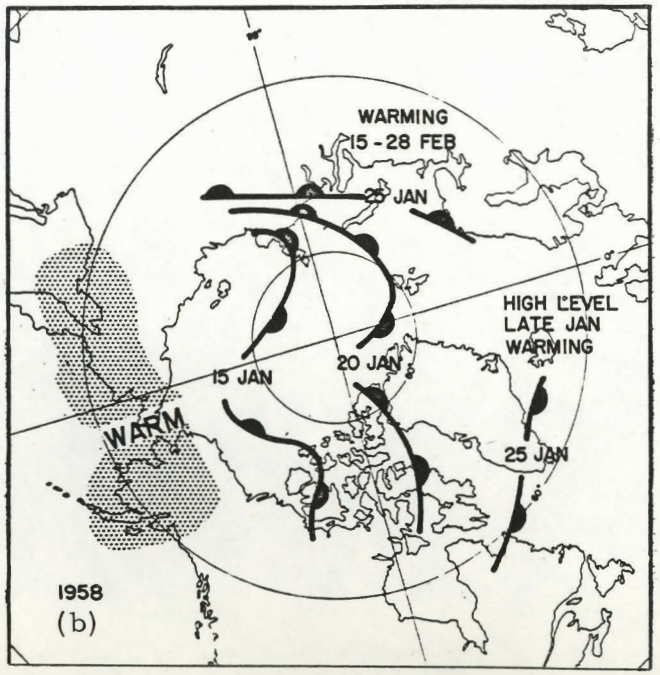

Fig. 28. Isochrones of the final-warmings, based on 100-mb temperature data, for the 1956-57, 1957-58 and 1958-59 winters.

and early March, thus differing from the previous two winters. The warming moved eastward from Alaska across the Canadian Arctic in late February and spread over the entire Arctic basin. A strong warming did occur at all stratospheric levels over the North Atlantic in late January (as shown by the Keflavik temperatures in fig. 27) but the warming did not persist. The January, 1959 pressure anomalies show no strong cyclonic areas but have a very large positive anomaly over Iceland - Greenland stretching across the Arctic basin into the Aleutians. February, 1959 showed a strong negative anomaly over Greenland and the Pole, differing again from the previous two warming months.

These years indicate that early stratospheric warmings may have their initiating factor in intense cyclonic activity dynamically similar to the origin of the Aleutian anticyclone. This would appear to warrant detailed synoptic study of the events. A study of the 1958-59 final warming wave at the 25-mb level did not reveal any obvious differences between that wave and previous wave activity during the winter, except in the final effect on the basic zonal current.

5. DYNAMICAL PROBLEMS

The main terms in the momentum and energy budgets of the lower atmosphere have been calculated, at least for limited periods, by the U.C.L.A. and M.I.T. General Circulation projects and theoretical treatments have been given by Phillips (1956), Lorenz (1955) and others. The role of disturbances in the development has also achieved much attention, notably from Charney (1947), Eady (1949), Kuo (1952), Pocinki (1955) and Fleagle (1957). The fundamental problems involved in this area, and in particular their implications for stratospheric dynamics, will be discussed in the following pages.

5.1 Absolute Angular Momentum

In an inertial coordinate system Newton's second law takes the form:

$$\dot{V}a = -\alpha \nabla P + g_0 + F \quad \text{(for unit mass)} \qquad (5.1 - 1)$$

This may be transformed into a relative coordinate system rotating with the earth to yield the equation of motion for the zonal direction as

$$\dot{u} = 2\Omega \sin\phi\, v + \frac{uv}{a} \tan\phi - \alpha \frac{\partial P}{\partial x} + Fx \qquad (5.1 - 2)$$

From (2) the absolute angular momentum equation for the zonal direction takes the form

$$\dot{M} = \frac{d}{dt}(uR + \Omega R^2) = R\left(-\alpha \frac{\partial P}{\partial x} + Fx\right) \qquad (5.1 - 3)$$

Equations (2) and (3) together show that, for large scale meteorological processes, to assume the individual conservation of absolute angular

momentum is equivalent to ignoring the pressure force term in the equations of motion.

Equation (3) may be combined with the equation of continuity to give the local rate of change of absolute angular momentum per unit volume:

$$\frac{\partial}{\partial t}\left(\rho M\right) = -\nabla\cdot\rho MV - R\frac{\partial P}{\partial x} + R\rho F_x \qquad (5.1 - 6)$$

which may be integrated to give the change in a volume as:

$$\frac{\partial}{\partial t}\int\rho M d\nu = \int\rho M V_n \, ds - \int R\frac{\partial P}{\partial x} d\nu + \int R\rho F_x d\nu \qquad (5.1 - 7)$$

where the divergence term has been changed from a volume to a surface integral by virtue of Stokes' theorem.

The total momentum may be discussed to advantage with respect to zonal rings bounded by two latitude walls and slices bounded by "horizontal" surfaces, as in Fig. 29.

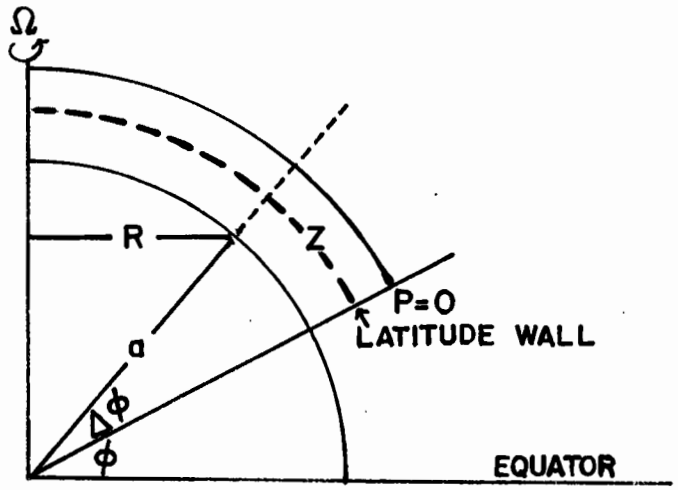

fig. 29

Schematic representation of zonal rings and polar caps

No loss of generality occurs if one considers a polar cap to eliminate the northern boundary and the top as P = o to eliminate the upper boundary, for slice elements may be recovered by simple subtraction. Then for an elevated polar cap, equation (7) becomes:

$$\frac{\partial}{\partial t}\int \rho M \, d\nu = \int_z^{\infty}\int_o^{2\pi} \rho M v R \, d\lambda \, dz + \int_{\phi}^{\pi/2}\int_o^{2\pi} \rho M w R a \, d\lambda \, d\phi - \int R \frac{\partial P}{\partial x} \, d\nu + \int R \rho F_x \, d\nu \qquad (5.1 - 8)$$

which may be written synbolically as:

$$\Delta M_T = {}_vM_T + {}_wM_T + P_\tau + F_\tau \qquad (5.1 - 9)$$

The transport terms may be further considered with respect to a Reynolds' type resolution for the wind such that

$$u = \bar{u} + u^* \qquad v = \bar{v} + v^* \qquad w = \bar{w} + w^* \qquad (5.1 - 10)$$

$$\text{where } (\bar{\ }) = \frac{1}{2\pi}\int_o^{2\pi} (\ )\, d\lambda, \qquad \lambda = \text{longitude}$$

then the horizontal momentum transport, ${}_vM_T$, becomes:

$${}_vM_T = \int_z^{\infty} 2\pi R^2 \rho \left(R\Omega \bar{v} + \bar{u}\bar{v} + \overline{u^*v^*}\right) dz \quad \text{or} \qquad (5.1 - 11)$$

$$= \frac{2\pi R^2}{g}\int_o^P \left(R\Omega \bar{v} + \bar{u}\bar{v} + \overline{u^*v^*}\right) dP$$

and the vertical momentum transport, ${}_wM_T$, becomes:

$${}_wM_T = \int_{\phi}^{\pi/2} 2\pi R^2 a\rho \left(R\Omega \bar{w} + \bar{u}\bar{w} + \overline{u^*w^*}\right) d\phi \quad \text{or} \qquad (5.1 - 12)$$

$$= \int_{\pi/2}^{\phi} \frac{2\pi R^2}{g} a \left(R\Omega \bar{\omega} + \bar{u}\bar{\omega} + \overline{u^*\omega^*}\right) d\phi$$

First consider a polar cap extending from the ground to P=o; then the vertical transport terms disappear, and:

$$\Delta M \Big]_o^{\infty} = {}_vM_T + P_\tau + F_\tau \qquad (5.1 - 13)$$

Thus

(I) The total absolute angular momentum of a polar cap can change only as a result of

(a) ${}_{v}M_{\tau}$ -- the horizontal meridional transfer across the latitude wall.

(b) P_{τ} -- the pressure torque. This term will only be non-zero if pressure is discontinuous along a horizontal surface in the zonal (x-) direction, i.e., if a mountain barrier crosses the latitude circle. Hence it is referred to as the mountain torque. It will generally act in the same direction as the friction term and, for the purposes of discussion, may be considered along with it.

(c) F_{τ} -- the friction torque. This represents an absolute angular momentum source for east winds at the ground and a sink for west winds at the ground.

(II) In any long-term steady state $\Delta M \cdot \big]_{0}^{\infty} = 0$, and it follows that, in this case:

(a) A net meridional transfer of M can only take place in the presence of ground torques (P_{τ} and F_{τ}), or as an alternative statement:

(b) The existence of zonal pressure and frictional torques at the ground requires a meridional transfer of absolute angular momentum.

(c) The existence of a zonal frictional torque at the ground implies a cross-isobar flow towards lower pressure in the friction layer

and for continuity a cross-isobar flow towards higher pressure in the free atmosphere; i.e., it requires a mean meridional circulation.

Now consider an elevated polar cap extending from some level, Z, in the free atmosphere to the top of the atmosphere. Then the pressure and frictional torques become negligible, and:

$$\Delta M\Big]_z^{\infty} = vM_T + wM_T \qquad (4.1 - 14)$$

Hence the total absolute angular momentum of an elevated polar cap can change only as a result of a momentum transfer through the boundaries.

The role and efficiency of the various transport terms will now be discussed.

(I) The horizontal omega-transport, $(R\Omega\bar{v})$

For the integral of this term around a latitude circle to be non-zero there must be a mass transfer across that latitude circle; thus in any long-term steady state the term is unimportant. It may be important in the establishment of zonal currents, but cannot contribute to their long-term maintenance against dissipative forces.

(II) The vertical omega-transport, $(R\Omega\bar{w})$

This term requires a mean meridional circulation, but not necessarily a mass transfer. It is clear from equation (13) that it cannot contribute to transfers from one latitude to another for zonal rings extending to the ground.

However, the term is a very efficient vertical transporting agency. Consider fig. 30, showing a mean meridional circulation with no mass transfer.

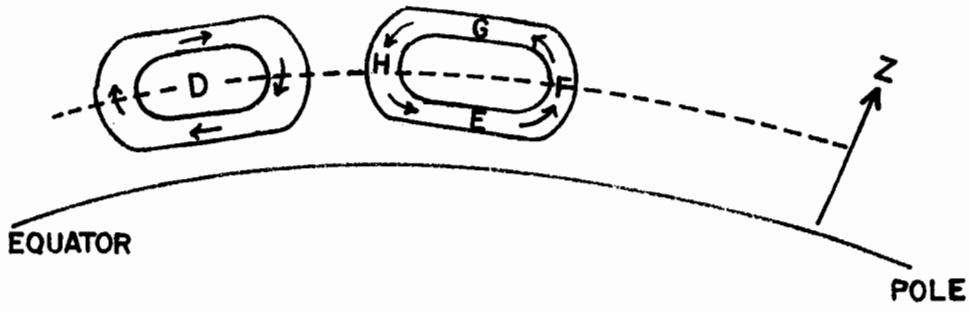

fig. 30
Schematic mean meridional circulation

The horizontal inflow and outflow of omega-momentum at E and G are equal, and there is no accumulation of momentum across any complete latitude wall. But since ϕ_F is different from ϕ_H, it follows that the omega-momentum transported downwards at H is greater than the upward transport at F, resulting in a net downward transfer of momentum across HF. Similarly, for the elevated section HFG, the inflow of Ω-momentum at F is clearly less than the outflow of $-\Omega$-momentum at G; hence the term contributes to a depletion of absolute angular momentum in HFG.

The transported velocity is Ω R, the linear velocity of the earth; hence any appreciable latitude difference between the upward and downward branches will result in large momentum transfers in the vertical, even for weak circulations.

If the sense of the circulation is defined with respect to a poleward temperature gradient (decrease), then:

(a) A thermally direct mean meridional circulation transfers omega-momentum upwards;

(b) A thermally indirect mean meridional circulation transfers omega-momentum downwards.

It should be noted that any meridional circulation postulated for other purposes must take into consideration the consequent vertical redistribution of momentum.

(III) The horizontal drift term, $(\overline{u}\ \overline{v})$

The term depends on a mean meridional circulation, $\overline{v} \neq o$, and a systematic variation of $\overline{u}$ and $\overline{v}$ with height. In the presence of a poleward temperature gradient, a direct meridional cell transfers momentum northward, and an indirect cell southward. With slow meridional circulations the term will be an inefficient transfer agent.

(IV) The vertical drift term, $(\overline{u}\ \overline{w})$

The term depends on the systematic variation of $\overline{u}$ and $\overline{w}$ with latitude. Since a vertical omega-transfer is always associated

with a variation of $\overline{w}$, the drift term is negligibly small in comparison.

(V) The horizontal eddy-flux term, $\overline{(u^* \; v^*)}$

The term is generally considered to be the main horizontal transfer term. It depends on the correlation of the instantaneous values of u* and v*, and does not require a mass transfer or a mean meridional circulation.

(VI) The vertical eddy-flux term, $\overline{(u^* \; w^*)}$

The term is very difficult to assess, requiring a correlation between the instantaneous values of u* and w*. It must be the important small scale term in the surface boundary layer. In the synoptic scale it may be important locally, but probably transfers momentum the wrong way from a general circulation viewpoint (e.g., upwards in the westerlies).

The Geostrophic Approximation: If the geostrophic approximation is used for u and v in equation (11), one obtains:

$$(v_g)M_T = \int_o^{P_o} \frac{2\pi R^2}{g} \quad \overline{u_g v_g} \quad dP \qquad (5.1 - 15)$$

Since the isobars or geopotential height lines are drawn continuously, then $\overline{v_g} = o$. Mean meridional circulations cannot be identified under the approximation, and equation (13) becomes:

$$\Delta M \Big]_o^{\infty} = \int_o^{P_o} \frac{2\pi R^2}{g} \quad \overline{u_g v_g} \; dP + (P_\tau + F_\tau) \qquad (5.1 - 16)$$

Now equation (16) is physically incomplete since it implies no meridional circulation, yet from II (c) it is clear that in the presence of ground

friction meridional circulations are required. However, it has also been shown that meridional circulations transfer little momentum horizontally; hence equation (16) should be a good approximation to reality.

It can readily be shown that since u_g and v_g are functions of the geopotential height (or pressure) field, a northward transfer occurs with troughs having a NE-SW tilt with latitude, and a southward transfer, with troughs having a NW-SE tilt, as in fig. 31.

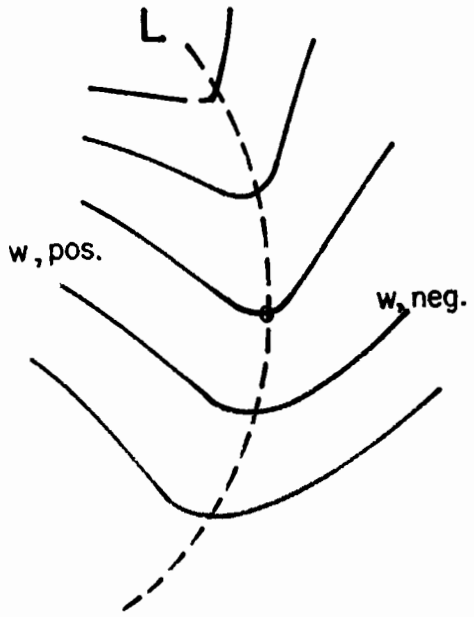

fig. 31
Schematic - tilted trough momentum transport

In atmospheric systems developing troughs can be expected to have the orientation shown in fig. 31, the zero tilt being at the point of maximum amplitude, with northward momentum transport in the southern

part and southward momentum transport in the northern part. Similarly, with the usual tropospheric structure of ascent to the east of a developing trough and descent to the west, the zonal overturning, via the vertical eddy-flux term, $\overline{u^* w^*}$, will contribute to an upward flux of zonal momentum in the southern part of the trough and a downward flux in the northern part. It thus appears that in the free atmosphere the momentum equation may usefully be approximated by:

$$\Delta M \Big]_z^{\infty} \simeq \int_0^P \frac{2\pi R^2}{g} \left(R\Omega v + \overline{u_g^* v_g^*} \right) dP + \int_{\phi}^{\pi/2} 2\pi R^2 a\rho \left(R\Omega \bar{w} + \overline{u^* w^*} \right) d\phi \qquad (5.1 - 17)$$

In summary, it appears that, due to the stabilizing factor of the earth's rotation, constraints are placed on atmospheric circulation such that:

(i) Large net mass transfers in the meridional direction are unlikely because of the attendant excessive transfer of absolute angular momentum. Mass transfers, on a large scale, probably only occur to the extent necessary to satisfy the zonal thermal wind equation (i.e., to achieve geostrophic balance).

(ii) Mean meridional circulations are similarly restricted and occur largely as a result of frictional torques. They only achieve sufficient strength to maintain mass continuity and to accomplish the required vertical momentum transfers.

(iii) Eddy circulations in the horizontal are expected to carry out the required horizontal transfer of angular momentum (and most other general circulation elements).

(iv) Vertical (eddy) circulations required to achieve heat balance are restricted mainly to overturning in zonal planes.

Clearly, then, the fact that the atmosphere must achieve a balance of angular momentum through transport processes provides a valuable diagnostic tool in the study of the general circulation and of individual motion systems.

5.2 Energy

The role of energy transformations in modern general circulation studies has been developed by Starr (1951) and others following the classical papers of Hadley (1735), Margules (1906) and Jeffreys (1926). Starr described the total kinetic energy of an arbitrary volume as

$$\frac{\partial K}{\partial t} = A + W + S + D \qquad (5.2 - 1)$$

where $A = \int E v_n \, ds$; the advection of kinetic energy by fluid elements crossing the boundary surface,

$W = \iint p\,(v\,dx - u\,dy)\,dz$; the performance of work by pressure forces at the boundary.

$S = \iiint p \left(\frac{\partial u}{\partial x} + \frac{\partial v}{\partial y} \right) dx\,dy\,dz$; the production of kinetic energy within the volume.

$D = \iiint F\,dx\,dy\,dz$; the dissipation of kinetic energy by frictional forces.

In a mechanically closed system the first two terms vanish as surface integrals. Then for a global balance the frictional dissipation must be balanced by an internal production of kinetic energy. This requires a covariance between horizontal divergence and pressure. As Starr points out divergence is the rule in the sub-tropical and migratory high pressure areas and convergence the rule in low pressure areas. This confirms the fundamental role of these systems in the general circulation.

Lorenz (1955) has taken a somewhat different approach. He follows the customary meteorological practice of combining potential and internal energy as total potential energy, but finds that the latter varies little and is not a useful variable. He then defines available potential energy, AIP, as the difference between the total potential energy, IP, and the minimum that could arise from an adiabatic redistribution of mass. In an adiabatic frictionless atmosphere

$$\frac{\partial}{\partial t}(\overline{AIP} + \bar{K}) = 0 \qquad (5.2 - 2)$$

However, large increases in $\bar{K}$ are usually accompanied by large increases in $\overline{AIP}$ and it follows that large changes in the mean kinetic energy of the atmosphere must involve non-adiabatic affects. The available potential energy may be partitioned into a zonal distribution, AIP_z and into an eddy distribution, AIP_e, by analysis of variance of the temperature field. The major terms in the energy conversion processes (C) are then found to be:

$AIP_z \rightleftharpoons K_z = C_z \; ; \alpha(\overline{T'w'})$; mean meridional circulation

$AIP_e \rightleftharpoons K_e = C_e \; ; \alpha(\overline{T^*w^*})$; eddy overturning (in the zonal plane)

$AIP_z \rightleftharpoons AIP_e = C_A \; ; \alpha(\overline{T^*v^*})$; eddy transport of sensible heat

$K_z \rightleftharpoons K_e = C_k \; ; \alpha(\overline{u^*v^*})$; eddy transport of momentum

The asterisk * represents the deviation of an individual value from the mean taken around a latitude circle. The prime ' represents the deviation of an individual mean for a latitude circle from a further mean

with respect to latitude.

Phillips (1956) conducted a numerical general circulation experiment using a two-level geostrophic model. The experiment realized the expected distribution of zonal winds, the existence of a jet and the required net poleward transport of energy. The energy exchange processes were similar to those of Lorenz and a conversion from zonal kinetic to zonal potential energy was found; a result tentatively confirmed by Nielsen (1959).

The theoretical ratios of Lorenz together with computed values by Starr and White and Pisharoty (1955) have been combined with the experimental system of Phillips and the more recent (J.N.W.P.)* model computations of Nielsen into a tentative hemispheric general circulation scheme on fig. 32. Here the zonal kinetic energy is maintained by a conversion (C_k) from eddy kinetic energy associated with an eddy momentum transport. It may be noted that for the values given the kinetic energy would become negligible in about a month in the absence of generating and conversion processes.

The hemispheric radiative imbalance represents the primary generating mechanism, G_z. Perhaps the most surprising result is the numerical difference between the conversion fron zonal P.E. to eddy P.E. (C_A) and the conversion from eddy P.E. to eddy K.E. (C_e).

---

* Joint Numerical Weather Prediction Unit, Suitland, Md.

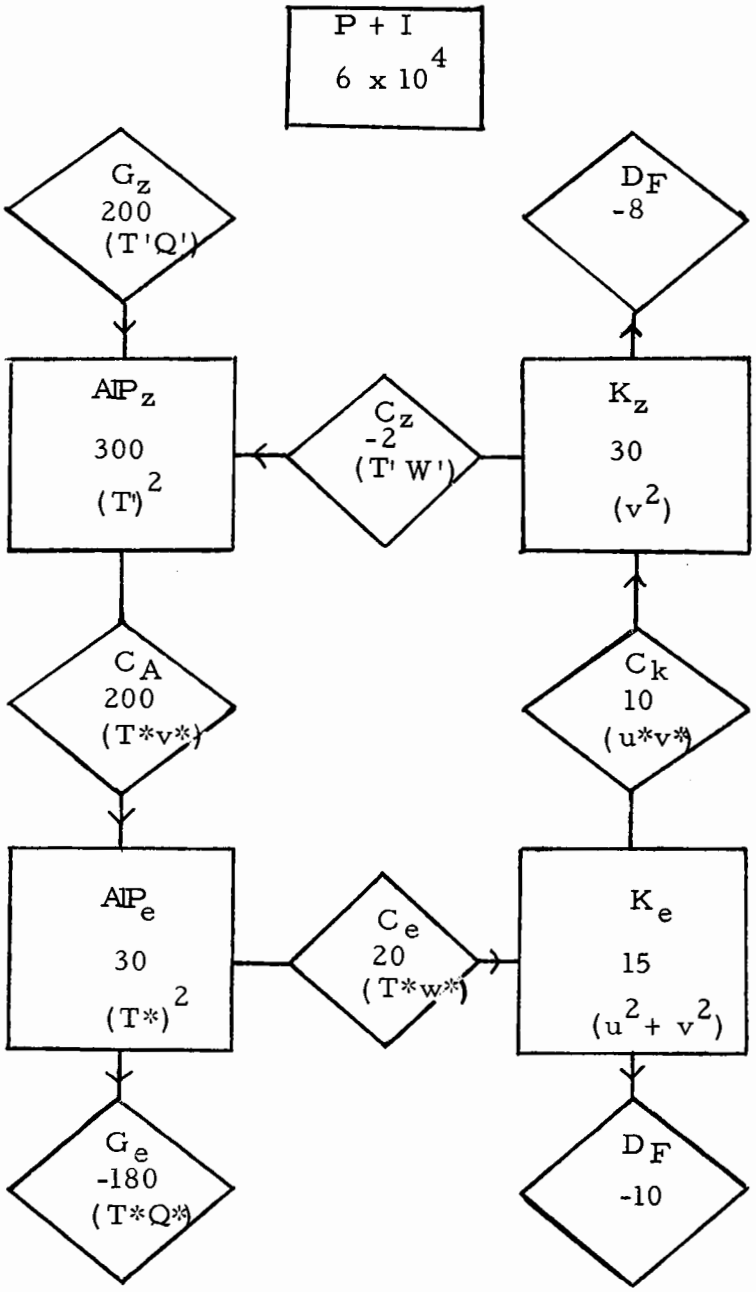

Fig. 32. Tropospheric energy components of the general circulation.
Rectangles - energies----------10^{16} kilo-joule
Diamonds - energy conversion--10^{10} kilo-joule sec^{-1}

In order to balance this difference the eddy generating process, (G_e) must be large and negative (a negative covariance between T* and Q*). This would be mainly achieved by the heating of cold air over warm surfaces and the cooling of warm air. The zonally distributed heat sources and sinks thus play a fundamental role in the nature and strength of the general circulation of the troposphere. Stratospheric circulations should be largely insulated from a direct influence of these surface effects and quite different ratios for the conversion processes may be expected.

It is possible to deduce directly from the second law of thermodynamics certain constraints that theories of general circulation energetics must observe. Thus a thermodynamically driven circulation is only possible in those regions of the atmosphere where heat is added at higher temperatures and lost at lower temperatures. This is clearly equivalent to the Lorenz formulation for the generating mechanism, G_z, requiring a positive covariance between T' and Q'. In the following treatment it is assumed that temperature curves are maintained at approximately their mean values by thermodynamic processes against radiative losses or gains.

The temperature profiles in fig. 33 are based on available reconstructions plus high-level radiosonde data and some rocket data, Stroud et al (1960). In fig. 33 consider the TROPICAL and the POLAR

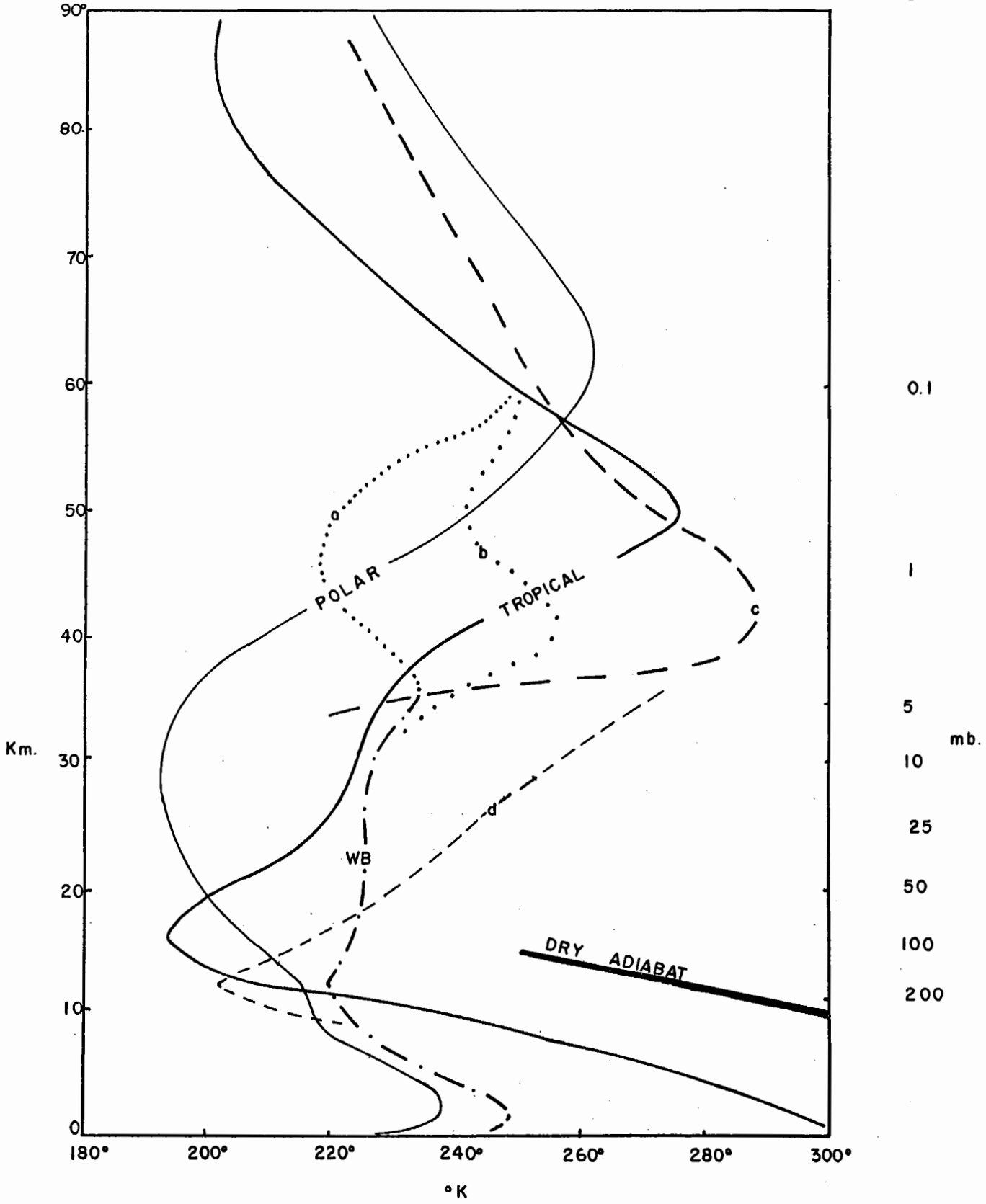

Fig. 33. Reconstructed temperature profiles for typical winter conditions.

temperature curves. In the troposphere heat is added at high temperatures and lost at low temperatures (by radiation), hence exchange processes converting potential to kinetic energy are permissible. Just above the tropopause conditions are reversed and the heat exchange can only be achieved by doing work on the system i.e. the circulation must be wind driven. The tropospheric system is generally considered to extend to about 20 km, with the main poleward temperature contrast occurring in the lowest 5 km which, of course, contain half the mass of the system.

For the same curves above 20 km a new system arises. From 20 km to the stratopause there is a poleward temperature gradient, and from the stratopause upward an equatorward gradient. From a thermodynamic viewpoint it is clear that, with strong radiative cooling near the pole, the region below the stratopause is the driving circulation and that such a circulation in the mesosphere is not possible. It follows that in order to maintain a heat balance (against radiative losses) there must be a circulation in the middle and upper stratosphere which converts potential energy to kinetic energy $\{P, K.\}$ with enough available work to drive the circulation in the mesosphere. From a static stability viewpoint the most favourable region on the curve for the development of unstable baroclinic disturbances is the region from about 20-30 km, the middle stratosphere.

It is well known that the lower stratosphere in the mid-winter jet stream period is not characterized by the TROPICAL - POLAR temperature contrast but rather by the TROPICAL - WB (warm belt) contrast (Hare, 1960). The vertical temperature profile in the warm belt may initially be similar to curve (WB-a) in fig. 33. This does not yield a simple poleward temperature gradient in the middle stratosphere nor a zonal flow similar to the central part of fig. 8. Between curve POLAR and WB-a there is a driving circulation from about 15 km to 40 km (with maximum zonal wind at 40 km) and a driven circulation above 40 km. This flow is in high latitudes north of the warm belt and forms the polar-night westerlies. To the south another possible driving region lies between curve - a - and TROPICAL from about 40 to 60 km, the maximum zonal wind being at the stratopause. The static stability and latitude of that flow would probably preclude unstable waves of the Fleagle type.

Churchill rocket data and high-level radiosondes suggest that as a consequence of large amplitude dynamical activity in the stratosphere (often called sudden warmings) curve (WB-a) may change to curve (WB-b) or even to curve (WB-c). From the similarities of curves (WB-b) or (WB-c) and TROPICAL it is apparent that little zonal flow could exist in the mesosphere. Radiative factors would then suggest the possibility of a reversal of the temperature pattern

below the mesopause (~80 km) with a westerly maximum at that level.

In summary thermodynamic considerations suggest that

(1) the driving region of the stratospheric winter circulation lies in the middle stratosphere (20-35 km) where a mean poleward temperature gradient exists and static stability is least opposed to vertical motion. This factor makes a study at 25 mb - the mass center of the middle and upper stratosphere - a logical choice.

(2) the strengthening of the middle latitude warm belt, as the tropospheric winter circulation intensifies, shifts middle latitude temperatures to tropical values in the middle stratosphere and effectively separates the stratosphere into two regimes:

(a) The strong poleward temperature gradient region from 15 to 40 km between middle latitudes and the pole (the driving polar-night westerlies) and

(b) a weaker cold region in the vicinity of 45 km at lower latitudes for which the radiative imbalance is uncertain but probably small.

(3) An excessive warming of the middle stratosphere at moderately high latitudes would prohibit any effective flow in middle latitudes at the stratopause level. Should this happen early enough in the winter season, radiative factors suggest the inversion of the mesopheric temperature gradient and the establishment of a separate westerly flow

in the upper mesosphere.

(4) The mode of the circulation in one atmospheric system is strongly influenced by the character of the thermally driven regions (the warm belts) in the system underneath. This defines one area of probable inter-dependence in the vertical.

5.3 Waves

The fundamental role of waves in atmospheric studies has already been indicated by the importance of the horizontal eddy circulation as a transporting agent, outside the tropics. In addition, the principal mechanism for the growth of large scale waves in the atmosphere has emerged as the conversion of available potential energy into kinetic energy. The emphasis in theoretical studies on unstable wave growth has thus shifted from barotropic dynamic instability to baroclinic instability (e.g. Pocinki, 1955). From the viewpoint of stratospheric dynamics the instability formulation by Fleagle (1957) seems most readily applicable. Since the formulation is tested here not only for the characteristic growth rates but also for vertical motion and energy conversion the pertinent parts are given below.

On the basis of the observed structure of the atmosphere Fleagle postulated a stream surface of maximum slope in mid-troposphere (fig. 34). The perturbation equations, in coordinates on such a surface, are greatly simplified since the vertical velocity, w, and its vertical derivative, $\partial w/\partial z$, are eliminated. The frequency equation, assuming perturbations periodic in latitude, longitude and time was obtained on that stream surface. The slope of the stream surface was then

eliminated to yield a solution as in equations (1) and (2) below.

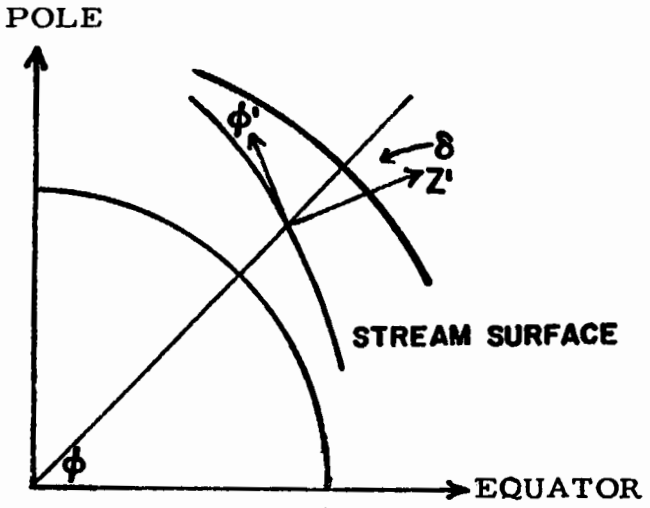

fig. 34

Schematic diagram - stream surface of maximum slope.

$$\sigma_R - mK = - \frac{mL\gamma (LU_z + \beta S_z / L\gamma)}{a \cos\phi \, (2S_z \bar{a}^2 + g\gamma^2 L^2)} \qquad (5.3 - 1)$$

$$\sigma_i = \frac{mL\gamma (LU_z + \beta S_z / L\gamma)^{1/2}}{a \cos\phi (2S_z \bar{a}^2 + g\gamma^2 L^2} \left\{ LU_z - \beta \left(\frac{S_z}{L\gamma} + \frac{g\gamma L}{\bar{a}^2} \right) \right\}^{1/2} \qquad (5.3 - 2)$$

where

σ_R, σ_i = the real and imaginary part of the frequency

K_r = the relative angular velocity of the air

L = $2(\Omega + K) \sin\phi$

γ = coefficient of piezotropy

U_z = the baroclinic parameter, $\partial U / \partial z$, the vertical shear of the basic current

β = the Rossby parameter = $- \frac{1}{a} \frac{\partial L}{\partial \phi}$

S_z = the stability parameter = $\frac{1}{\theta} \frac{\partial \theta}{\partial z}$; θ = potential temperature

a = the radius of the earth

$\bar{a}^2 = \frac{1}{a^2}\left(\frac{m^2 - \sin^2\phi}{\cos^2\phi} + \nu^2\right)$

m, ν = the zonal and meridional wave numbers

g = gravity

The criterion for unstable wave growth is given by the radical in equation (2) as

$$LU_z > \beta\left(\frac{S_z}{L\gamma} + \frac{g\gamma L}{\bar{a}^2}\right) \qquad (5.3 - 3)$$

Thus there is a minimum vertical wind shear (or horizontal thermal gradient) required for instability. Wave growth thus depends on the thermal gradient, the static stability, the latitude and the wave number. The solutions for the troposphere appear to yield results consistent with the known structure. The polar-night regime has a similar thermal regime (i.e. isentropic surfaces at 25 mb sloping upwards towards the pole) and apparent baroclinic wave development but rather different static stability. The growth rates for appropriate stratospheric stability are shown in fig. 35. They indicate that the most unstable waves have zonal wave numbers of six or less. This is in agreement with observations.

By selecting the dimension of greatest instability Fleagle has also been able to express the vertical velocity in fairly simple form. At the stream surface of maximum slope the ratio of the vertical velocity, w, to the south-north perturbation velocity, v, is given by

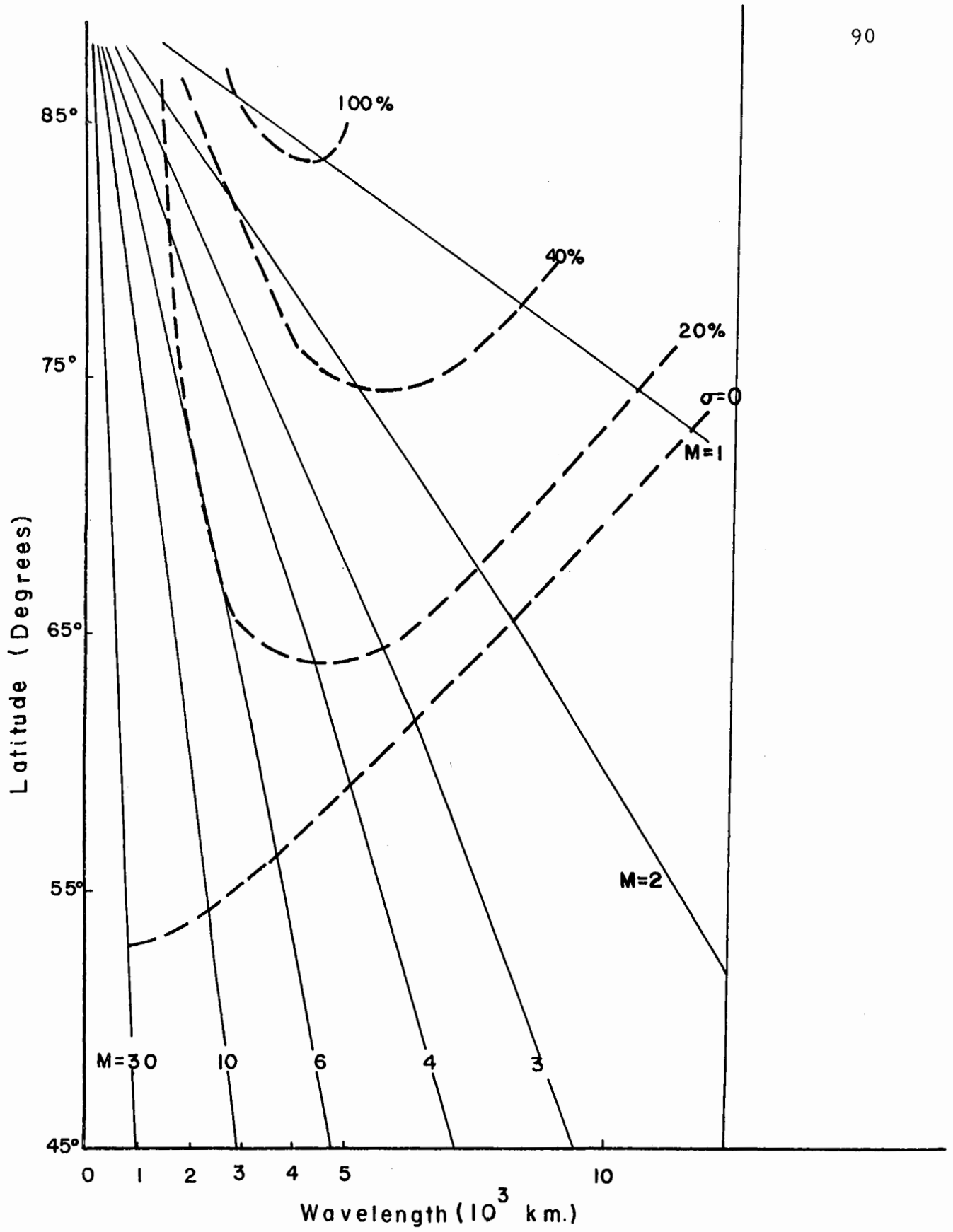

Fig. 35. Perturbation growth rates as a function of wave number and latitude for an isothermal lapse rate and a meridional temperature gradient of 1 degree C per lat. deg. (after Fleagle, 1957).

$$\frac{w}{v} = \frac{2LUz\,\bar{a}^2 - g\beta\gamma L}{2gSz\,\bar{a}^2 + g^2\gamma^2L^2} \pm \frac{iL\gamma\, a\cos\phi\,\sigma_i}{mSz} \qquad (5.3-4)$$

Equation (2) has been differentiated with respect to $\bar{a}^2$ to determine the dimension of greatest instability with only meridional extent considered so that $\bar{a}^2 \sim m^2/a^2\cos^2\phi$ and

$$\bar{a}^2(m) = \frac{g\gamma^2L^2(LUz + 3\beta Sz/L\gamma)}{2Sz(LUz - \beta Sz/L\gamma)} \qquad (5.3-5)$$

from which

$$\sigma_i = \frac{LUz - \beta Sz/L\gamma}{2\sqrt{2gSz}} \qquad (5.3-6)$$

Then substitution in (4) gives

$$\frac{w}{v} = \frac{1}{2gSz}\left[LUz + \frac{\beta Sz}{L\gamma} \pm i\frac{(LUz - \beta Sz/L\gamma)^{3/2}}{(LUz + 3\beta Sz/L\gamma)^{1/2}}\right. \qquad (5.3-7)$$

If v is approximated geostrophically

$$v \simeq \frac{g}{LR}\frac{\partial Z}{\partial\lambda} \simeq \frac{g}{L}\frac{\partial Z}{\partial x} \qquad R = a\cos\phi \qquad (5.3-8)$$

and for periodic disturbances Z may be represented by

$$Z = A(z)e^{i(m\lambda - \nu\phi - \sigma t)} \qquad (5.3-9)$$

$$\frac{\partial Z}{\partial\lambda} = A(z)\,im\,e^{i(m\lambda - \nu\phi - \sigma t)} \qquad (5.3-10)$$

$$\frac{\partial^2 Z}{\partial\lambda^2} = -A(z)\,m^2e^{i(m\lambda - \nu\phi - \sigma t)} \qquad (5.3-11)$$

$$i\frac{\partial Z}{\partial \lambda} = \frac{1}{m}\frac{\partial^2 Z}{\partial \lambda^2} \qquad (5.3-12)$$

$$i\frac{\partial Z}{\partial x} = \frac{i}{R}\frac{\partial Z}{\partial \lambda} = \frac{1}{mR}\frac{\partial^2 Z}{\partial \lambda^2} \simeq \frac{1}{a}\frac{\partial^2 Z}{\partial x^2} \qquad (5.3-13)$$

Then substitution of v from (8), $\frac{i\partial Z}{\partial x}$ from (13) and $\overline{\alpha}$ from (5) into equation (7) yields:

$$w = \tfrac{1}{2}\left(\frac{U_z}{S_z} + \frac{\beta}{\gamma L^2}\right)\frac{\partial Z}{\partial x} \pm \frac{1}{\gamma L}\left(\frac{S_z}{2g}\right)^{1/2}\left(\frac{\left(\frac{U_z}{S_z} - \frac{\beta}{\gamma L^2}\right)^2}{\left(\frac{U_z}{S_z} + \frac{3\beta}{\gamma L^2}\right)}\right)\frac{\partial^2 Z}{\partial x^2} \qquad (5.3-14)$$

or symbolically

$$w = W_1\frac{\partial Z}{\partial x} + W_2\frac{\partial^2 Z}{\partial x^2} \qquad (5.3-15)$$

This form may be solved by superposition of solutions and is very convenient for application to a Fourier representation of the contour height, Z. It can readily be seen that in this formulation upward vertical motion occurs with southerly winds and cyclonic vorticity.

6. QUANTITATIVE DYNAMICAL ANALYSIS

In the remainder of this thesis an attempt will be made to utilize objective and quantitative methods of dynamical analysis of the observed data. This attempt will only be partially realized, since the starting point is a set of analyzed maps, not observed data, and the complexity of the answers requires interpretation as well as specification. Since the basic data were isolines on hemispheric charts it was natural to turn to Fourier series for analytic specification. The practical techniques of the method have been outlined recently by Boville and Kwizak (1959) followed by a more extended exposition by Godson (1959). In addition to scalar field representation the method permits the determination of geostrophic momentum, kinetic energy and fluxes as a function of circumpolar wave-number, an advantage emphasized by the work of Eliasen (1958) and Saltzman (1957). In addition to extending the above applications, the author has utilized the Fleagle wave model to permit energy conversion computations.

6.1 The Fourier series approach

The geopotential height field, Z, (or any other continuous scalar field) which is given by N equally spaced values around a latitude circle may be represented, in usual Fourier notation, by:

$$Z = A_0 + \sum_n A_n \cos n\lambda + \sum_n B_n \sin \lambda$$

$$= A_0 + \sum_n C_n \cos (n\lambda - \theta_n)$$

the representation being precise with $\frac{N-1}{2}$, the maximum number of waves. In this project the latitude circle was specified by 36 points at 10 degree longitude intervals. The polar cap was then represented by 9 latitude circles from 40N to 80N plus the value at the pole. The specification was done for the 500-mb, 100-mb and 25-mb geopotential height fields and the 25-mb temperature field giving a total of 46,800 pieces of input data.

The use of a constant 36-point division on the contracting latitude circles is open to criticism on the basis of equal area sampling. However, the constant grid is much simpler for data extraction and error checking and the sampling problem is partially balanced by a subsequent reduction of high frequency noise.

The data were put on cards and processed through McGill's I.B.M.-650, 4000-word digital computer. The output for each latitude was the total variance, σ^2, the mean value, A_o, and for each wave number the amplitudes, A_n, B_n and C_n^2, the phase angle, θ_n, and the trough position. Initially the programme was run to thirteen waves but the variance attributable to the high wave numbers proved to be mainly noise at 25 mb, and the number at that level was reduced to nine. It became evident early in the project that errors in data extractions or card punching could be readily recognized and typed by spurious amplitude variations in the high Fourier wave numbers.

It is thus considered that all significant errors of that type have been eliminated and for that reason alone it is desirable to carry the wave analysis into the noise level.

The establishment of accuracy and significance limits for Fourier expansions of this type is a difficult problem. It becomes particularly important for kinetic energy computations where random errors may be additive. Godson (1959) has given a solution based on the assumption that the grid point data contain m harmonic wave components plus a random error field dispersed equally among the Fourier components. His significance ratio test was used in the following modified form

$$\frac{\sum_r \gamma^2_{(m+1)}}{\sum_r 2\,\sigma^2_m} = \frac{4}{r(N-1-2m)} \quad Sqr(P)$$

where r = the number of cases

γ = the computed Fourier amplitude,

m = the last significant wave

σ^2_m = the remainder variance; the total variance minus the variance of waves 1 to m.

N = the number of sample points (36)

$Sqr(P)$ = a statistical factor obtained from the solution of:

$$\Gamma(qr, S) = (qr - 1)!\,P$$

where Γ is the incomplete gamma function and P is the probability. The factor S has been tabulated by Godson. In addition, the standard

errors of the computed amplitudes are given by:

$$\sigma^2_{\alpha_n} = \sigma^2_{\beta_n} = \frac{2\sigma_z^2}{N-1} = \frac{2}{N-1-2m} \sigma_m 2$$

where α and β are the computed Fourier amplitudes and z is the amplitude component resulting from a random error field. In this project the number of cases, r, for any given level and latitude was 36. The waves were tested one at a time (q = 1) starting at the highest wave number until the significant wave was found using a probability, P, of 95%. The Fourier amplitudes were tested at two latitudes, 50N and 70N, for each level with the following results.

Table 2.

Significant Fourier wave numbers

level	m	Ce^2
25 mb	4	30
100 mb	7	45
500 mb	8	60

where m is, on the average, the last significant wave and Ce^2 is the Fourier noise level (i.e. $2\sigma^2_{\alpha}$) for heights in tens of ft. These results were applied not to the computations of the Fourier coefficients but to subsequent programmes using the coefficients. There the cut off was made on the basis of the noise level rather than by wave number.

A programme factor eliminated all waves from the computations where C^2 did not exceed the noise level.

The Fourier resolution, theoretically, permits rather simple computations for linear correlation coefficients between variations at a given wave number. Unfortunately the phase relationships for a given wave tend to oscillate considerably in latitude and height within the atmosphere, so that such correlations are often meaningless. The kinetic energy averaged over a large latitude interval eliminates some phasing problems and provides a correlation tool. The correspondence between the 500-mb level and the 25-mb level for wave number one is shown on fig. 36 by means of the vector amplitude. The figure shows wave number one at 70N for the five-day charts from October through March numbered consecutively from one to thirty-six. The scalar factor is the Fourier amplitude, C, of the geopotential height, and the angle represents the trough position. It is apparent that there is a marked, but complex, relation between the two levels. In early October the two troughs are in phase in octant one, but in the second half of the month the 25-mb trough shifts into octant three and effectively remains there till mid-March. The mid-October shift has been associated earlier in this study with the formation of the Aleutian anticyclone over the intense tropospheric cyclone region. Through the winter, the 500-mb and 25-mb systems tend to have a similar but reversed phase.

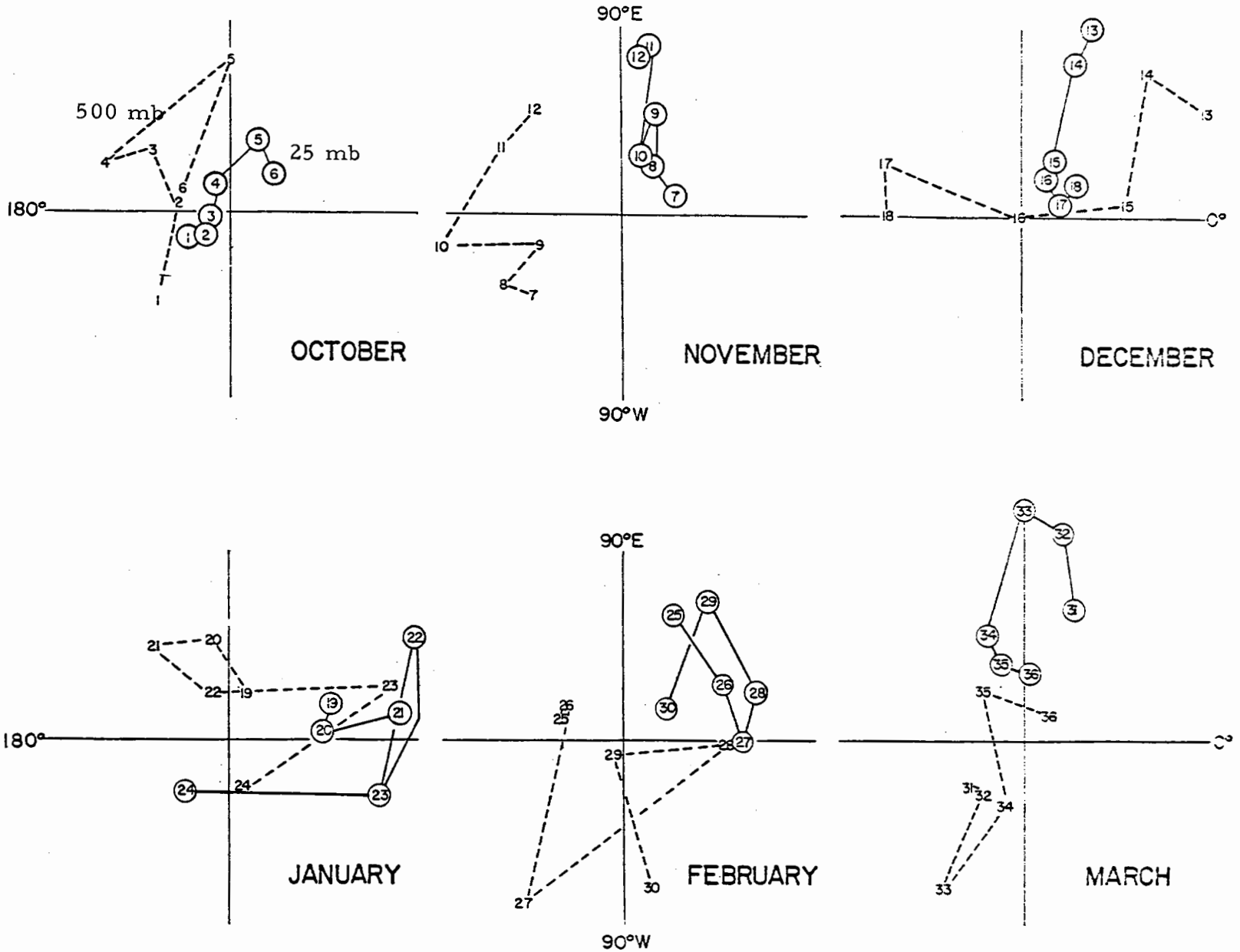

Fig. 36. The amplitudes and longitudinal trough positions of wave number one at 500 mb and 25 mb shown as consecutive vectors for the 36 charts at five-day intervals October, 1958 - March, 1959.

The 500-mb eccentric trough is much more variable than the 25-mb system, but the major changes at 500-mb appear to be reflected in the 25-mb vector amplitudes. The one chart (A-24, Jan. 28th) on which the 25-mb trough moved into octant one was associated with a similar strong vector change at 500-mb.

The relationships in the domain of wave number 2 are simpler. The troughs at the three levels tend to be closely in phase, near 60-70W, so that angular changes are not significantly different. The amplitude changes as a function of time for wave number 2 are shown in fig. 37. The isolines have been drawn continuously even though 5-day continuity is questionable, particularly at 500-mb. The isoline interval has been varied by the factors 2: 3: 4 to keep the ranges similar. It is apparent that the large amplitude changes take place at the same time at each level but that there is usually a shift with height in the latitude of maximum amplitude. The relationship in wave number three is difficult to assess due to the sharp drop in amplitude at 25 mb. At higher wave numbers the relationships cannot be studied individually at 5 day intervals.

6.2 Kinetic Energy

The Kinetic energy per mb for a zonal ring of width $\Delta \phi$, using the geostrophic approximation, is given by

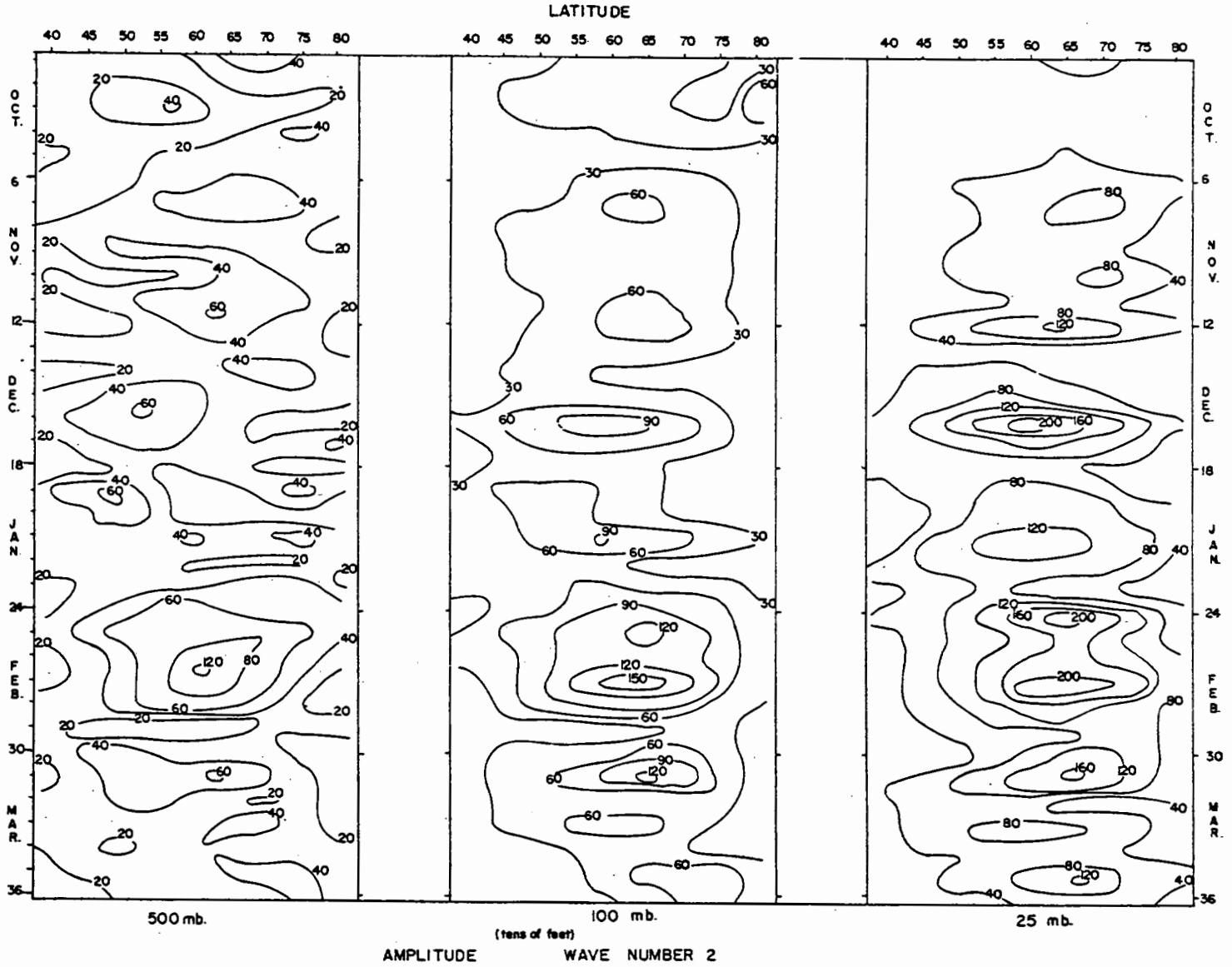

Fig. 37. Isoline representation of the amplitudes of wave number two at 500 mb, 100 mb and 25 mb based on the charts at five-day intervals October, 1958 - March, 1959.

$$KE = \frac{\pi g}{8\Omega^2(\Delta\phi)^2}\left\{\frac{\sin\phi_1 - \sin\phi_2}{\sin^2\frac{\phi}{2}}\right\}\left\{2(\Delta A_0)^2 + \sum_n\left[(\Delta A_n)^2 + (\Delta B_n)^2\right] + \frac{(\Delta\phi)^2}{\cos^2\frac{\phi}{2}}\sum_n n^2 C_n^2\right\} \quad (6.2 - 1)$$

For computing purposes the map was divided into 4 rings and 2 zones as shown below:

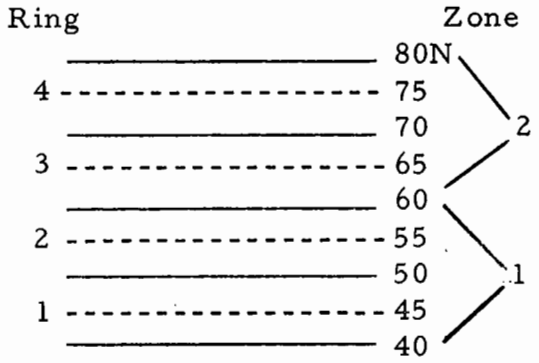

The kinetic energy was computed for ten degree rings, accumulated internally and an output was obtained for each wave number from 0 to n for zones one and two. The total kinetic energy at each level through the period is shown on fig. 38. The average kinetic energy for the 36 maps from 40N to 80N is given for each level in the following table and shown graphically in fig. 39. The spectrum of the stratosphere is different from the troposphere as would be expected. The maximum wave energy at 500 mb is in wave number three and a high energy level is maintained out through wave number eight with appreciable energy occasionally out to number eleven. At 25 mb the energy level drops

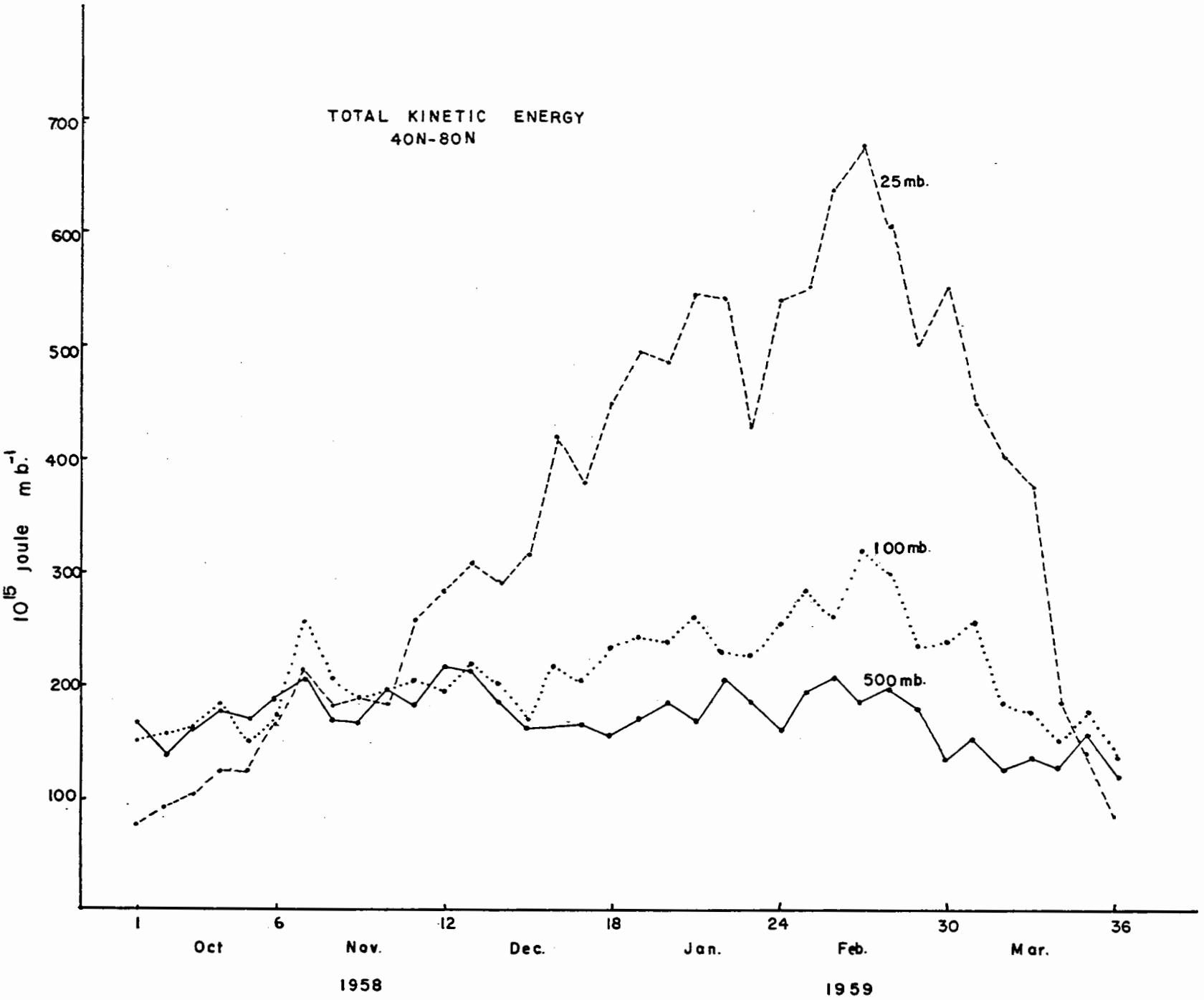

Fig. 38. The total kinetic energy 40N to 80N at 500 mb, 100 mb and 25 mb based on the 36 charts, October, 1958 - March, 1959 (10^{15} joule mb^{-1}).

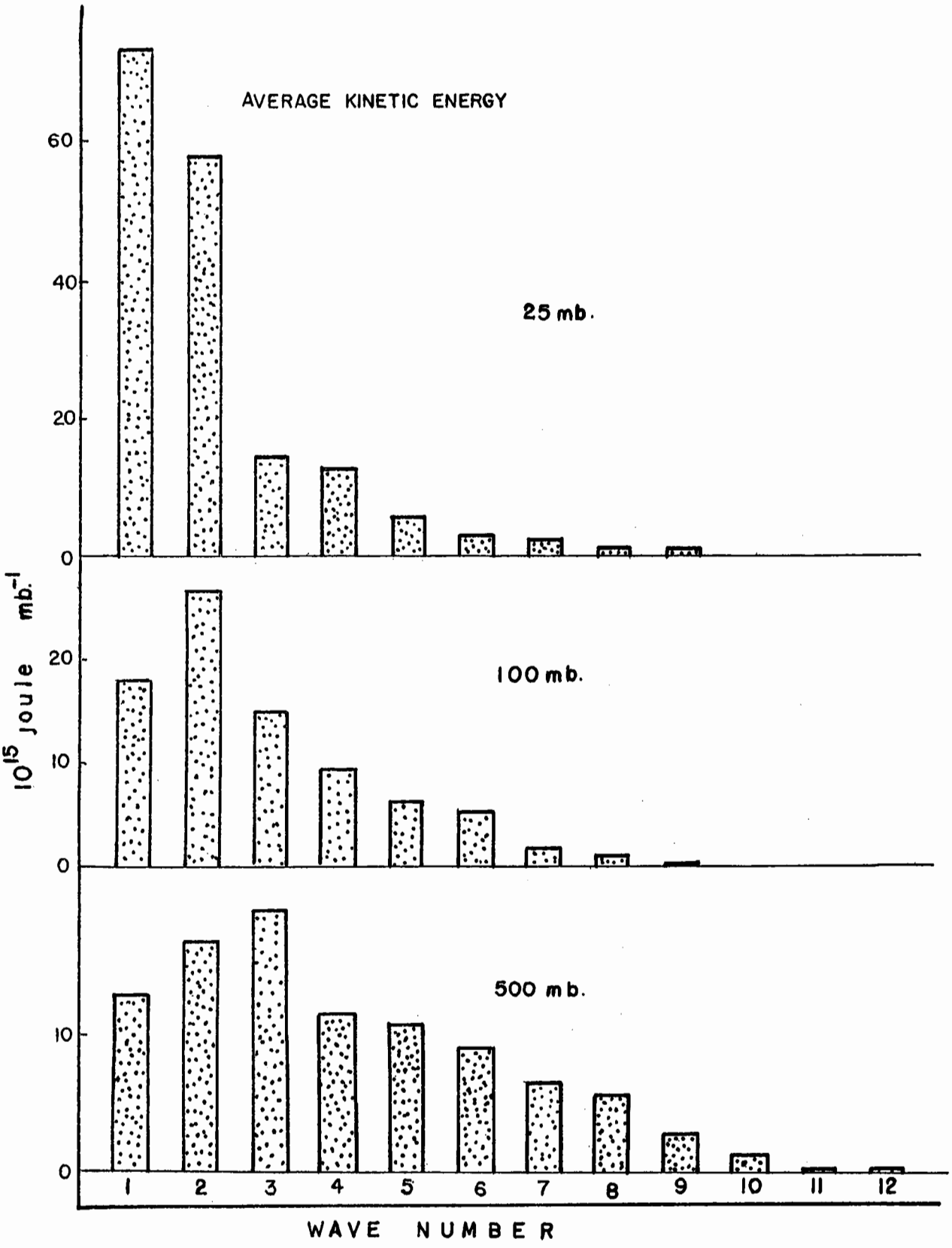

Fig. 39. The average kinetic energy October, 1958 - March, 1959 as a function of wave number at 500 mb, 100 mb and 25 mb. (10^{15} joule mb^{-1}).

rapidly from wave number two to number three; number three and four reach appreciable energy levels about one-sixth of the time but there is little energy beyond number four.

Table 3. Average kinetic energy, 40N-80N, 10^{13} joule mb^{-1}

	Wave #	500 mb	100 mb	25 mb
	0	6694	12800	16860
	1	1335	1856	7393
	2	1714	2743	5829
	3	1893	1471	1441
	4	1179	962	1288
	5	1100	606	537
	6	866	465	358
	7	631	174	266
	8	570	137	155
	9	258	33	82
	10	130		
	11	62		
	12	42		
	13	--		
Total	1 to n	9780	8447	17349

The variations with wave number are shown clearly by fig. 39. Linear correlations were computed for the kinetic energy from 40N to 80N for the three levels, by wave number. The in phase correspondence of wave number two is confirmed by the values in table number 4. The values at the high wave numbers are not likely to be meaningful due to the sampling interval.

Table 4. Linear correlation coefficients for the total kinetic energy, 40N-80N.

	500-100 mb	500-25 mb	100-25 mb
Total	.45	.22	.86
Zonal, #0	.19	-.27	.79
Wave # 1	.51	-.04	.52
2	.82	.68	.86
3	.64	.22	.63
4	.76	.35	.52
5	.78	.06	.35
6	.56	.55	.60

6.3 Momentum

The Fourier coefficients of geopotential height form the basis for the computations of relative angular momentum, momentum transport and momentum divergence.

The relative angular momentum of a zonal ring is given by

$$M \text{ per mb} = \frac{-\pi a^2}{\Omega \Delta\phi} \left\{ \frac{\sin\phi_1 - \sin\phi_2}{\tan\phi} \right\} (\Delta A_0) \qquad (6.3 - 1)$$

The computations were done for the polar ring (80N - 90N) in addition to the previous rings to give the zonal angular momentum for each circumpolar ring from 40N to the pole.

The eddy momentum transport across latitude circles was computed from the geostrophic transport formula:

$$M_T \text{ per mb} = \frac{\pi g}{4\Omega^2(\Delta\phi)} \frac{\cos\phi}{\sin^2\phi} \left\{ \sum_n n(A_n \Delta B_n - B_n \Delta A_n) \right\} \qquad (6.3 - 2)$$

The momentum divergence was computed by subtracting the transports for adjacent latitude circles.

The relative angular momentum computations for each level for the polar cap north of 50 degrees are given on fig. 40. The two dramatic events in the stratosphere, the sudden increase in mid-December and the decrease in March, have no apparent counterparts in the mid-troposphere.

The December increase has been discussed synoptically by Hare (1960b). The 25-mb kinetic energy showed that the increase in the zonal current was almost the same as the energy decrease in wave number one. At 500 mb there was a similar change in wave number one which is illustrated by the vector amplitude changes on

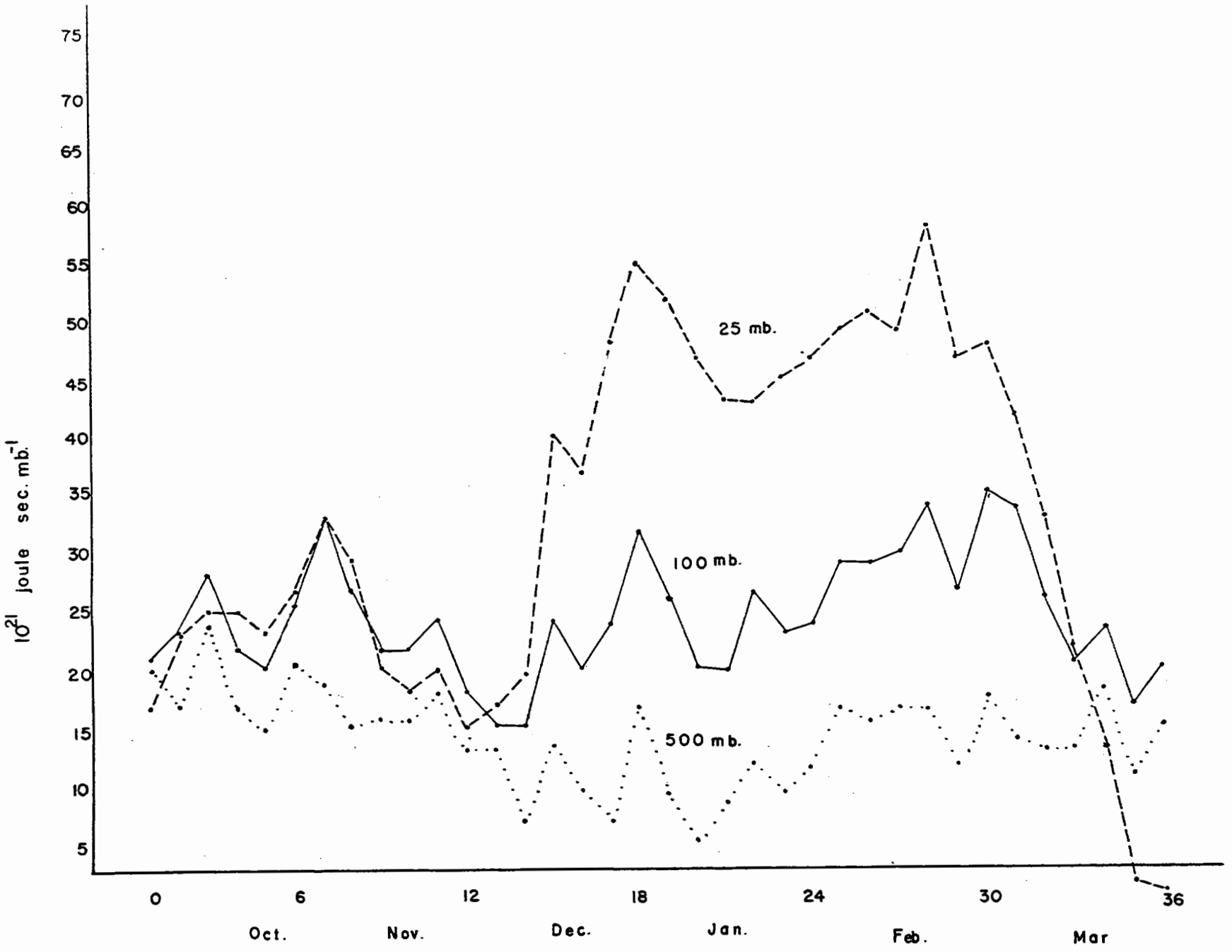

Fig. 40. The relative angular momentum for the polar cap north of 50N, October, 1958 to March 1959 at 500 mb, 100 mb and 25 mb. (10^{21} joule sec mb^{-1}).

fig. 36. This change in eccentricity of the 25-mb vortex required a large transport of momentum into the stratospheric polar cap. The mean temperature for the 50N latitude circle increased one degree and that for the 80N circle dropped ten degrees, indicating that any meridional overturning would probably transport momentum the wrong way. A net mass transfer is a possibility for such short period changes, but cannot be measured geostrophically.

The change in relative angular momentum from day 14 to day 15 (Dec. 9th to 14th) was a maximum in ring 3 (60N to 70N) amounting to 11×10^{21} joule sec mb^{-1}. The momentum convergence into that ring on day 15 was 2423×10^{13} joule mb^{-1} which if maintained for five days would amount to $\sim 10 \times 10^{21}$ joule sec mb^{-1} change. The close similarity between the momentum change and the momentum convergence is partially fortuitous for inspection shows that no simple relation exists between the momentum changes and the momentum transports at 5-day intervals. However the fact that the order of magnitude and the sign are right suggest that eddy transport may be the significant term.

The decay of the relative angular momentum in March followed the commencement of the final warming on March 1st. Meridional overturning apparently would again transfer momentum the wrong way. There is no indication of an eddy flux in March that could dissipate

the momentum and the transfer should be due to a net mass transfer or a vertical eddy flux.

The average horizontal momentum transport at 25 mb by wave numbers for the 36 maps is tabulated below in Table 5. The table again emphasizes the dominant effect of the low wave numbers, with the maximum transport occurring at wave number two.

Table 5. Average horizontal momentum transport at 25 mb, 10^{13} joule mb^{-1}

Wave number	Momentum transport
1	697.6
2	914.1
3	249.7
4	266.5
5	142.0
6	56.9
7	31.5
8	13.6
9	9.7

6.4 Heat Transport

The horizontal eddy heat transport may be computed manually

by the geostrophic contour channel technique (Mintz and Kao,1955). Such computations were made at 55N from the maps at five-day intervals in January and February for the 25-mb, 100-mb and 500-mb levels. The average transports for the 12 maps at each level are given in table 6.

Table 6. Heat transports across 55N, Jan.-Feb., 1959

25 mb	6.75×10^{12} joule $sec^{-1} mb^{-1}$
100 mb	5.28
500 mb	5.39

The values at the lower levels are comparable to similar computations by Mintz (1955). They suggest that the required northward heat flux may be present in the eddy terms but give no indication of the scale of the transporting waves.

The wave distribution of the heat transport at 25 mb was calculated from the height and temperature Fourier coefficients. The applicable formula for the computations is

$$H_T = 2\pi R\, c_p\, \overline{T^* v^*}\, \frac{\Delta P}{g}$$

$$= \frac{0.6595 \times 10^{10}}{\sin\phi} \sum_n n(a_n B_n - b_n A_n) \text{ joule sec}^{-1} \text{ mb}^{-1} \qquad (6.4 - 1)$$

The net transports across each of the nine latitude circles from 40N to 80N were obtained along with the transports by wave number averaged

over all latitudes. The net transports as functions of latitude and time are shown on fig. 41. The transport is mostly northward with a trend for convergence into the 60N to 70N zonal ring. The average monthly transports as a function of wave number are given in table 7 and the overall averages are shown on fig. 42. It appears that the major heat transport is carried out by the low wave numbers with little transport by waves higher than number five. Wave numbers two, three and four have maximum transports in January, the month of maximum baroclinic activity.

Table 7. Average northward heat transport at 25-mb by wave number (10^{10} joule $sec^{-1}mb^{-1}$)

	Oct.	Nov.	Dec.	Jan. 1958 -	Feb. 1959	Mar.	Average
1.	82.6	379.6	180.2	287.1	157.8	316.2	250.6
2.	35.5	7.6	103.4	351.2	-53.3	81.3	87.6
3.	8.2	40.7	48.3	69.0	39.8	23.7	38.3
4.	4.9	4.0	22.1	49.3	-30.4	12.6	10.4
5.	2.9	- 2.3	1.4	-17.9	9.4	2.0	-0.8
6.	0.2	6.2	1.2	3.3	-4.0	.4	1.22
7.	0.2	-0.2	-5.7	4.2	6.5	.9	1.0
8.	0.3	0.7	-0.5	2.7	1.2	0.1	0.8
9.	0.3	0.1	-1.2	-1.1	-0.2	-0.1	-0.4

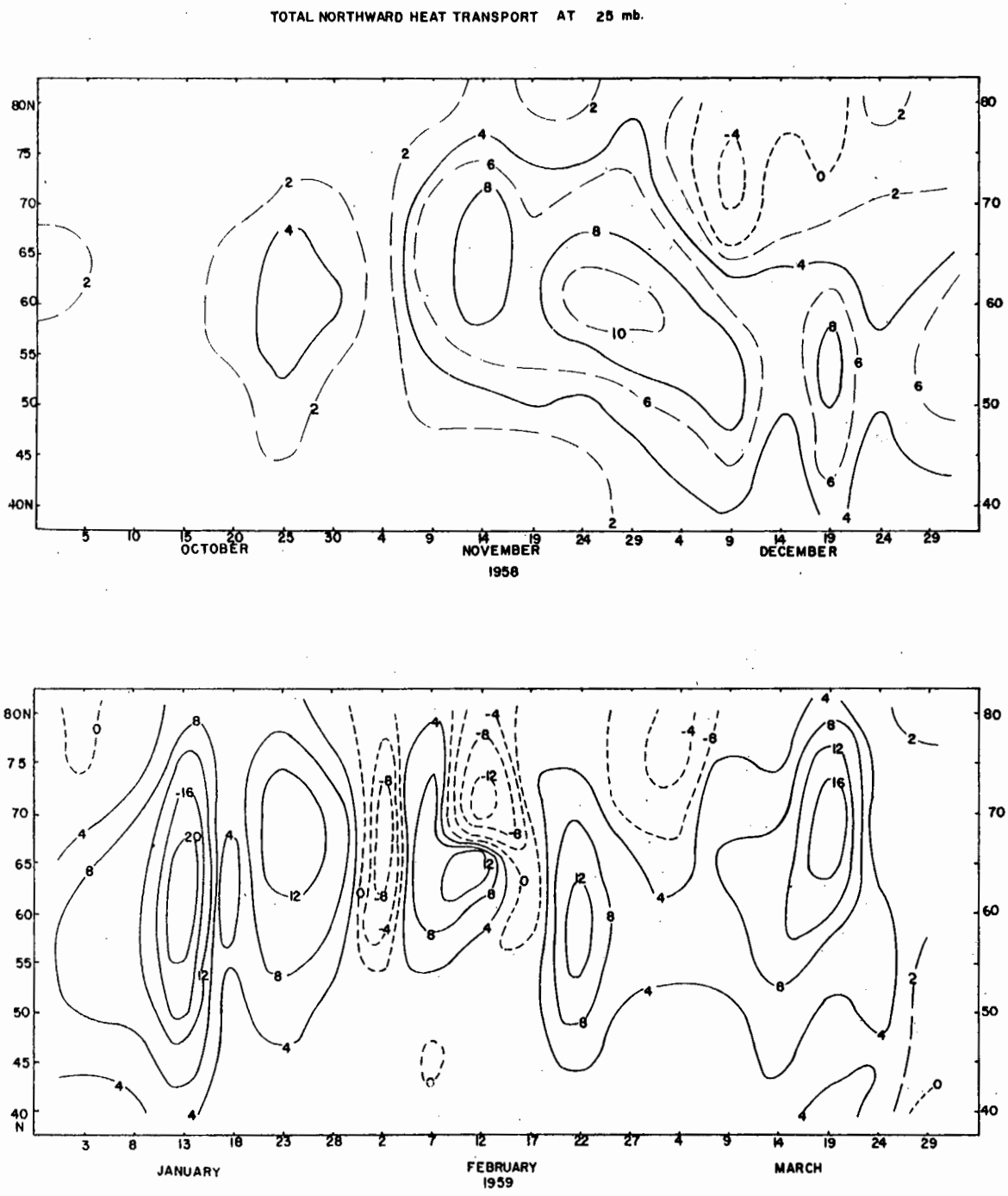

Fig. 41. Isolines of geostrophic heat transport across latitude circles at 25 mb, October, 1958 - March, 1959. (10^{12} joule $sec^{-1} mb^{-1}$).

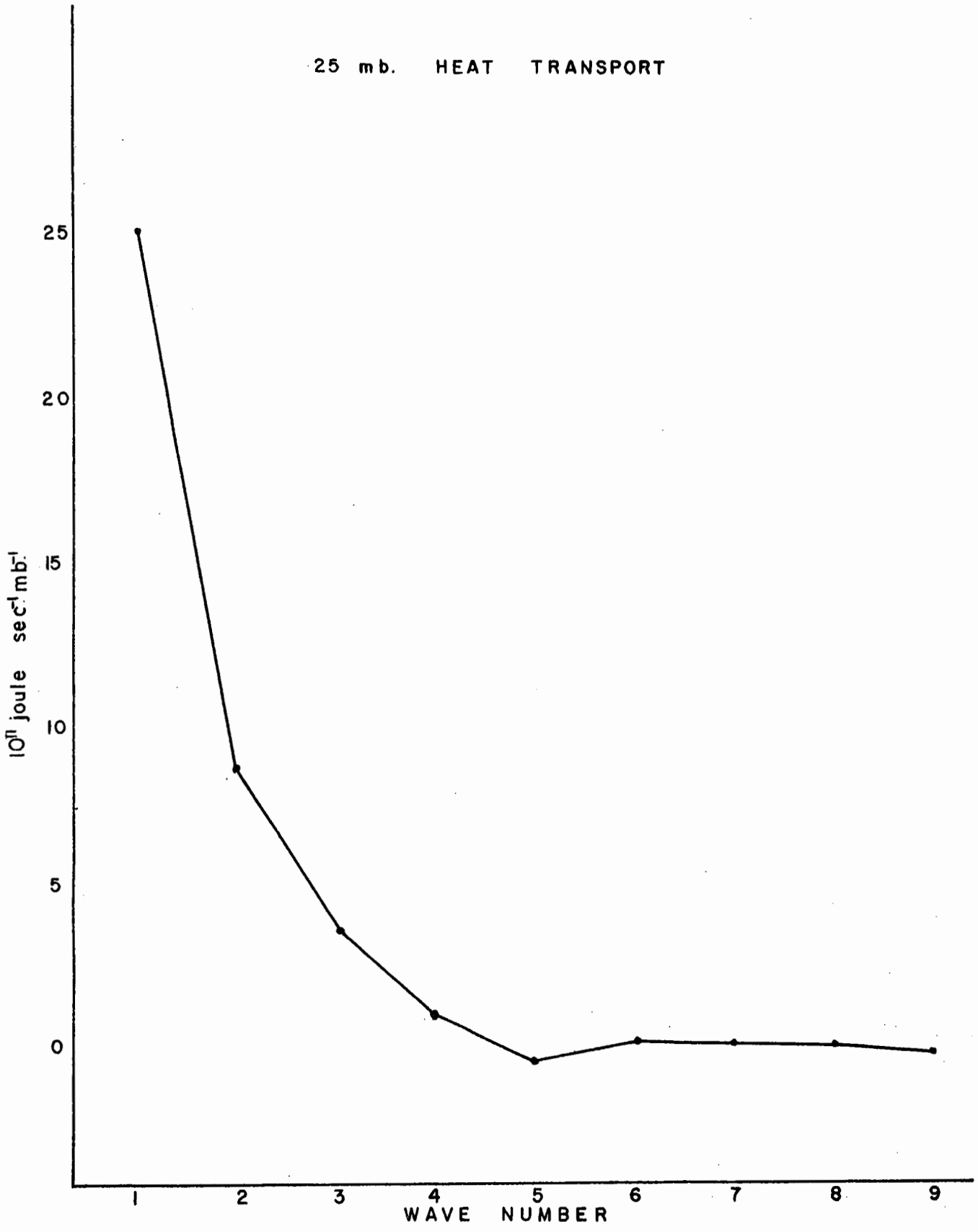

Fig. 42. The average heat transport at 25 mb as a function of wave number. (10^{11} joule $sec^{-1}mb^{-1}$).

6.5 Energy Conversions

The most difficult of the energy conversions to obtain are those involving vertical motion, for the latter cannot be measured directly on any broad scale basis. The vertical motions of the Fleagle model, as given in section 5.3., may be derived directly from the geopotential height field. It follows from equation (5.3 - 15) that

$$w = \sum_{n=1}^{\infty} w_n = W_1 \sum_{n=1}^{\infty} \left(\frac{\partial Z}{\partial x}\right)_n + W_2 \sum_{n=1}^{\infty} \left(\frac{\partial^2 Z}{\partial x^2}\right)_n \qquad (6.5 - 1)$$

and then the application of the Fourier expansion to Z gives:

$$Z = A_0 + \sum_n A_n \cos n\lambda + \sum_n B_n \sin n\lambda \qquad (6.5 - 2)$$

The partial derivatives of this function with respect to x are

$$\frac{\partial Z}{\partial x} = \frac{1}{R} \sum_n \left(nB_n \cos n\lambda - nA_n \sin n\lambda \right) \qquad (6.5 - 3)$$

$$\frac{\partial^2 Z}{\partial x^2} = -\frac{1}{R^2} \sum_n \left(n^2 B_n \sin n\lambda + n^2 A_n \cos n\lambda \right) \qquad (6.5 - 4)$$

and substitution back into (1) gives a new Fourier series for w, which is

$$w = \sum_n \left\{ \frac{W_1}{R} nB_n - \frac{W_2}{R^2} n^2 A_n \right\} \cos n\lambda - \sum_n \left\{ \frac{W_1}{R} nA_n + \frac{W_2}{R^2} n^2 B_n \right\} \sin \lambda \qquad (6.5 - 5)$$

Thus this vertical motion can be described, on a hemispheric basis, by the coefficients in the above series. However, from a computational viewpoint it is advantageous to proceed directly to the potential

to kinetic energy conversion. Following the outline in section 5.2., the conversion may be represented by

$$\underline{\left\{P, K\right\}} \text{ per mb} \simeq \frac{1}{\bar{T}} \overline{w^* T^*}\, 2\pi a^2 (\sin\phi_1 - \sin\phi_2) \qquad (6.5 - 6)$$

where $\underline{(\,)} = \frac{1}{2\pi} \int_0^{2\pi} (\,)\, d\lambda$, the average taken around a latitude circle. Then where the temperature is also represented by a Fourier series:

$$T = a_0 + \sum_n a_n \cos n\lambda + \sum_n b_n \sin n\lambda \qquad (6.5 - 7)$$

equations (5), (6) and (7) may be combined and integrated around a latitude circle to yield.

$$\left\{P, K\right\} \text{ per mb} = \pi \frac{(\sin\phi_1 - \sin\phi_2)}{(a_0 + 273)\cos^2\phi} \sum_n \left\{W_1 R n (a_n B_n - A_n b_n) - W_2 n^2 (a_n A_n + b_n B_n)\right\} \qquad (6.5 - 8)$$

The physical significance of equation (8) may be interpreted more readily in the phase angle form. Thus when

$$\begin{aligned} a_n &= c_n \cos k_1 \qquad & b_n &= c_n \sin k_1 \\ A_n &= C_n \cos k_2 \qquad & B_n &= C_n \sin k_2 \end{aligned} \qquad (6.5 - 9)$$

then

$$(a_n B_n - b_n A_n) = c_n C_n \sin (k_2 - k_1) \qquad (6.5 - 10)$$

which shows that a phase difference $(k_1 - k_2 \neq o)$ must exist for the term to operate. The temperature field must lag behind the height field for a positive P. E. → K. E. conversion. The term derives from the $\partial Z / \partial x$ term of the vertical motion, and hence requires the southerly ascending winds to be associated with warmer air than the descending northerly winds. Similarly the last part of equation (8) yields

$$-(a_n A_n + b_n B_n) = -c_n C_n \cos (k_1 - k_2) \qquad (6.5 - 11)$$

This term has its maximum positive value when the two curves are 180° out of phase. The term derives from the $\partial^2 Z / \partial x^2$ term of w

hence a positive PE → KE conversion requires that the warmer air be in ascending regions of cyclonic curvature and the colder air in descending regions of anticyclonic curvature.

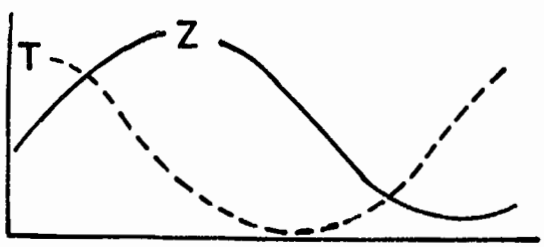

the $\partial Z/\partial x$ term

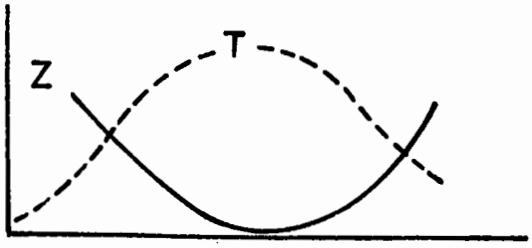

the $\partial^2 Z/\partial x^2$ term

The phase difference for maximum conversion depends on the relative magnitude of the terms, but clearly will occur when the thermal trough lags behind the geopotential height trough by one-quarter to one-half of a wave-length.

For computing purposes it is convenient to write equation (8) as

$$\left\{P, K\right\} \text{ per mb} = \frac{1}{273+a_0}\left[d_\phi \sum_n n(a_nB_n - b_nA_n) - e_\phi \sum_n n^2(a_nA_n + b_nB_n)\right] \quad (6.5 - 12)$$

where

$$d_\phi = c_1(-c_3\Delta a_0 + c_4) \qquad e_\phi = c_2\left[\frac{(-c_3\Delta a_0 - c_4)^2}{-c_3\Delta a_0 + 3c_4}\right] \quad (6.5 - 13)$$

the constants c_1, c_2, c_3 and c_4 being computed from the equations for W_1 and W_2 (5.3 - 14). A standard stability was used, the value chosen corresponding to an isothermal lapse rate. The machine computations of the conversions were done internally by rings with a print-out by wave-number and the total for the two zones (40-60N and

60-80N). Since the theory is only applicable when the meridional temperature gradient exceeds the critical value, such a criterion had to be applied to the computations. The criterion was only satisfied during periods in December, January and February. The average energy conversions as a function of wave number are shown in fig. 43. for January, the active month. The major contributions in these computations are from waves one and two with negligible amounts beyond wave number four. The monthly figures are given in table 8 and discussed later.

The remainder of the hemispheric energy exchanges, as given in section 5.2, may now be calculated for the 25-mb level. The Lorenz (1955) formulation is followed with the simplifications required to fit the available computations. In the main, this required omitting the vertical motion from the transporting terms. The kinetic energy components, K_e and K_z, and the eddy conversion, C_e, have already been formulated. The non-adiabatic zonal generation of available potential energy is given by

$$G_z = \frac{1}{g}\int_0^{\overline{P_0}} \frac{\Gamma_H}{\Gamma_d - \overline{\Gamma}} \frac{\overline{T'Q'}}{\overline{T}}\, dP \qquad (6.5 - 14)$$

where Q is the rate of heat addition per unit mass. This may be transformed to a total for the polar cap north of 40N at 25 mb.

$$G_z \simeq 5.02 \times 10^{10}\ \overline{T'q'} \text{ joule sec}^{-1} \text{ mb}^{-1} \qquad (6.5 - 15)$$

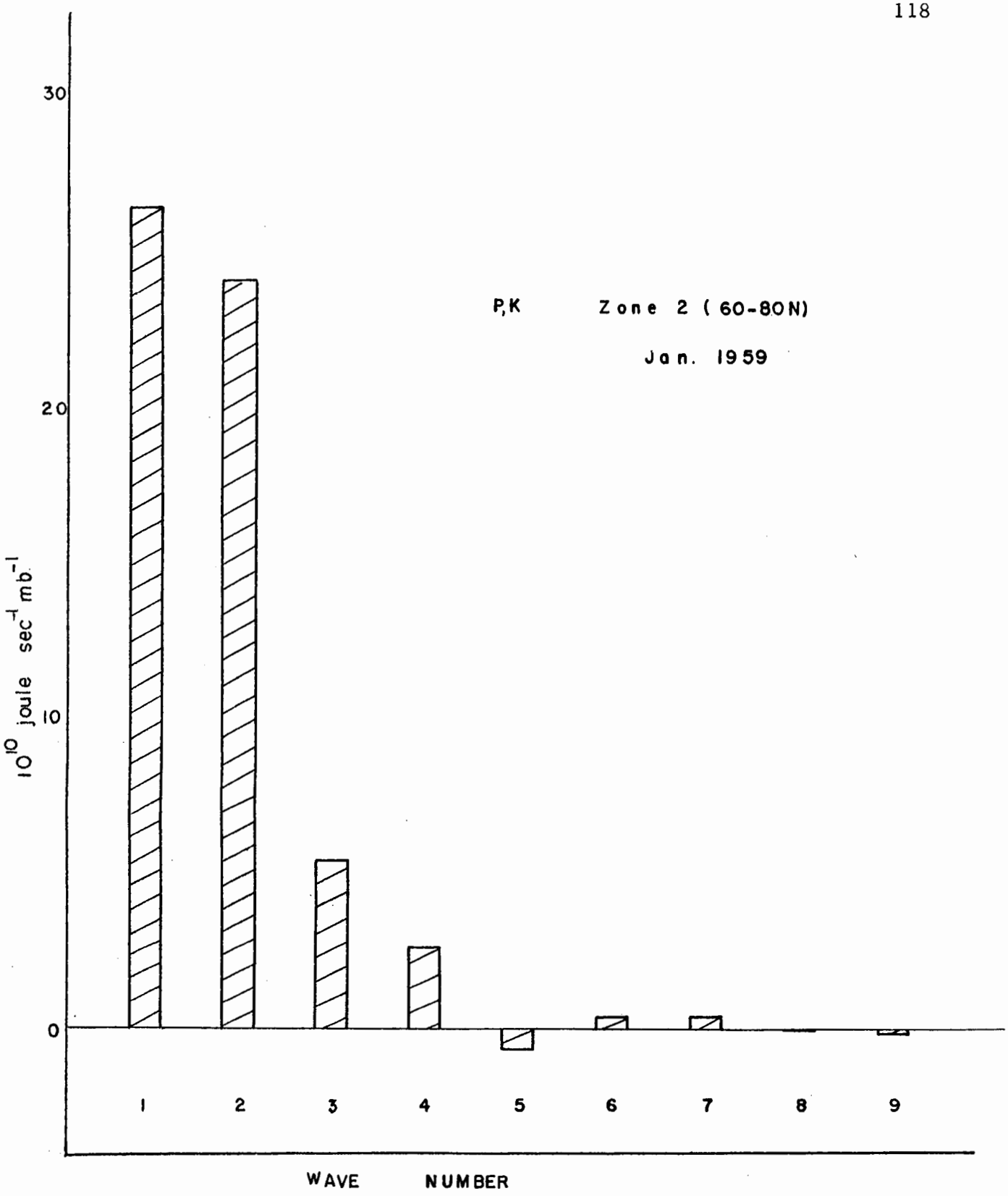

Fig. 43. The average eddy potential to eddy kinetic energy conversion at 25 mb for January, 1959 as a function of wave number. (10^{10} joule sec^{-1} mb^{-1}).

where q' is the heat added in ^{o}K per day. The available potential energy components for the polar cap north of 40N at 25-mb are given by

$$AP_z \simeq 44.0 \times 10^{16} \; \bar{T} \left(\frac{\overline{T'}}{\bar{T}}\right)^2 \text{ joule mb}^{-1} \qquad (6.5 - 16)$$

$$AP_e \simeq 44.0 \times 10^{16} \; \bar{T} \left(\frac{\overline{T^*}}{\bar{T}}\right)^2 \text{ joule mb}^{-1} \qquad (6.5 - 17)$$

Where the * represents deviations of individual values from the average taken around the latitude circle and the ' represents the deviation of the average for a latitude circle from the average for all latitude circles. The exchange between zonal available potential energy and eddy available potential energy is

$$C_A = -\frac{R}{g}\int_0^{\bar{P}_0} \frac{\bar{\theta}}{\bar{T}} \left[\overline{(T^*v^*)}\frac{\partial}{\partial y} + \overline{(T^*\omega^*)}\frac{\partial}{\partial P}\right]\left(\frac{\Gamma_d}{\Gamma - \bar{\Gamma}}\frac{1}{\theta}T'\right)dP \qquad (6.5 - 18)$$

The horizontal component of this conversion may be computed from the heat transports and the mean meridional temperature gradients. For a ten-degree wide latitude ring the computational form at 25 mb is:

$$C_A = -0.287\left[\overline{H_T \Delta\left(\frac{T'}{\bar{T}}\right)}\right] 10^{10} \text{ joule sec}^{-1} \text{ mb}^{-1} \qquad (6.5 - 19)$$

The exchange between eddy kinetic energy and zonal kinetic energy is given by

$$C_K = -\frac{1}{g}\int_0^{\bar{P}_0} \cos\phi \left(\left[\overline{u^*v^*}\right]\frac{\partial}{\partial y} + \left[\overline{u^*\omega^*}\right]\frac{\partial}{\partial P}\right)\cdot\left(\frac{[\bar{u}]}{\cos\phi}\right)dP \qquad (6.5 - 20)$$

The horizontal component of this conversion may be computed from the momentum transports and the zonally averaged geopotential heights. For a ten-degree latitude ring at 25 mb this is

$$C_K = -1.16 \times 10^{-4} \frac{\overline{M_T \cdot \Delta^2 A_0}}{\cos\phi \sin\phi} 10^{10} \text{ joule sec}^{-1} \text{ mb}^{-1} \quad (6.5 - 21)$$

Table 8. Energy exchange computations at 25 mb

Averages for 40N - 80N

(Energies - 10^{16} joule mb^{-1}; Conversions - 10^{10} joule $sec^{-1} mb^{-1}$)

G_z	Oct.	Nov.	Dec.	Jan. (-10.0)	Feb.	Mar.	6 months
AlP_z	1.9	0.5	7.7	11.2	10.3	2.9	5.7
C_A	1.8	1.2	7.2	24.6	1.5	-2.3	5.7
AlP_e	2.3	10.2	6.6	12.6	12.3	11.2	9.2
C_e	-	-	8.2	42.2	-6.7	-	7.3
K_e	3.8	13.4	16.2	24.5	26.2	20.0	17.3
C_k	8.6	2.2	5.3	26.8	79.4	40.6	27.2
K_z	7.6	8.3	20.4	26.3	31.1	7.4	16.9

The energy exchange processes for the 25-mb level averaged by months are given in table 8. The components of the kinetic energies and the available potential energies were all of the same order, and the kinetic energies generally averaged about twice the potential

energies. In March, after the major warming, the vortex centre moved off the pole into the Eurasian sector and the energy was predominantly in the eddy component.

The energy transfers and conversions present a more complex picture. From October to November the energy transfer, C_A, associated with the horizontal heat transport is insufficient for the indicated growth in eddy available potential energy. Similarly there are no unstable waves to support the increase in eddy kinetic energy. It thus seems necessary to have forced perturbations and vertical circulations to carry out the exchanges. During December and particularly in January, the exchange processes become large and the baroclinic activity appears to be associated with the major part of the exchange. During February the heat transport term becomes very small and the available potential to kinetic energy conversion becomes negative. The northward momentum transport is very large in this month. Forced perturbations and vertical circulations are thus again required to effect the energy exchanges. In March the heat transport exchange (C_A) becomes negative but the conversion C_k, associated with momentum transport is still contributing towards increased zonal flow despite the observed decrease. A satisfactory balance under these conditions requires a southward mass transport.

The radiative component of the exchanges is the most difficult

to interpret. The value given in brackets in January for G_z, the non-adiabatic generation, has been computed from the temperatures and heating rates given by Brooks (1958). The negative value stems from the fact that the computed cooling was greater in the warm belt than in the polar regions, at 25 mb. In the troposphere average radiative values are the same as the average heat transport terms. It would be difficult to justify a similar balance at a single radiative level, such as 25 mb. However, the trends may be of value. The average heat transport across 40N at 25 mb for the six months is equivalent to a heating rate for the polar cap of 0.20°C per day and that across 60N to a rate of 0.24°C per day. The maximum monthly value was that for transport across 60N in January, being 0.40°C per day. These figures are comparable to the observed cooling rates and would support an eddy-type circulation. The computed 25-mb energy components for the month of January are shown in fig. 44. The energy made available through radiative imbalance, G_z, was entered on the assumption that it approximates the heat transport term, C_A. A partial balance, in fig. 44., may be achieved if the energy conversion due to meridional overturning, C_z, has a significant negative value. Such an indirect circulation seems logical with forced subsidence in the warm belt and likely ascent in the cold core of the vortex. However, this would give a downward flux of (omega)

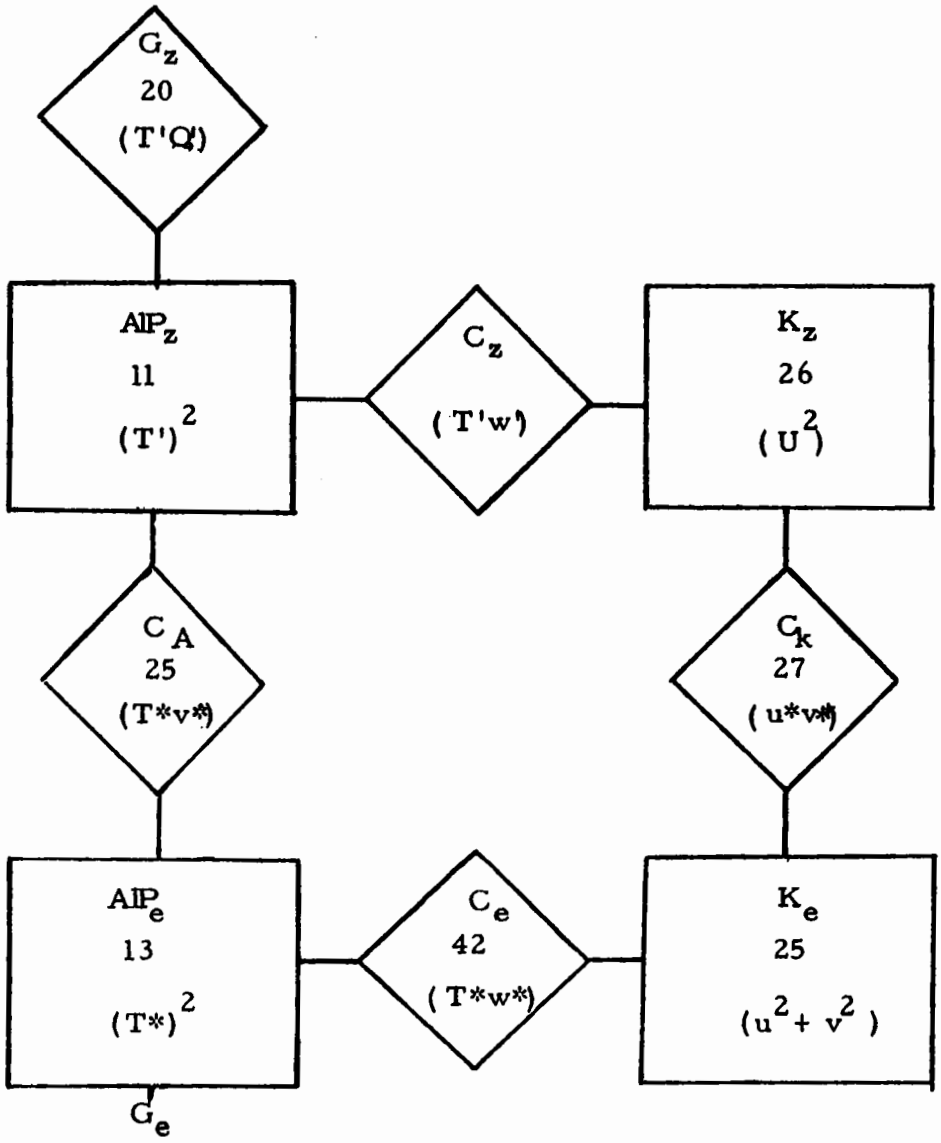

Fig. 44. 25-mb energy components for the month of January, 1959.
Rectangles - energies----------10^{16} joule mb^{-1}
Diamonds - energy conversion----10^{10} joule sec^{-1} mb^{-1}

momentum, according to section 5.1. (fig. 30) and would require a meridional mass flux. The computed terms in fig. 44 are comparable in magnitude to the tropospheric values, fig. 32, except for $A\mathbb{P}_z$ and C_A which are an order less. The storage of zonal available potential energy, $A\mathbb{P}_z$, is thus fairly small in the stratosphere and this may explain the apparent ease with which the basic winter circulation changes. The numerical values of the terms are biased by the small sample but should be fair estimates except for the vertical motion uncertainty in the conversion term C_e.

The foregoing application of linear theory to the 25-mb level indicates that the energy conversions associated with unstable baroclinic wave activity were of major importance in the month of January. During the fall and late winter the exchanges were apparently not ascribable to such activity and forced perturbations and mass transfers offer the logical alternatives.

7. DISCUSSION

The aim of this project on the middle stratosphere was to identify and describe its major perturbation systems, to relate its behaviour to that of the troposphere and to attempt a quantitative definition of its energetics. The large measure of success achieved on the first two parts and the significant progress on the third are summarized in this section.

7.1 Conclusions

The details of the energy budget terms in this study must be considered in the light of the paucity and limited accuracy of the observed data and the fact that the charts in the middle stratosphere were limited to one level every five days. However, the study has been sufficiently comprehensive to leave little doubt concerning the validity of the results with respect to the largest wave lengths in the atmosphere. The following conclusions stem from the study:

(i) Large scale waves are present in the middle stratosphere during the colder half of the year.

(ii) Most of the kinetic energy of these waves is found in wave numbers one and two.

(iii) The waves are effective transporters of heat and momentum and the conservative trace element, ozone.

(iv) Baroclinic wave development, fulfilling instability criteria

and energy conversions of the Fleagle type, appear to have been identified down to wave number four. The developments were evidently limited in number and occurred mainly in the January month.

(v) A significant correspondence between the middle stratosphere and the troposphere has been established in the eccentric and bi-polar wave numbers (one and two). The investigation of the Aleutian anticyclone and the Fourier resolutions suggest that the systems propogate upward in association with vertical circulations.

(vi) A partial energy budget for the middle stratosphere has been formulated primarily on the basis of energy computations and horizontal transports. This budget indicates that vertical circulations in zonal planes associated with forced or other types of perturbations probably play a significant role in the middle stratosphere.

(vii) Although the study supports the upward extension of large scale effects from the troposphere into the middle stratosphere the lack of sufficient information from higher levels precluded establishing the order or existence of effects from those levels.

7.2 Status of the problem

This study has achieved a considerable definition of the circulation of the middle stratosphere and confirmed the usefulness of the synoptic-dynamic approach for that regime. An extension of the wave analysis to a daily basis in the January month would probably resolve the questions of interaction with tropospheric activity and of the baroclinic energy exchanges through wave number four. An extension of the synoptic approach appears necessary to further formulate the nature of the interactions and the extent of the vertical circulations in the major late-winter warmings. The rocket information now becoming available into the mesosphere will be most readily interpreted in conjunction with this type of synoptic-dynamical analysis of the stratosphere.

The results of the study make it obvious that any realistic numerical solution of the stratospheric circulation must include the tropospheric domain. A further extension of the observational horizon through rocket networks followed by a more precise physical framework must precede such an ambitious solution.

References

Allington, K., B.W. Boville, and F.K. Hare, 1960: 'Midwinter ozone variations and stratospheric flow over Canada, 1958-59', Tellus, 12, No. 3.

Bjerknes, J., 'Preliminary study of the day to day changes of angular momentum during January-February and July-August 1949'. U.C.L.A.*

Boville, B.W., and M. Kwizak, 1959: ' Fourier analysis applied to hemispheric waves of the atmosphere'. Meteorological Branch, Canada, TEC-292.

Boville, B.W., 1960: 'The Aleutian stratospheric anticyclone', J.Meteor, 17, 329-336.

Brooks, D. L., 1958: 'The distribution of carbon dioxide cooling in the lower stratosphere'. J. Meteor, 15, 210-219.

Charney, J.G., 1947: 'The dynamics of long waves in a baroclinic westerly current', J. Meteor, 4, 135-162.

Craig, R. A., 1950: 'The observations and photochemistry of atmospheric ozone and their meteorological significance', Met. Monographs, 1, No. 2.

Craig, R. A. and W.S. Hering, 1959: 'The stratospheric warming of January - February, 1957', J. Meteor, 16, 91-107.

Cramer, H. E., and F. A. Record, 1955: 'Power spectra of the eddy-velocity components', J. Meteor, 12, 146-151.

Eady, E. T., 1949: 'Long waves and cyclone waves', Tellus, 1, 35-52.

Eliasen, E., 1958: 'A study of long atmospheric waves on the basis of zonal harmonic analysis', Tellus, 10, 206-215.

Fleagle, R. G., 1957: 'On the dynamics of the general circulation', Quart. J. R. Meteor. Soc., 83, 1-20.

Godson, W. L., and R. Lee, 1958: 'High-level fields of wind and temperature over the Canadian Arctic'. Beitr. zur Phys. der Atmos., 31, 40-68.

Godson, W. L., 1959a: 'The application of Fourier analysis to meteorological data'. Meteorological Branch, Canada, TEC-295.

Godson, W. L., 1959b: 'Paper presented to Seminar in Arctic and Stratospheric Meteorology. Montreal, McGill Univ., 27 July - 7 August, 1959.

Godson, W. L., 1960: 'Total ozone and the middle stratosphere over Arctic and sub-Arctic in winter and spring'. Quart. J. R. Met. Soc., 86, 301-317.

Götz, F. W. P., 1951: 'Ozone in the atmosphere'. Compendium of Meteor., 275-291.

Hadley, G., 1735: 'On the cause of the general trade winds', Phil. Trans. R. Soc. Lond., 437, 58.

Hare, F. K., 1960a: 'The summer circulation of the Arctic stratosphere below 30-km', Quart. J. R. Met. Soc., 86, 127-146.

Hare, F. K., 1960b: 'The disturbed circulation of the Arctic stratosphere', J. Meteor., 19, 36-51.

Jeffreys, H., 1926: 'On the dynamics of geostrophic winds', Quart. J. R. Met. Soc., 52, 85-104.

Julian, P. R., 1959: 'Tropospheric behaviour associated with the Arctic stratosphere warming phenomenon', Final Report - part 1, AF 19(604)-2190, The Pennsylvania State University.

Kuo, H. L., 1952: 'Three dimensional disturbances in a baroclinic zonal current' J. Meteor., 9, 260-278.

Lettau, H., 1951: 'Diffusion in the upper atmosphere', Compendium of Meteor., 320-333.

Lorenz, E. N., 1955: 'Available potential energy and the maintenance of the general circulation', Tellus, 7, 157-167.

Ludlam, D. M., 1958: Weatherwatch. Weatherwise, 11, 214-215.

Mateer, C. L., 1960: 'A rapid technique for estimating the vertical distribution of ozone from Umkehr observations', Meteorological Branch, Canada, TEC-314.

Margules, M., 1906: 'Über die Energie der Stürme', Met. Zeit, 23, 481-497.

McCreary, F. E., 1959: 'Stratospheric winds over the Tropical Pacific', Presented at the Conference on Stratospheric Meteorology, A.M.S., Minneapolis, Minn., Sept., 1959.

Meunch, H. S., 1958: 'Analysis of synoptic charts in the stratosphere', G.R.D. Research Notes, No. 1., Geophysics Research Directorate, Bedford, Mass.

Mintz, Y., 1955: 'Final computation of the mean geostrophic poleward flux of angular momentum and of sensible heat in the winter and summer of 1949', U.C.L.A.*

Mintz, Y., and S-K., Kao, 1955: 'The contour-channel method of computing the geostrophic poleward flux of atmospheric properties', U.C.L.A.*

Murgatroyd, R. J., 1957: 'Winds and temperatures between 20 km and 100 km - a review', Quart. J. R. Met. Soc., 83, 417-458.

Murgatroyd, R. J., and R. M. Goody, 1958: 'Sources and sinks of radiative energy from 30 to 90 km', Quart. J. R. Met. Soc. 84, 225-234.

Nielsen, A. W., 1959: 'A study of energy conversion and meridional circulation for the large-scale motion in the atmosphere', Mon. Wea. Rev., 87, 319-332.

Normand, C., 1953: 'Atmospheric ozone and the upper-air conditions', Quart. J. R. Met. Soc., 79, 39-50.

Ohring, G., 1958: 'The radiation budget of the stratosphere', J. Meteor., 15, 440-451.

Orvig, S., 1960: 'Extrapolation of 25-mb heights and temperatures over North America north of 50°', Arctic Meteorology Research Group, Publication in Meteorology No. 14, McGill University, Montreal.

Phillips, N., 1956: 'The general circulation of the atmosphere: a numerical experiment', Quart. J. R. Met. Soc., 82, 123-164.

Pisharoty, P., 1955: 'The kinetic energy of the atmosphere', U.C.L.A.*

Plass, G.N., 1956: 'The influence of the 15μ carbon-dioxide band on the atmospheric infra-red cooling rate', Quart. J. R. Met. Soc., 82, 310-324.

Pocinki, L.S., 1955: 'The stability of simple baroclinic flow with horizontal shear', G.R.P. 38, Geophysics Research Directorate, Bedford, Mass.

Pressman, J., 1955: 'Seasonal and latitudinal temperature changes in the ozonosphere', J. Meteor., 12, 87-89.

Reed, R. J., 1950: 'The role of vertical motions in ozone-weather relationships', J. Meteor., 17, 263-267.

Saltzman, B., 1957: 'Equations governing the energetics of the larger scales of atmospheric turbulence in the domain of wave number', J. Meteor, 14, 513-523.

Scherhag, R., 1952: 'Die explosionsartigen stratosphärenerwärmungen des Spätwinters 1951-52', Ber. Deut. Wetterd. U.S. Zone, 6, 51-63.

Starr, V. P., 1951: 'Application of energy principles to the general circulation', Compendium of Meteor. 568-577.

Stroud, W. G., W. Nordberg, W.R. Bandeen, F.L. Bartman and P. Titus, 1960: 'Rocket grenade measurements of temperatures and winds in the mesosphere over Churchill, Canada.' Inst. Aer. Sciences, Paper no. 60-47, New York meeting, January 25-27, 1960.

Teweles, S., 1958: 'Anomalous warming of the stratosphere over North America in early 1957', Mon. Wea. Rev., 86, 377-396.

Teweles, S., and F. G. Finger, 1960: 'Reduction of diurnal variation in the reported temperatures and heights of stratospheric constant pressure surfaces', J. Meteor., 17, 177-194.

Wexler, H. and W.B. Moreland, 1958: Polar atmosphere symposium, Part I, Permagon, London, 71-84.

.....'Studies of the atmospheric general circulation', Final Report, part 1, General Circulation Project, no. AF19(122)-153., Dept. of Meteor., Massachusetts Institute of Technology..

*.... *Investigations of the general circulation of the atmosphere', Final Report of General Circulation Project no. AF19(122)-48, Dept. of Meteor., University of California.

Appendix A

The 25-mb charts in this appendix were drawn by the author and formed the basis for the dynamical study of the stratosphere. The charts are being published by the Defence Research Board of Canada in "An Atlas of Stratospheric Circulation" D. Phys. R(G) Misc G4. For convenience, the charts at five-day intervals have been numbered consecutively and the dates corresponding to the reference numbers are listed below.

	A-1	-2	-3	-4	-5	-6	
October	5,	10,	15,	20,	25,	30,	1958
	A-7	-8	-9	-10	-11	-12	
November	4,	9,	14,	19,	24,	29,	1958
	A-13	-14	-15	-16	-17	-18	
December	4,	9,	14,	19,	24,	29,	1958
	A-19	-20	-21	-22	-23	-24	
January	3,	8,	13,	18,	23,	28,	1959
	A-25	-26	-27	-28	-29	-30	
February	2,	7,	12,	17,	22,	27,	1959
	A-31	-32	-33	-34	-35	-36	
March	4,	9,	14,	19,	24,	29,	1959

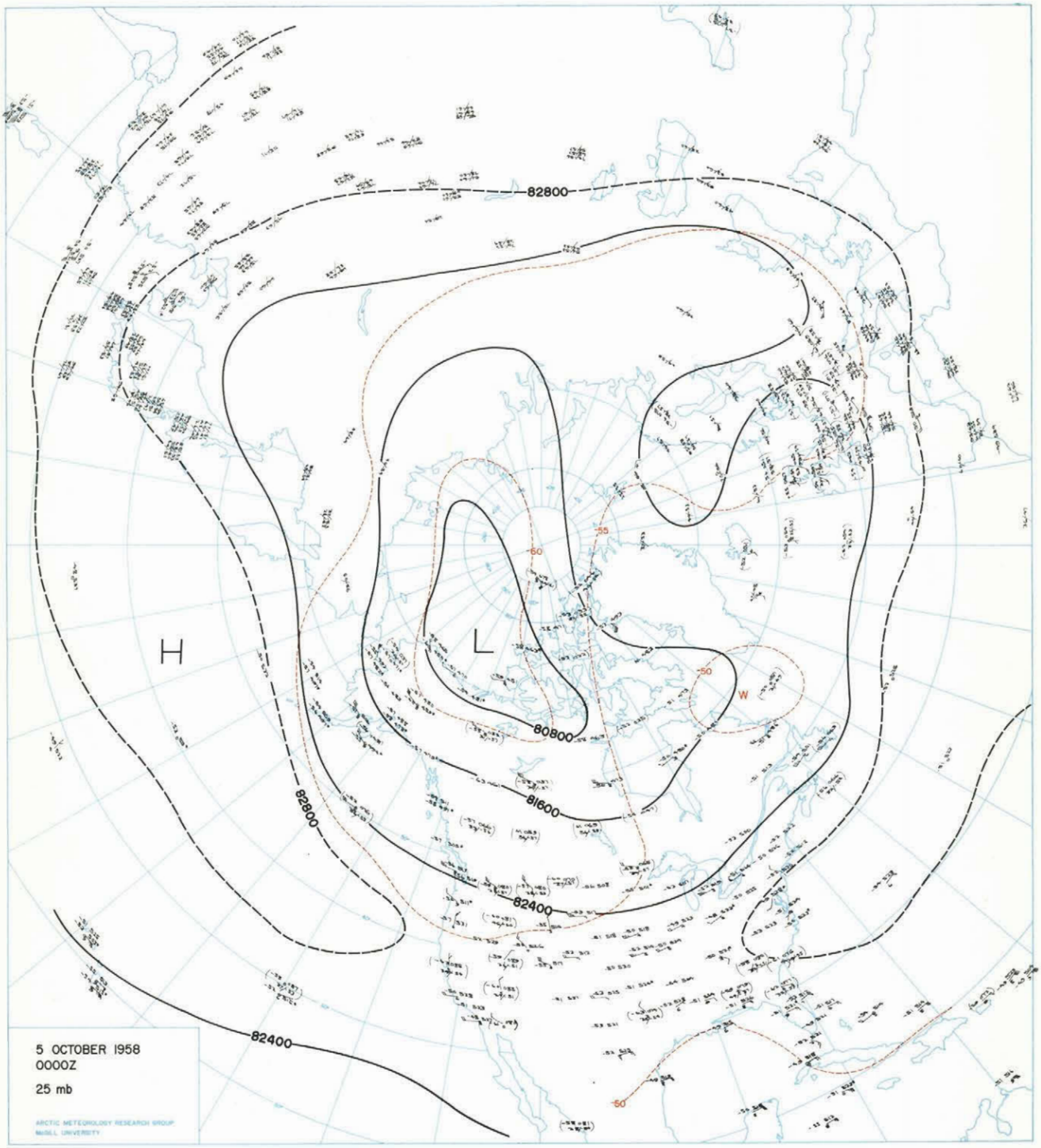
82800
H
L
-60
-55
-50
W
80800
81600
82800
82400
82400
-50
5 OCTOBER 1958
0000Z
25 mb
ARCTIC METEOROLOGY RESEARCH GROUP
McGILL UNIVERSITY

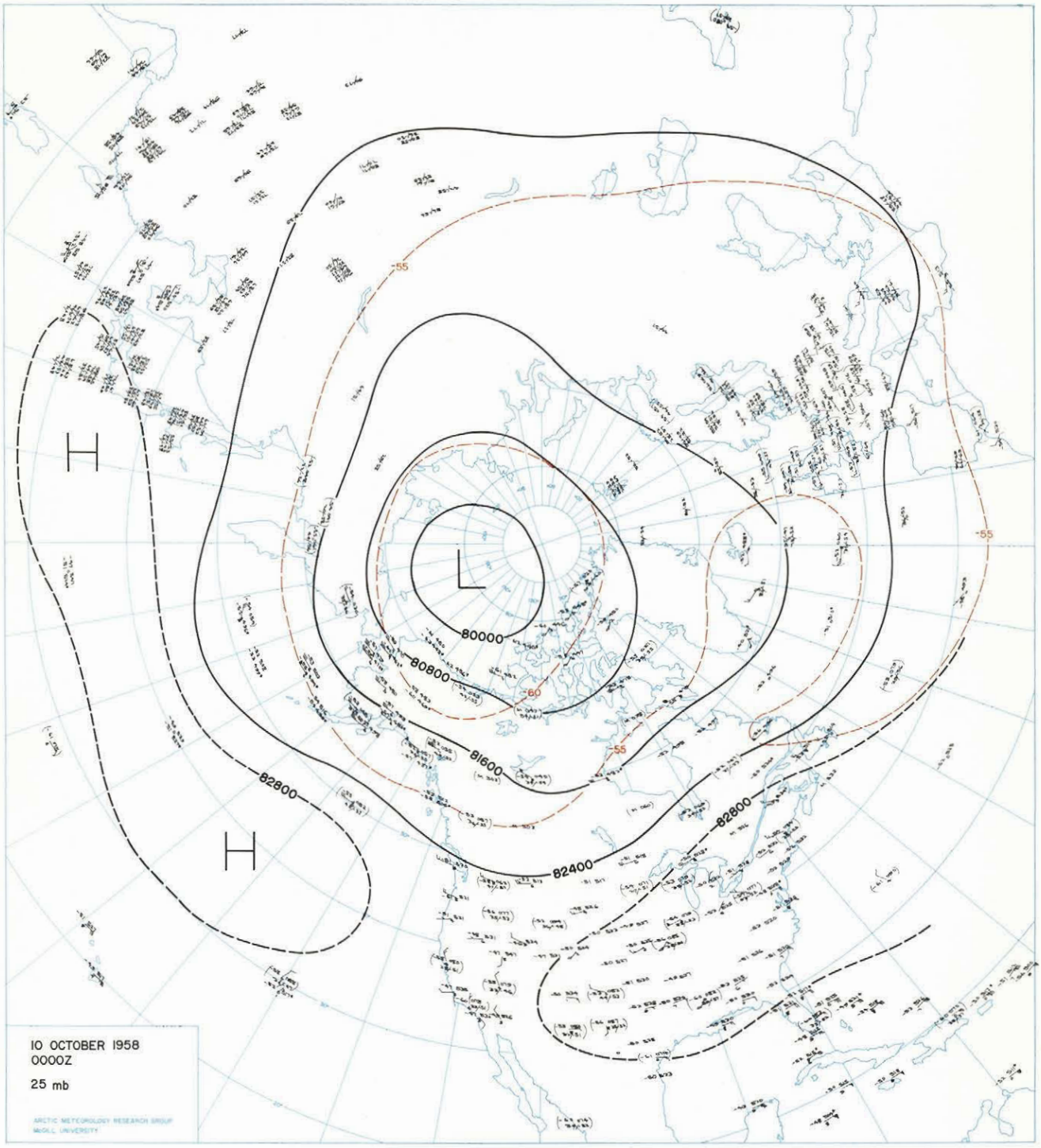
-55
-55
-60
-55
80000
80800
81600
82400
82800
82800
H
H
L
10 OCTOBER 1958
0000Z
25 mb
ARCTIC METEOROLOGY RESEARCH GROUP
McGILL UNIVERSITY

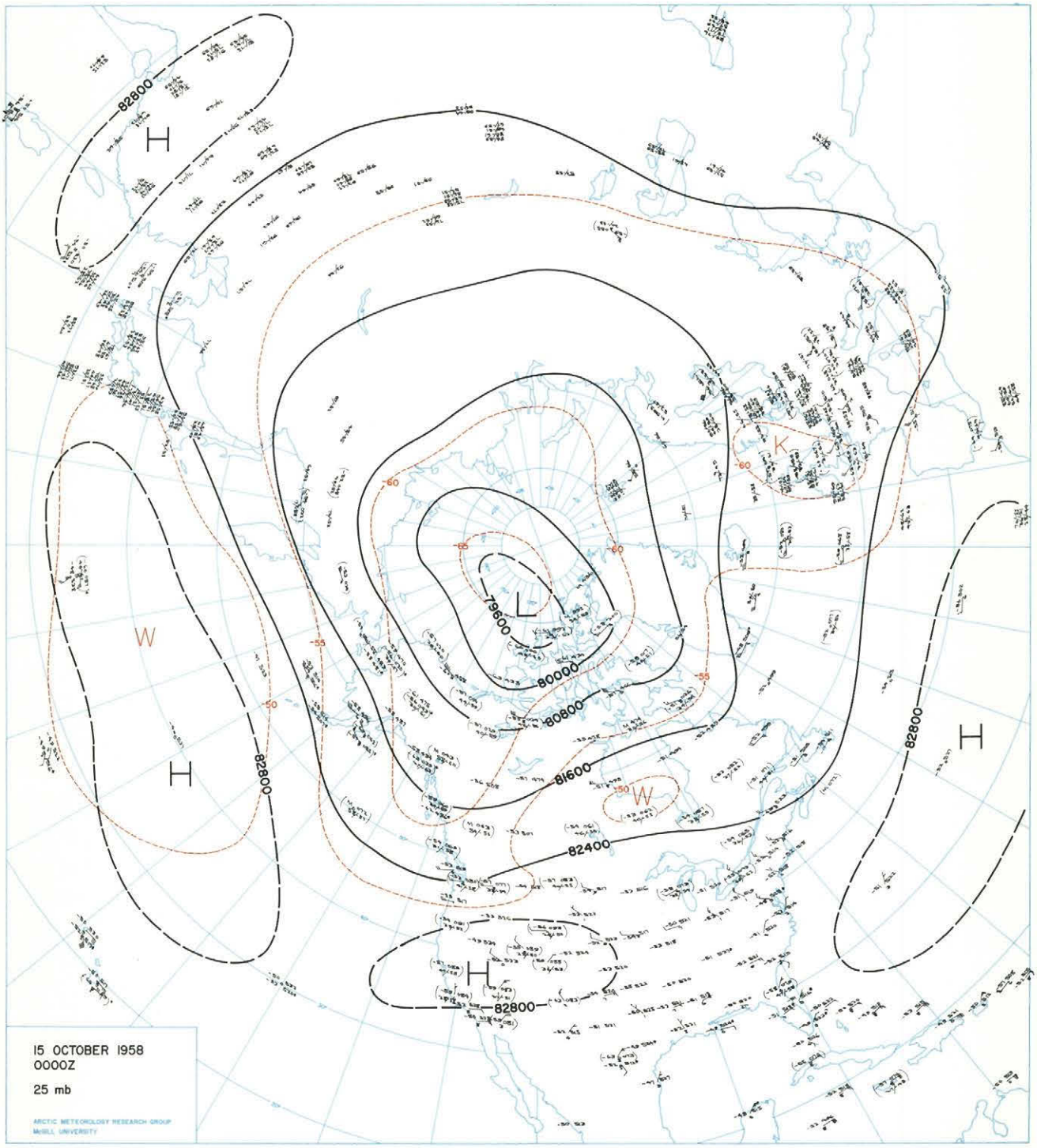
82800
H
K
-60
-65
-60
L
79600
80000
80800
-55
-55
W
-50
81600
-50
W
82400
82800
H
H
82800
H
82800
15 OCTOBER 1958
0000Z
25 mb
ARCTIC METEOROLOGY RESEARCH GROUP
McGILL UNIVERSITY

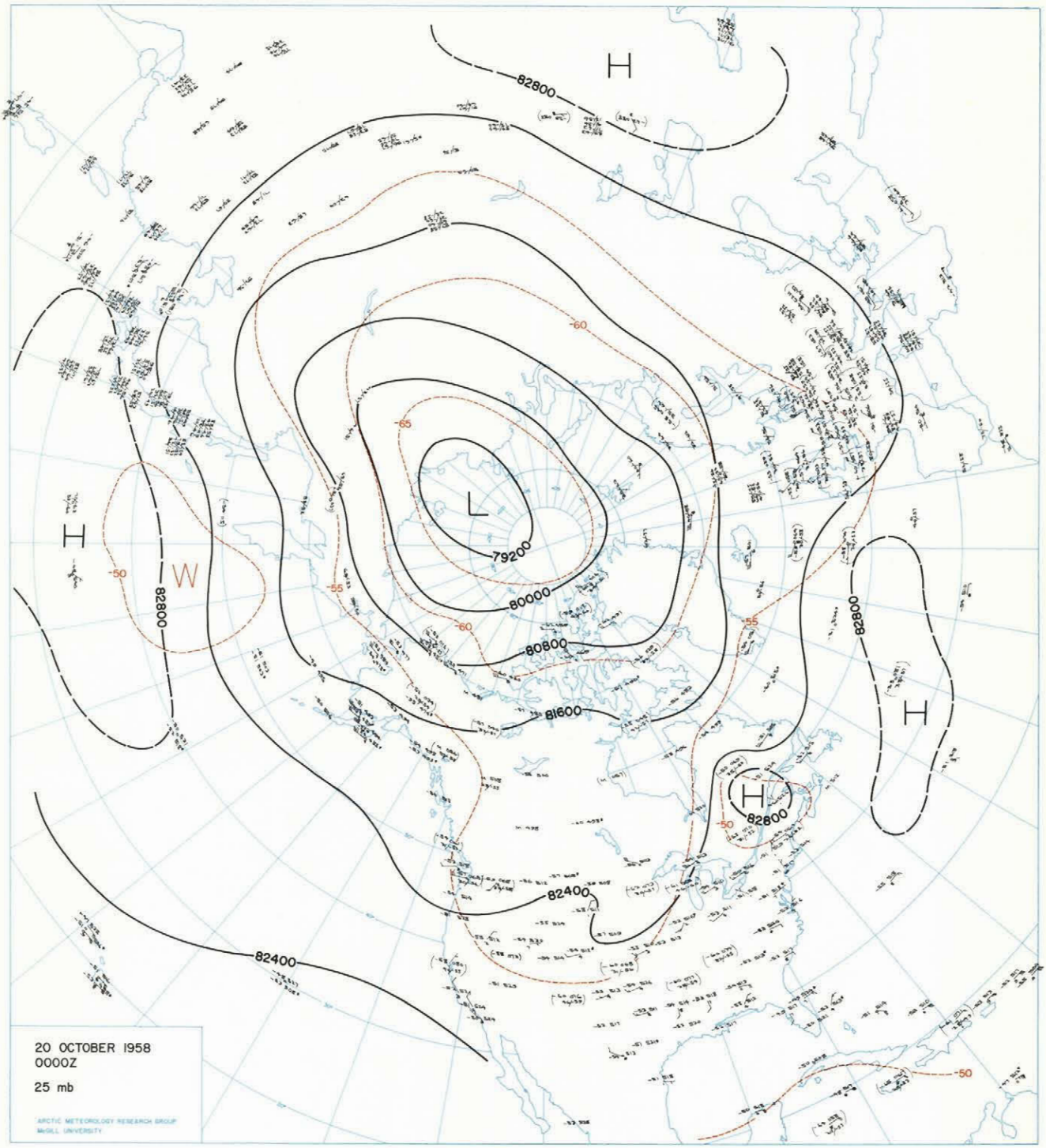
H
82800
-60
-65
L
79200
80000
80800
81600
H
W
-50
-55
82800
82400
82400
H
82800
-50
-55
82800
H
-50
20 OCTOBER 1958
0000Z
25 mb
ARCTIC METEOROLOGY RESEARCH GROUP
McGILL UNIVERSITY

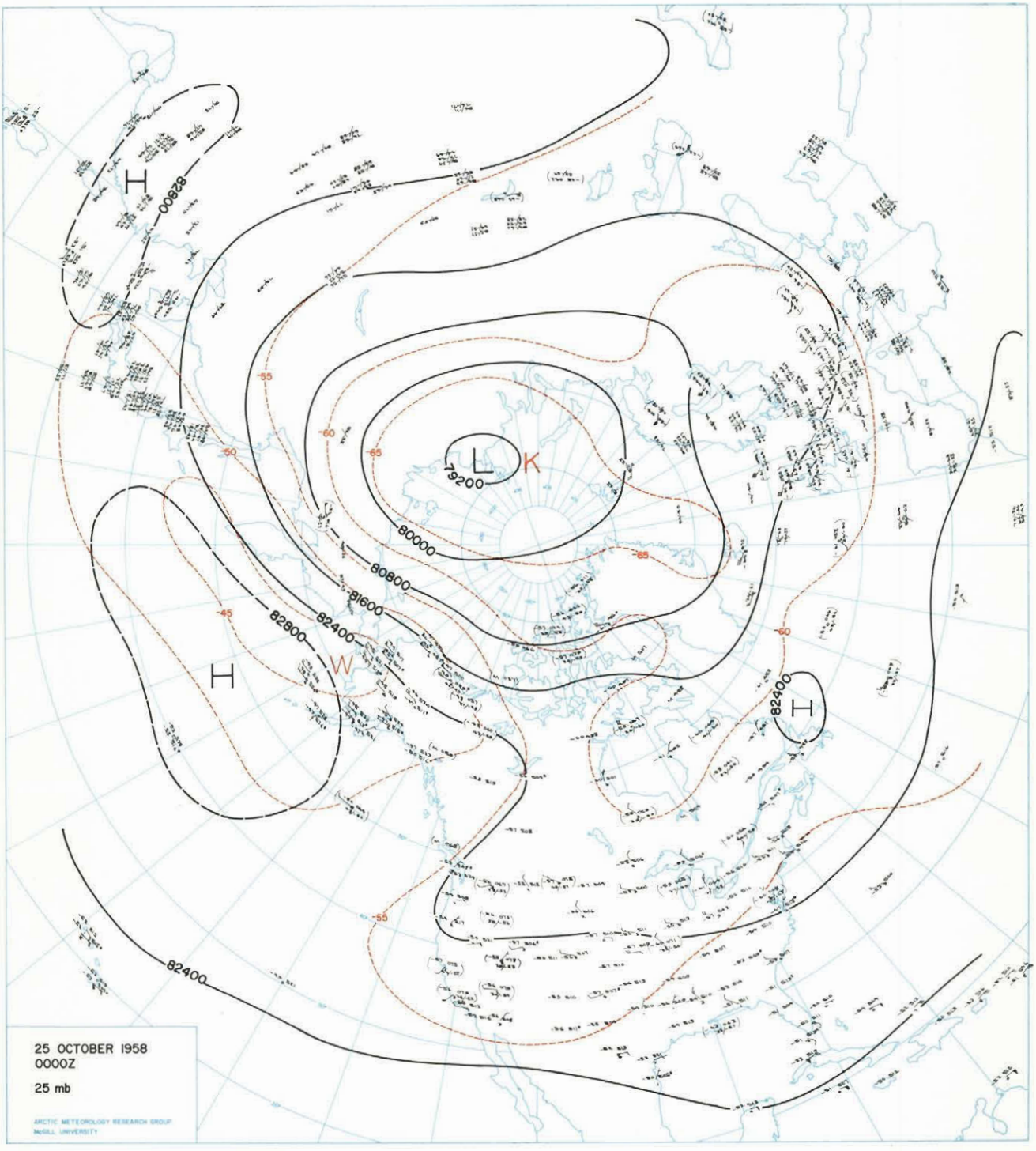
H
82800
L
K
79200
80000
80800
81600
82400
82800
H
W
-45
-50
-55
-60
-65
H
82400
82400
25 OCTOBER 1958
0000Z
25 mb
ARCTIC METEOROLOGY RESEARCH GROUP
McGILL UNIVERSITY

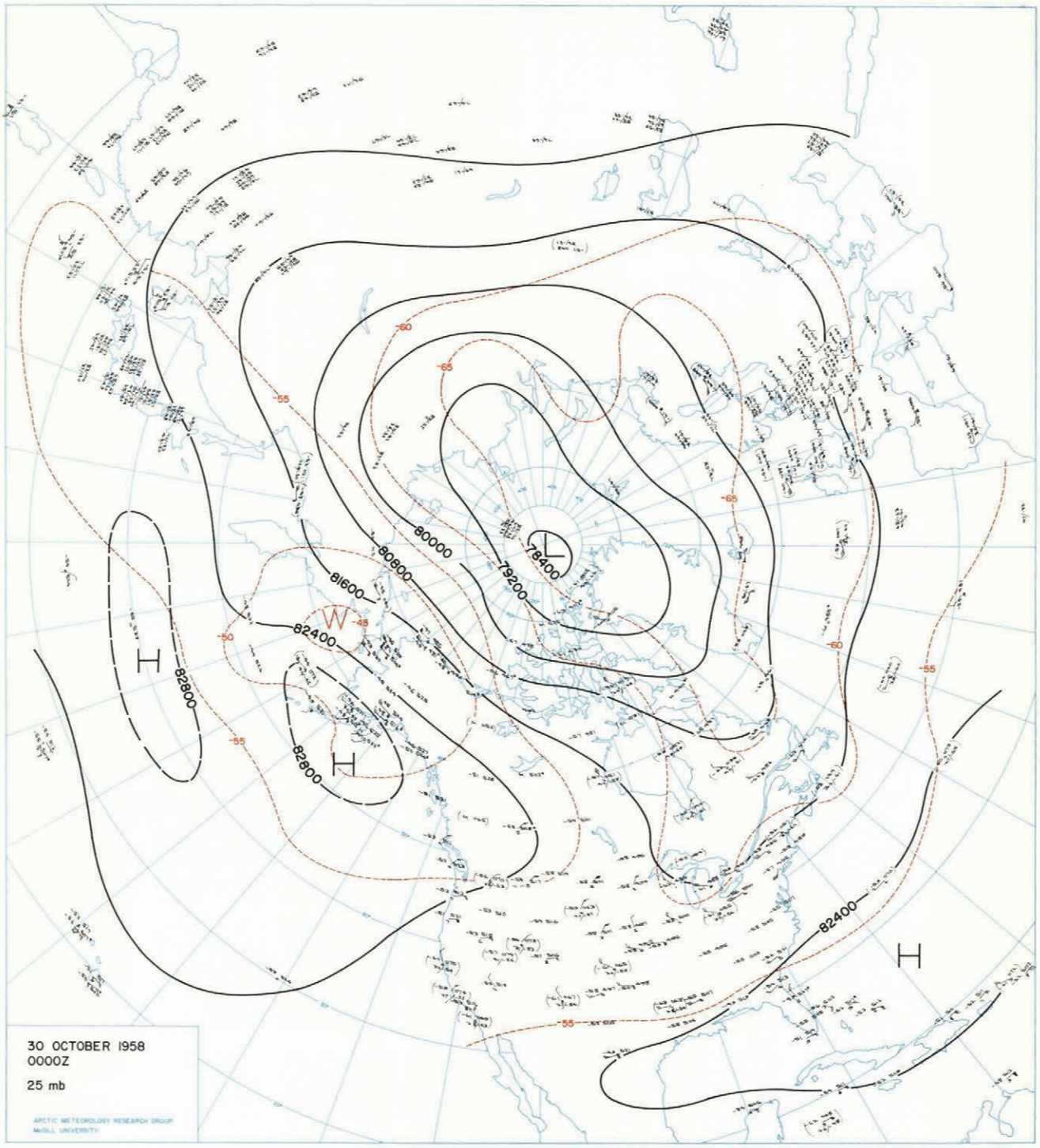
78400
79200
80000
80800
81600
82400
82800
82800
82400
H
H
H
W
-45
-50
-55
-60
-65
-55
-60
-65
-55
-55
30 OCTOBER 1958
0000Z
25 mb
ARCTIC METEOROLOGY RESEARCH GROUP
McGILL UNIVERSITY

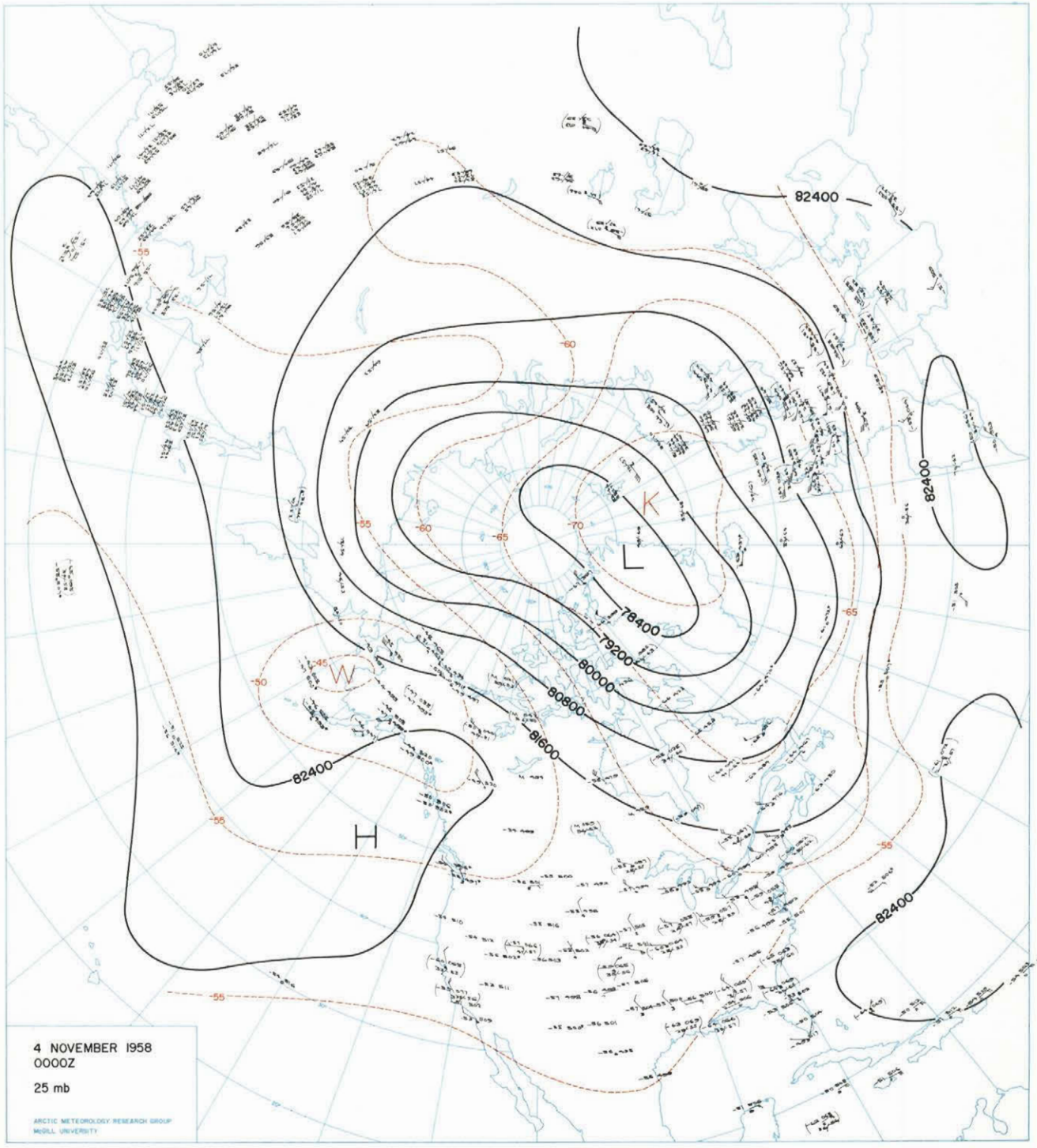
82400
82400
82400
82400
78400
79200
80000
80800
81600
K
L
W
H
-55
-60
-65
-70
-45
-50
4 NOVEMBER 1958
0000Z
25 mb
ARCTIC METEOROLOGY RESEARCH GROUP
McGILL UNIVERSITY

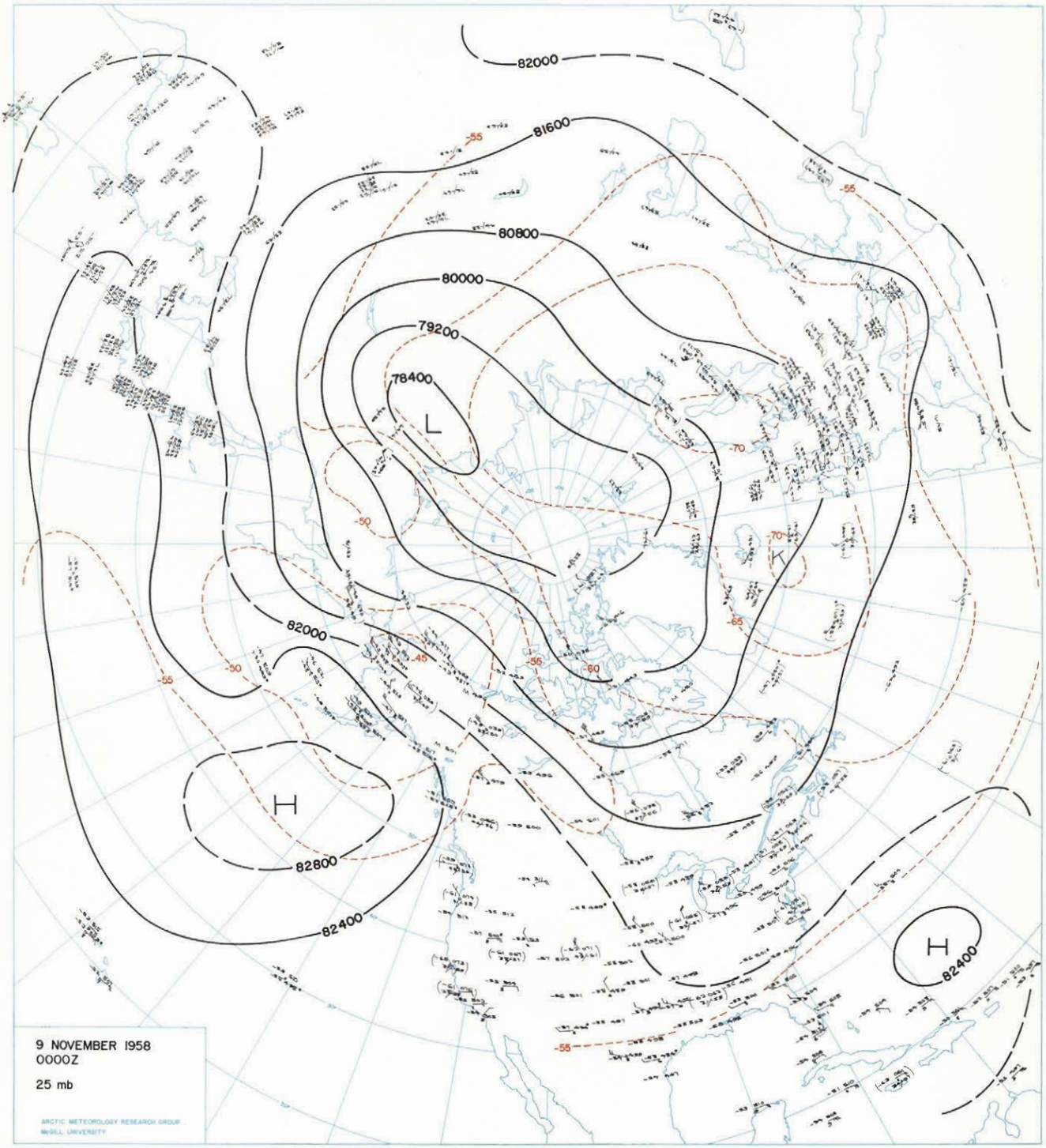
82000
81600
80800
80000
79200
78400
L
82000
82800
82400
H
K
H
82400
-55
-50
-45
-60
-70
-65
9 NOVEMBER 1958
0000Z
25 mb
ARCTIC METEOROLOGY RESEARCH GROUP
McGILL UNIVERSITY

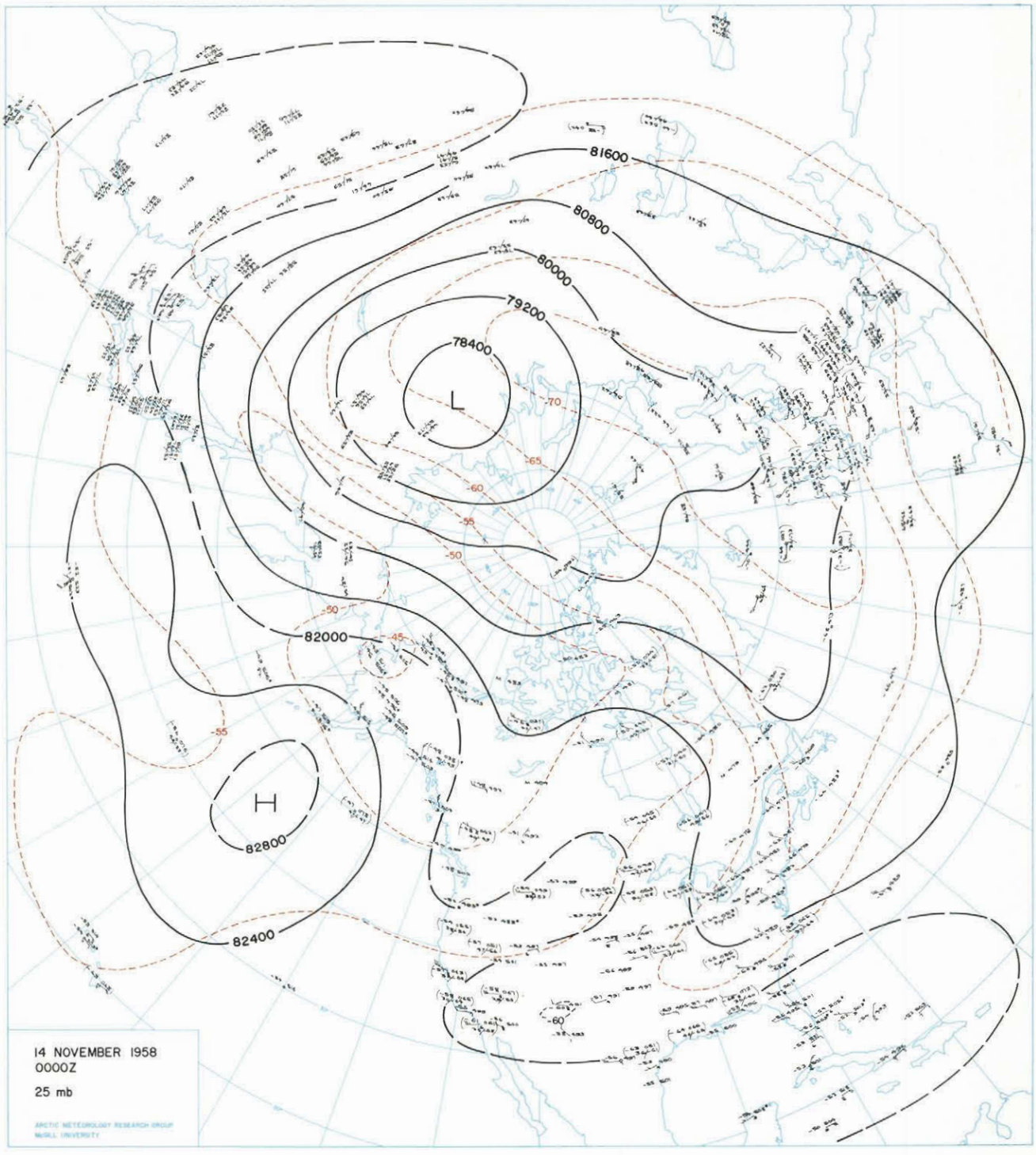
81600
80800
80000
79200
78400
L
-70
-65
-60
-55
-50
-50
82000
-45
-55
H
82800
82400
-60
14 NOVEMBER 1958
0000Z
25 mb
ARCTIC METEOROLOGY RESEARCH GROUP
McGILL UNIVERSITY

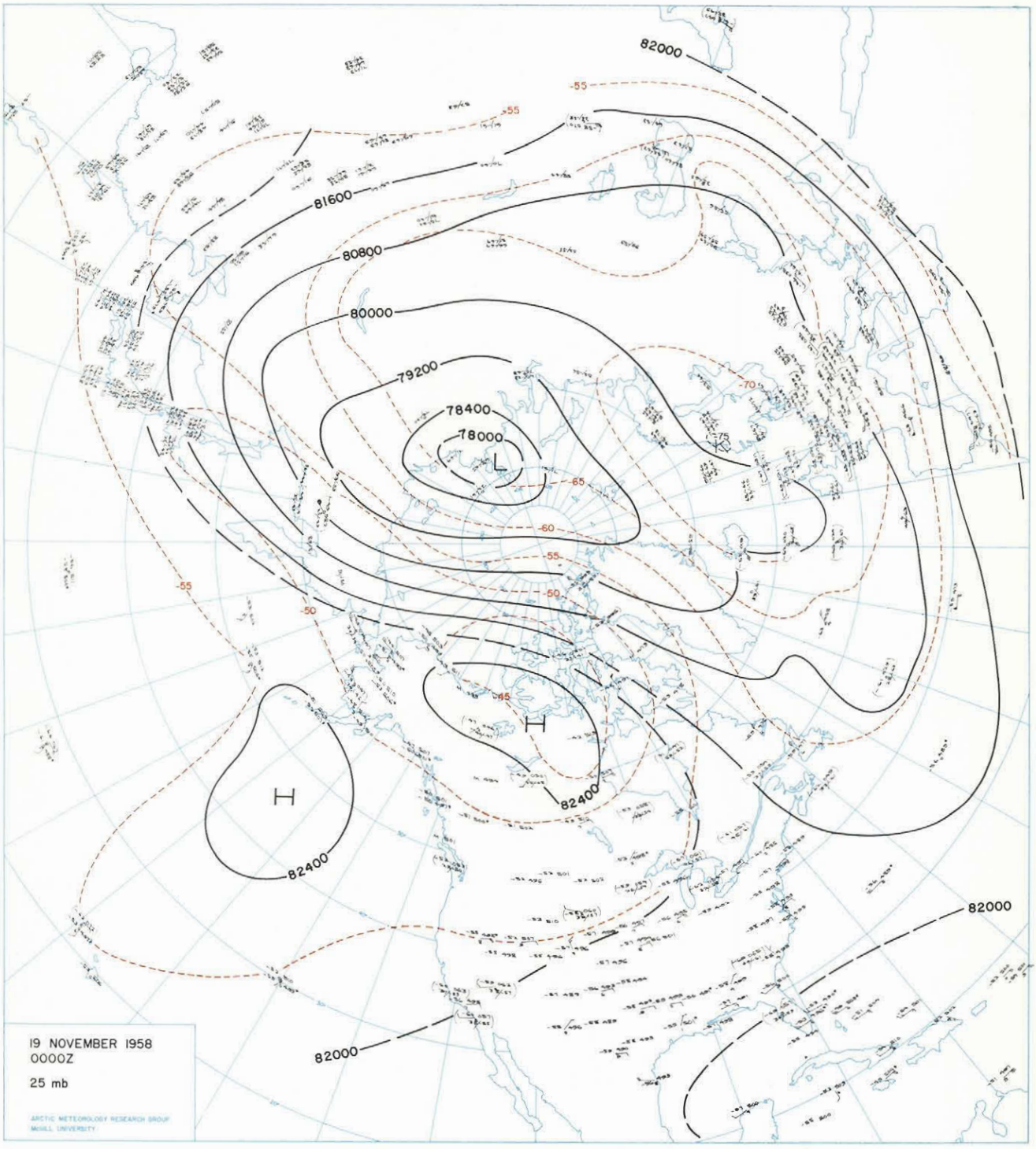
82000
-55
-55
81600
80800
80000
79200
78400
78000
L
-70
-75
-65
-60
-55
-50
-55
-50
-65
H
H
82400
82400
82000
82000
19 NOVEMBER 1958
0000Z
25 mb
ARCTIC METEOROLOGY RESEARCH GROUP
McGILL UNIVERSITY

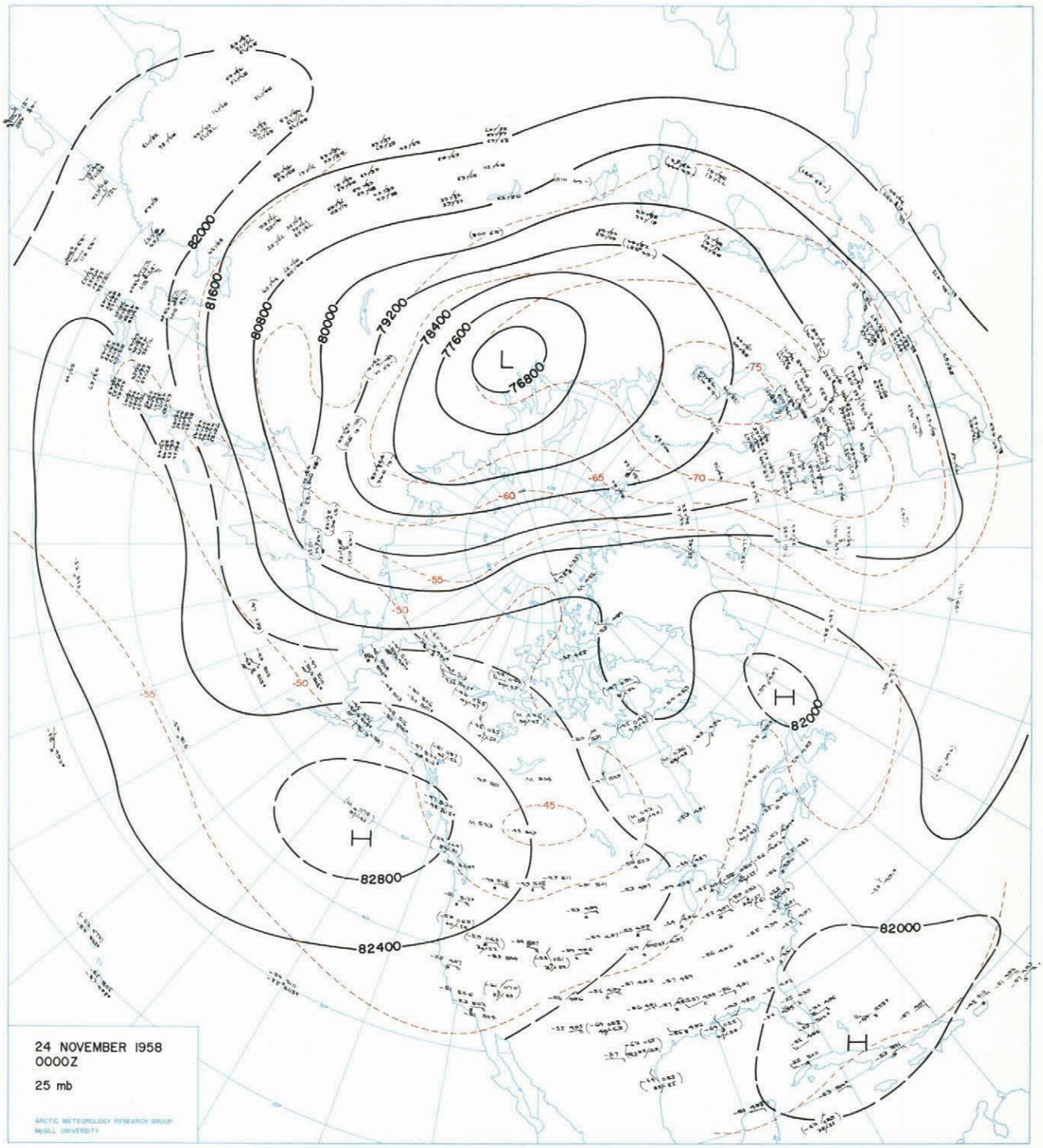
82000
81600
80800
80000
79200
78400
77600
L
76800
-75
-70
-65
-60
-55
-50
-55
-50
-45
H
82800
82400
H
82000
82000
H
24 NOVEMBER 1958
0000Z
25 mb
ARCTIC METEOROLOGY RESEARCH GROUP
McGILL UNIVERSITY

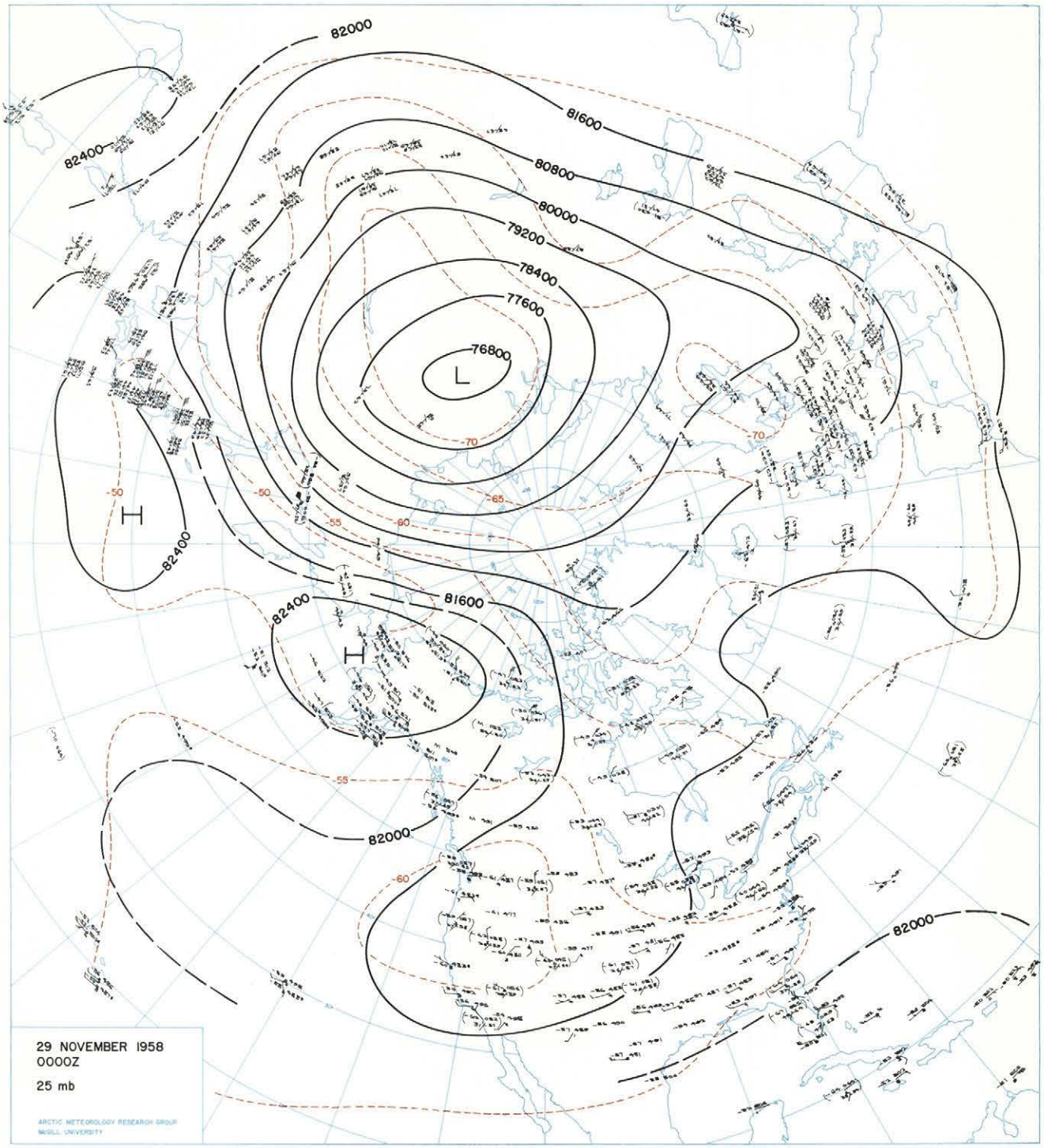
82000
81600
82400
80800
80000
79200
78400
77600
76800
L
H
H
-70
-50
-65
-55
-60
82400
81600
82400
-55
82000
-60
82000
29 NOVEMBER 1958
0000Z
25 mb
ARCTIC METEOROLOGY RESEARCH GROUP
McGILL UNIVERSITY

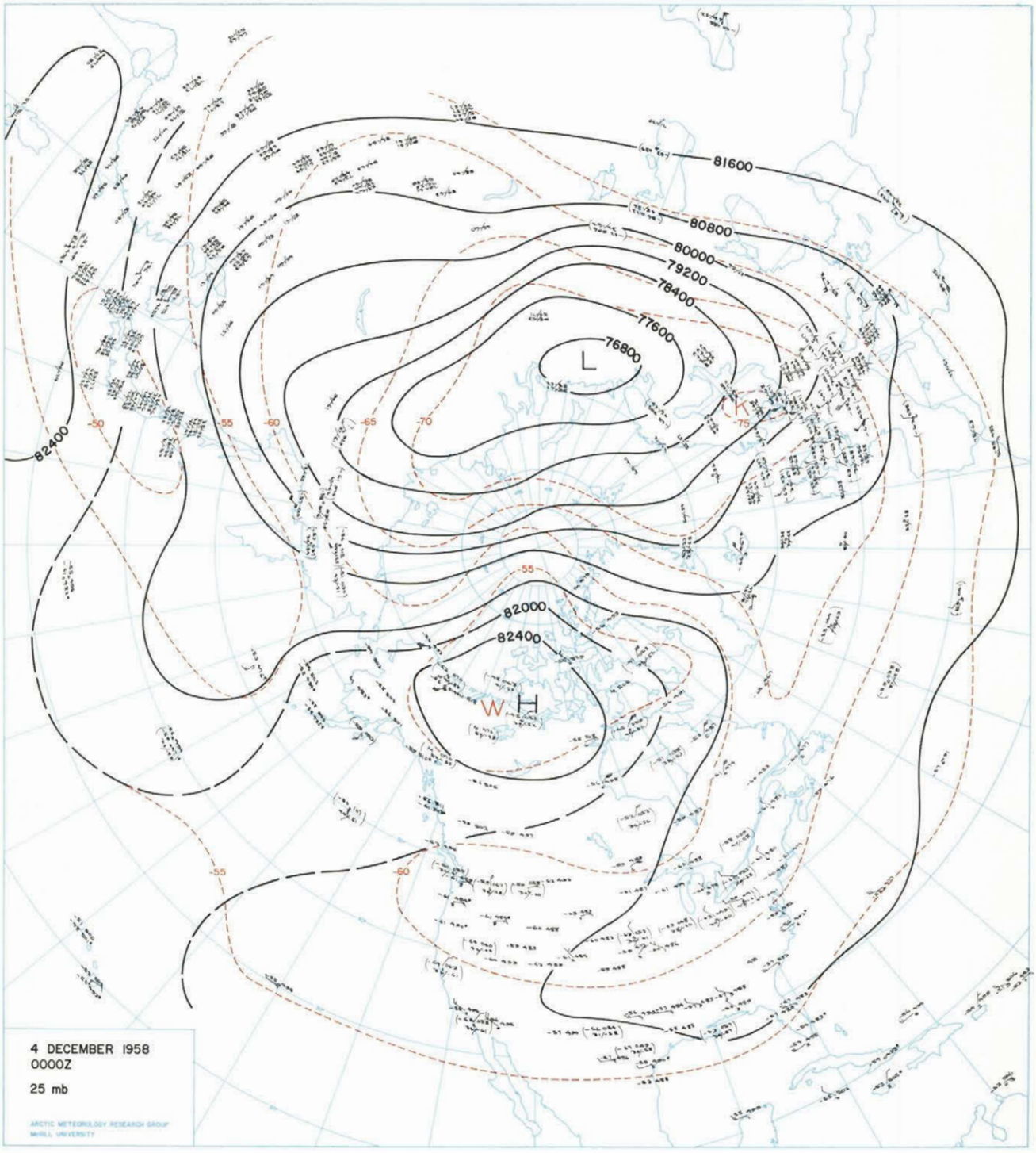
81600
80800
80000
79200
78400
77600
76800
L
H
82400
82000
82400
W H
-50
-55
-60
-65
-70
-75
-55
-55
-60
4 DECEMBER 1958
0000Z
25 mb
ARCTIC METEOROLOGY RESEARCH GROUP
McGILL UNIVERSITY

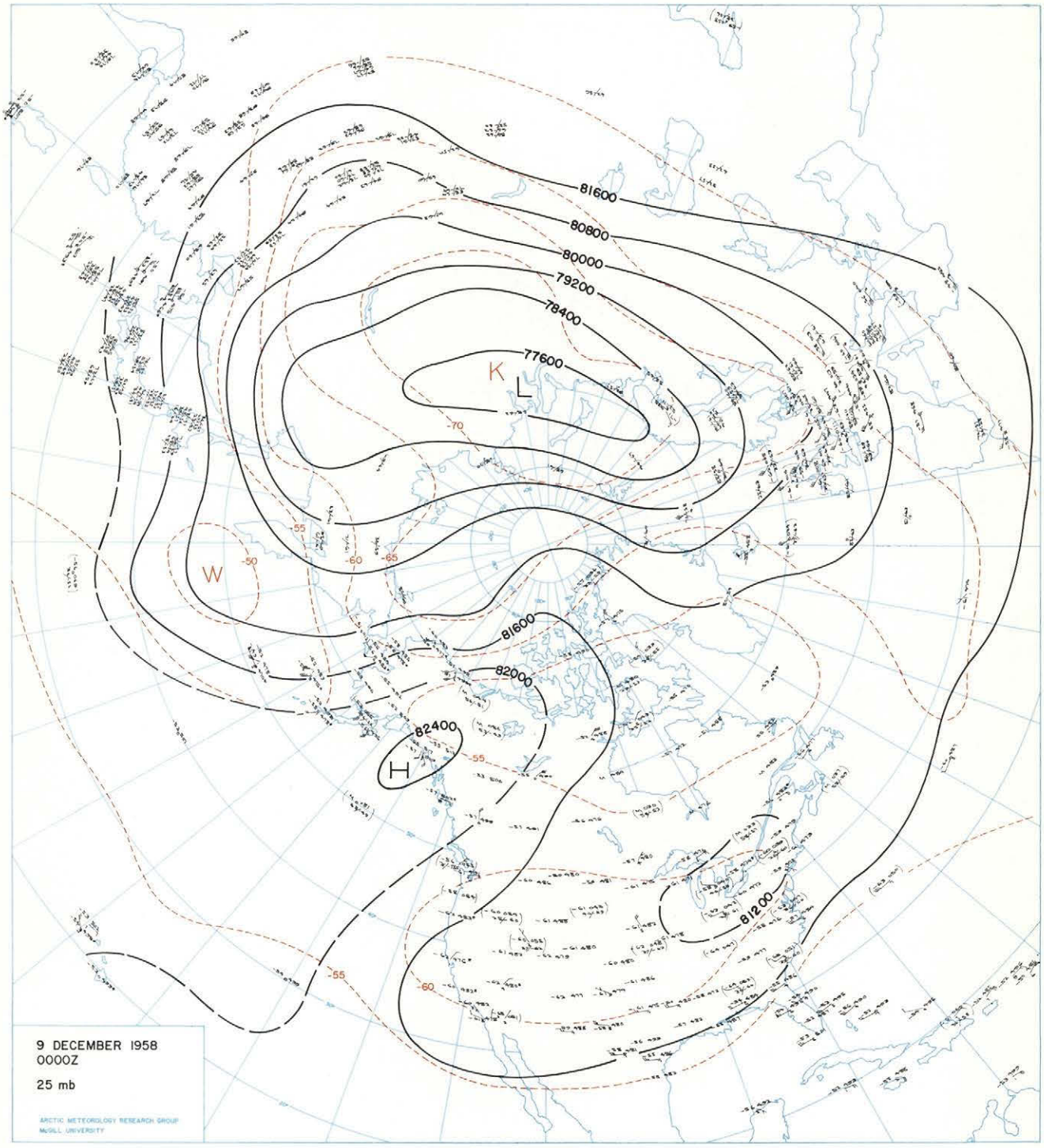
81600
80800
80000
79200
78400
77600
K
L
-70
-55
-50
-60
-65
W
81600
82000
82400
H
-55
-55
-60
81200
9 DECEMBER 1958
0000Z
25 mb
ARCTIC METEOROLOGY RESEARCH GROUP
McGILL UNIVERSITY

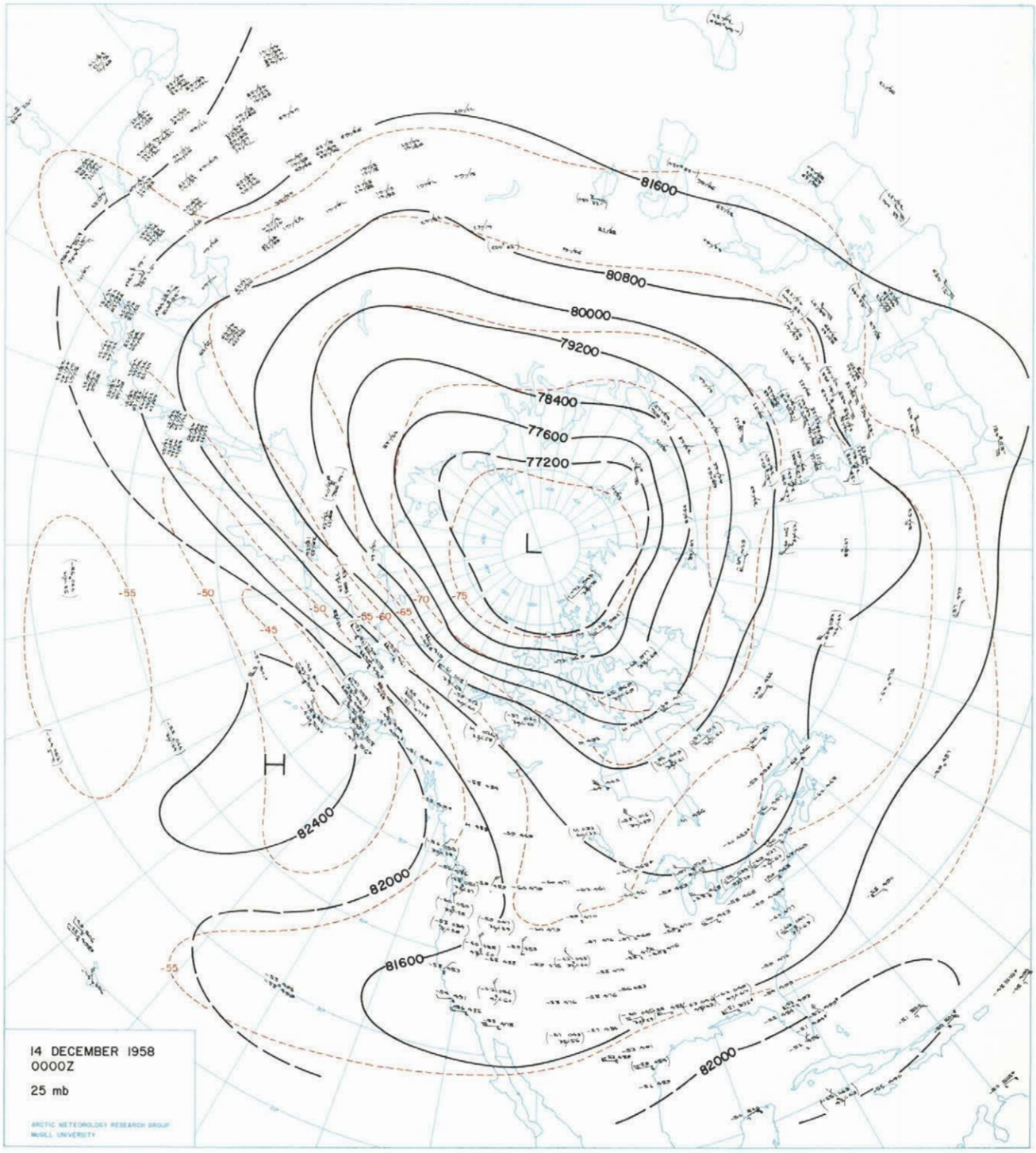
81600
80800
80000
79200
78400
77600
77200
L
H
82400
82000
81600
82000
-55
-50
-45
-50
-55
-60
-65
-70
-75
-55
14 DECEMBER 1958
0000Z
25 mb
ARCTIC METEOROLOGY RESEARCH GROUP
McGILL UNIVERSITY

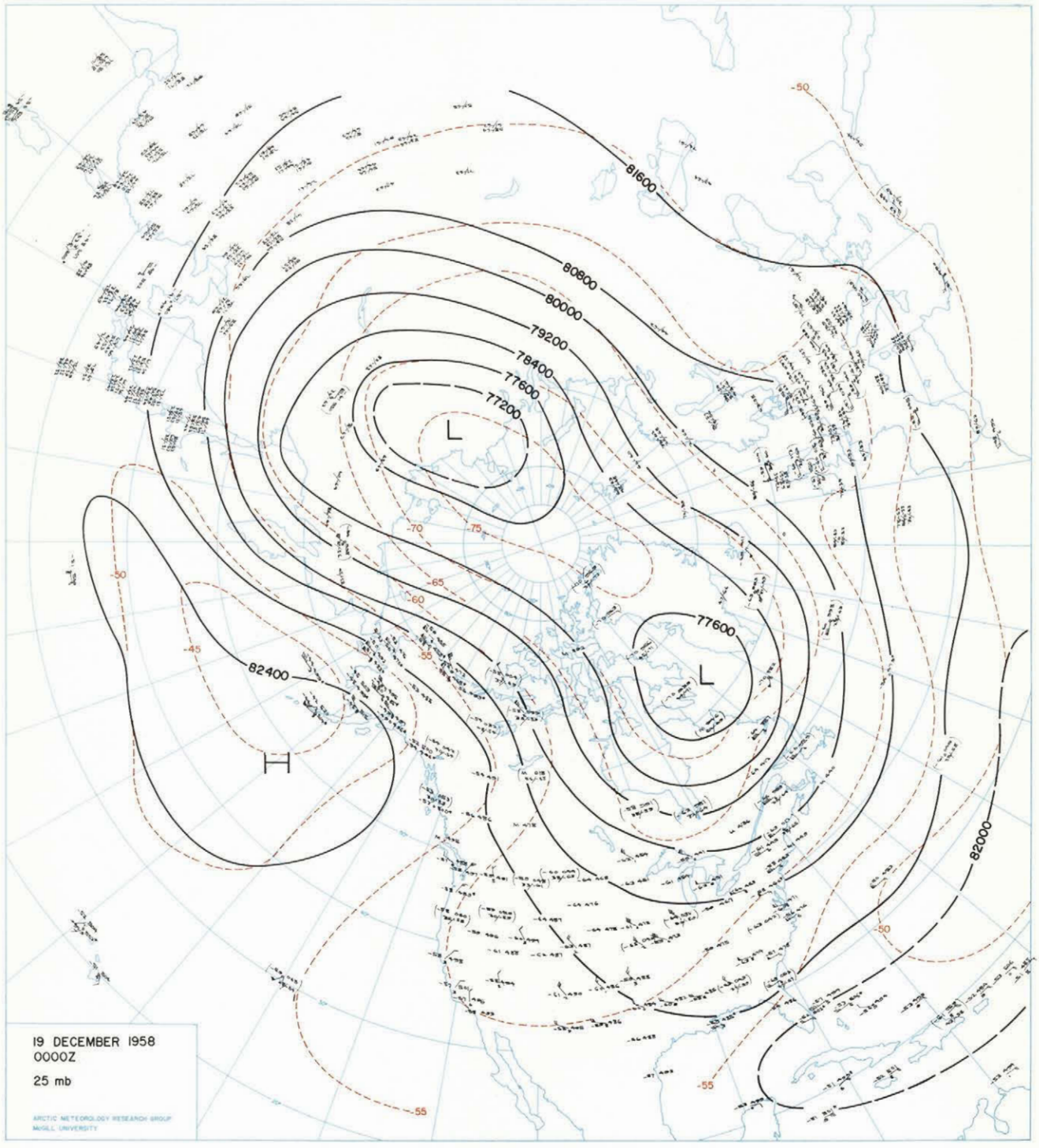
81600
80800
80000
79200
78400
77600
77200
L
-70
-75
-65
-60
-50
-45
-55
82400
H
77600
L
L
82000
-50
-55
-50
-55
19 DECEMBER 1958
0000Z
25 mb
ARCTIC METEOROLOGY RESEARCH GROUP
McGILL UNIVERSITY

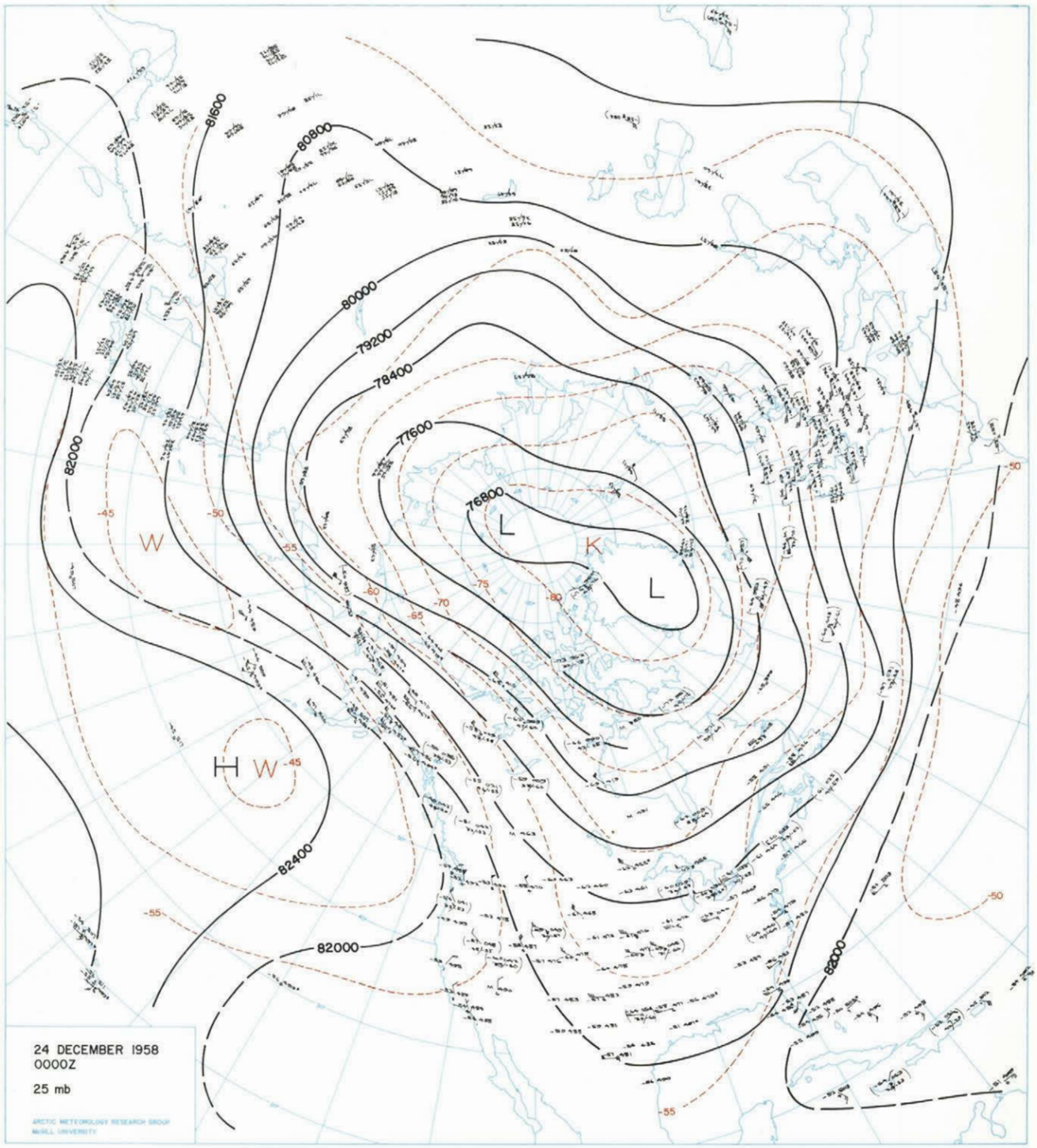
81600
80800
80000
79200
78400
77600
76800
82000
82400
L
K
L
W
H
W
-45
-50
-55
-60
-65
-70
-75
-80
-50
-55
24 DECEMBER 1958
0000Z
25 mb
ARCTIC METEOROLOGY RESEARCH GROUP
McGILL UNIVERSITY

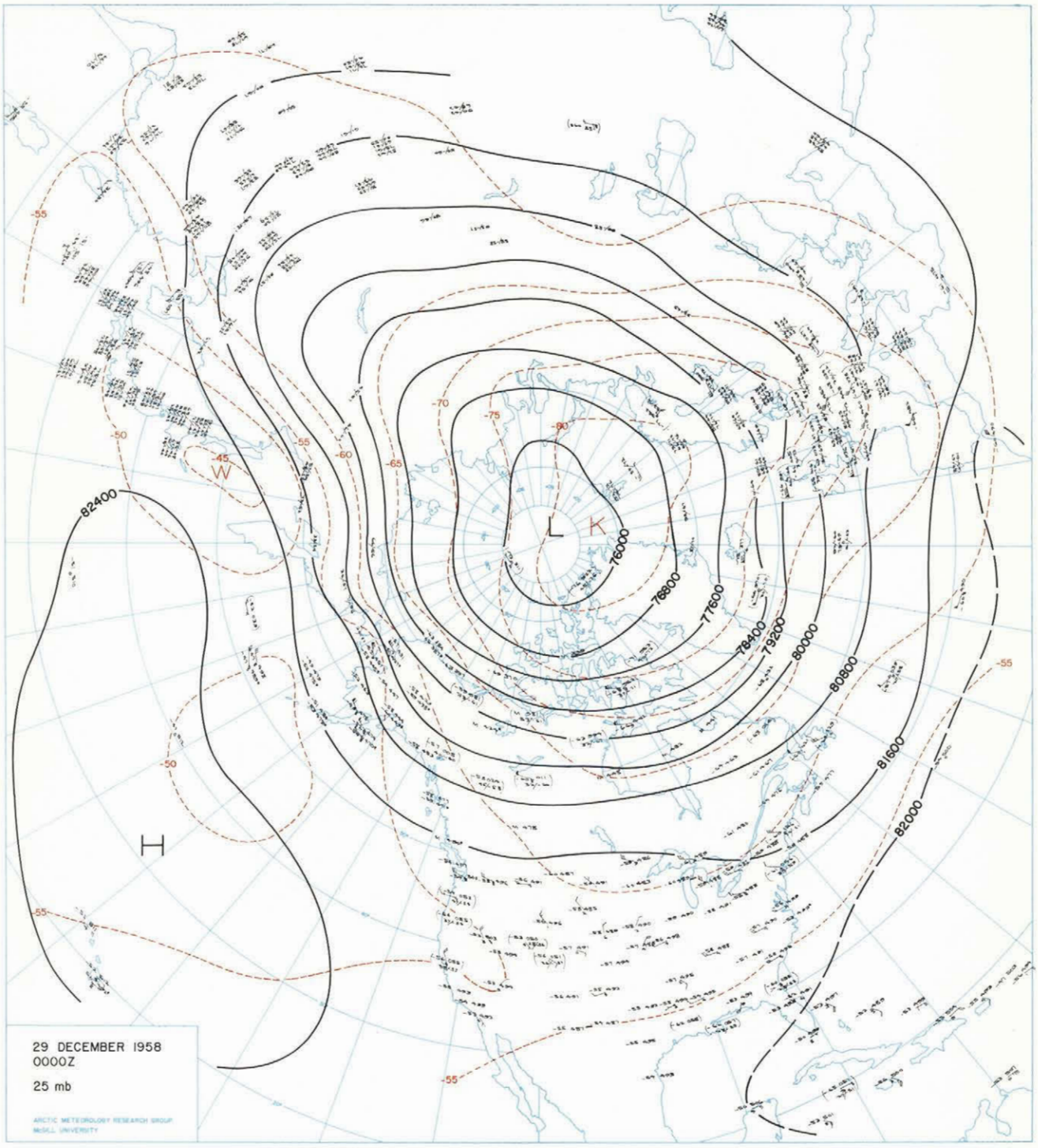
-55
-50
-45
W
-55
-60
-65
-70
-75
-80
82400
L
K
76000
76800
77600
78400
79200
80000
80800
81600
82000
-55
-50
H
-55
-55
29 DECEMBER 1958
0000Z
25 mb
ARCTIC METEOROLOGY RESEARCH GROUP
McGILL UNIVERSITY

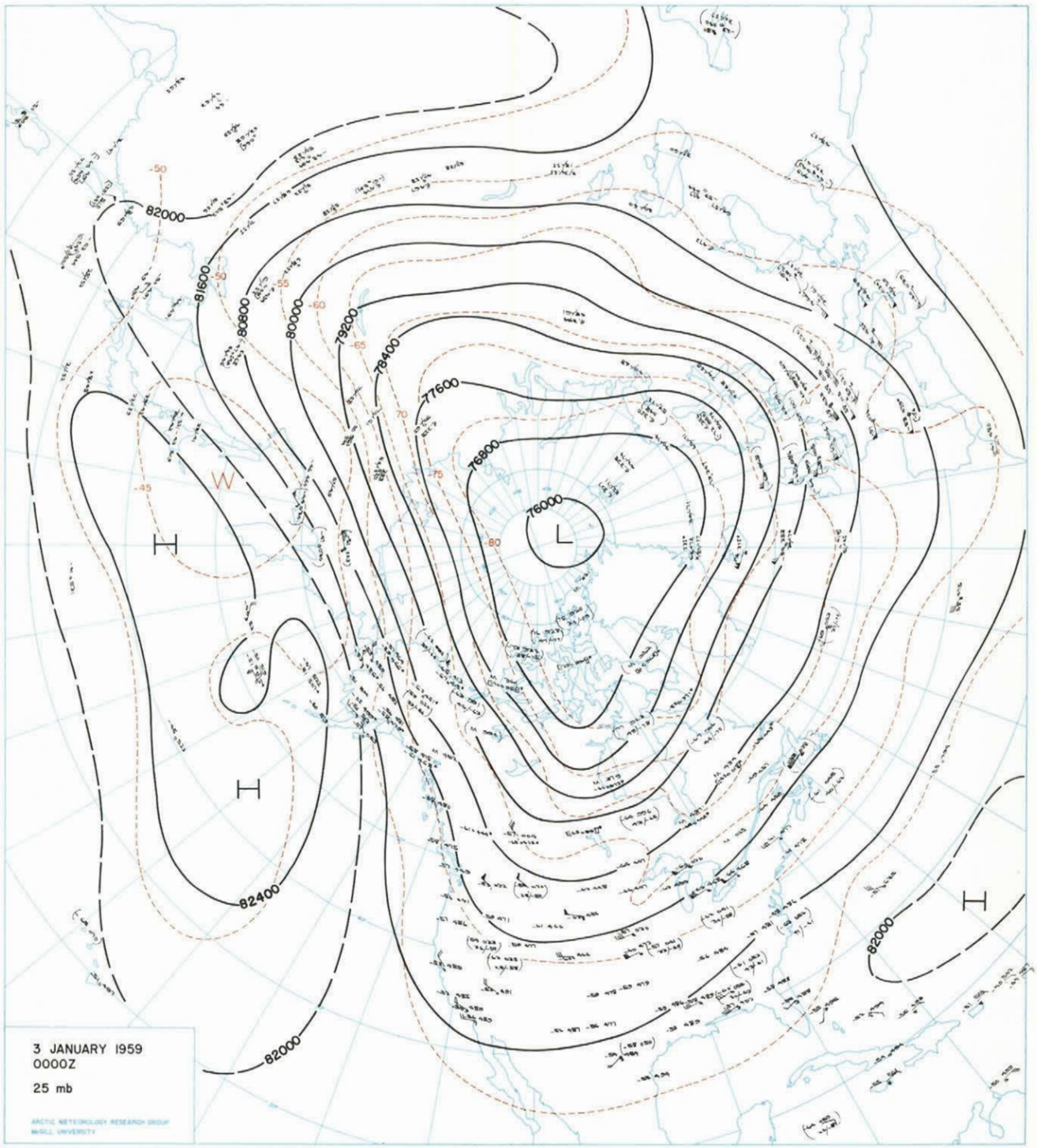
82000
81600
80800
80000
79200
78400
77600
76800
76000
82400
82000
82000
-50
-50
-55
-60
-65
-70
-75
-80
-45
W
H
H
H
L
3 JANUARY 1959
0000Z
25 mb
ARCTIC METEOROLOGY RESEARCH GROUP
McGILL UNIVERSITY

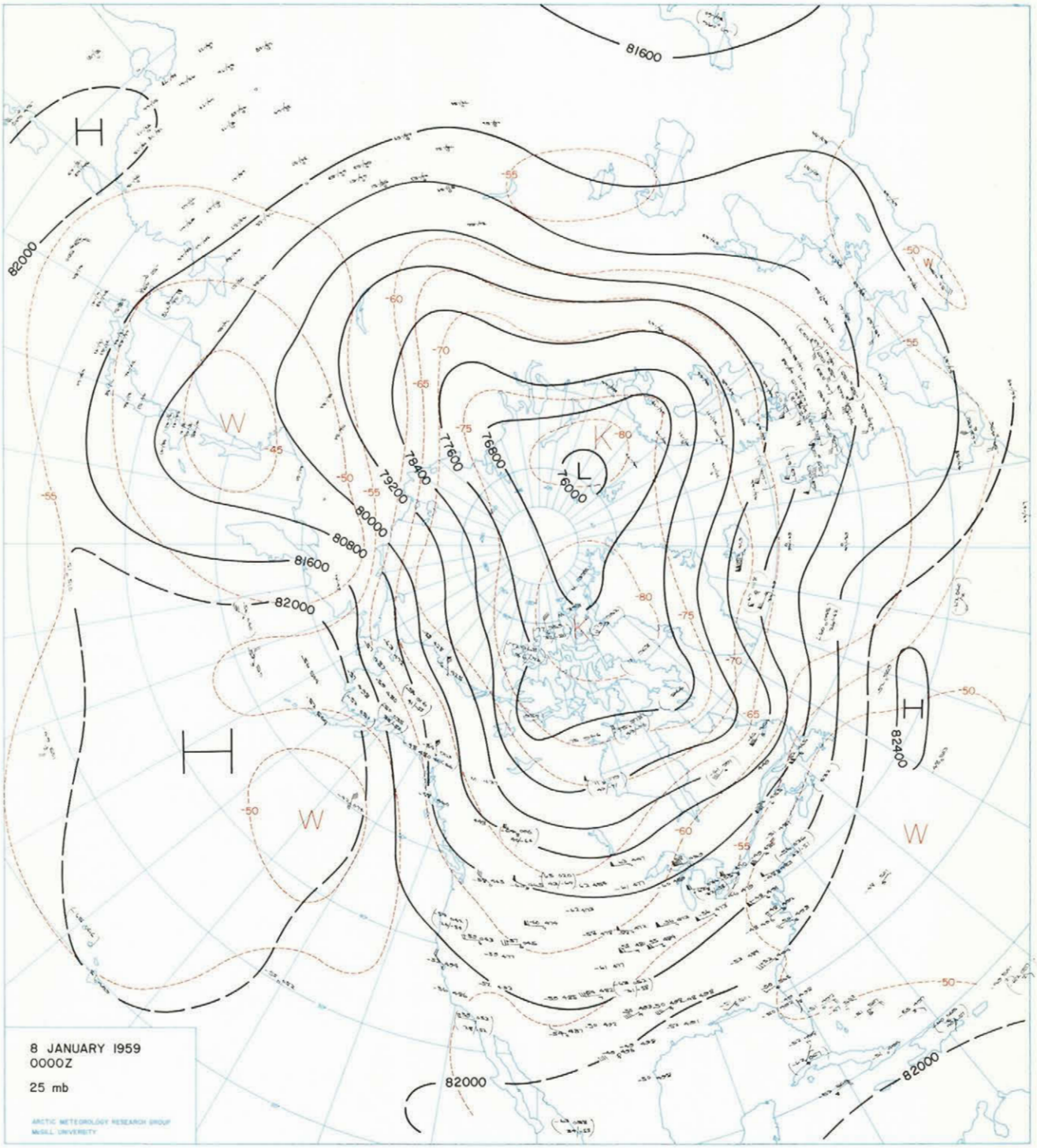
81600
82000
H
W
-55
-50
-60
-70
-65
-75
77600
76800
K
-80
76000
L
78400
79200
80000
80800
81600
82000
-45
-50
-55
H
W
-50
-80
-75
K
-70
-65
H
82400
-50
W
-60
-55
-50
82000
82000
8 JANUARY 1959
0000Z
25 mb
ARCTIC METEOROLOGY RESEARCH GROUP
McGILL UNIVERSITY

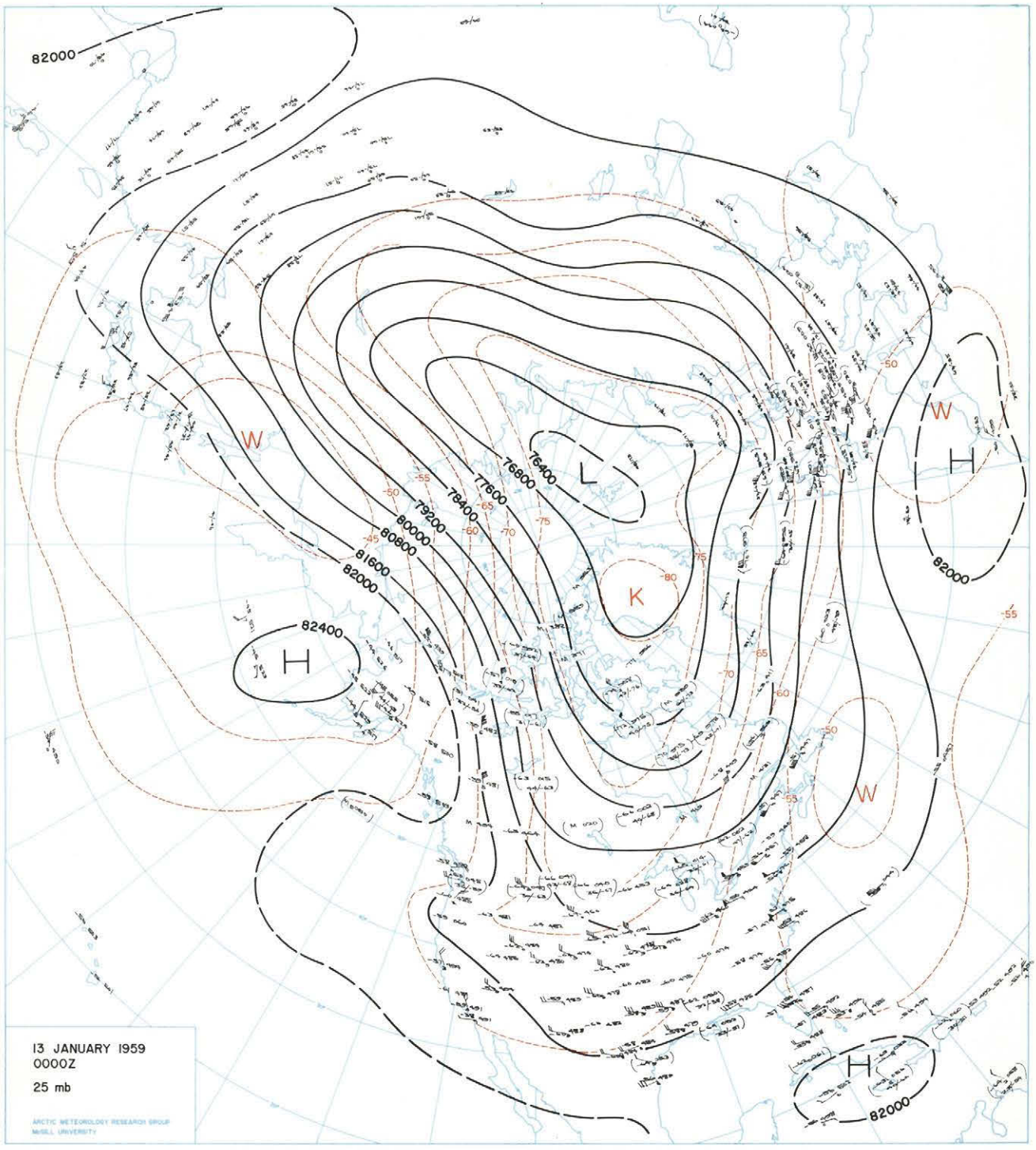
82000
W
76400
76800
77600
78400
79200
80000
80800
81600
82000
L
K
82400
H
W
H
82000
W
H
82000
-50
-55
-60
-65
-70
-75
-80
-45
13 JANUARY 1959
0000Z
25 mb
ARCTIC METEOROLOGY RESEARCH GROUP
McGILL UNIVERSITY

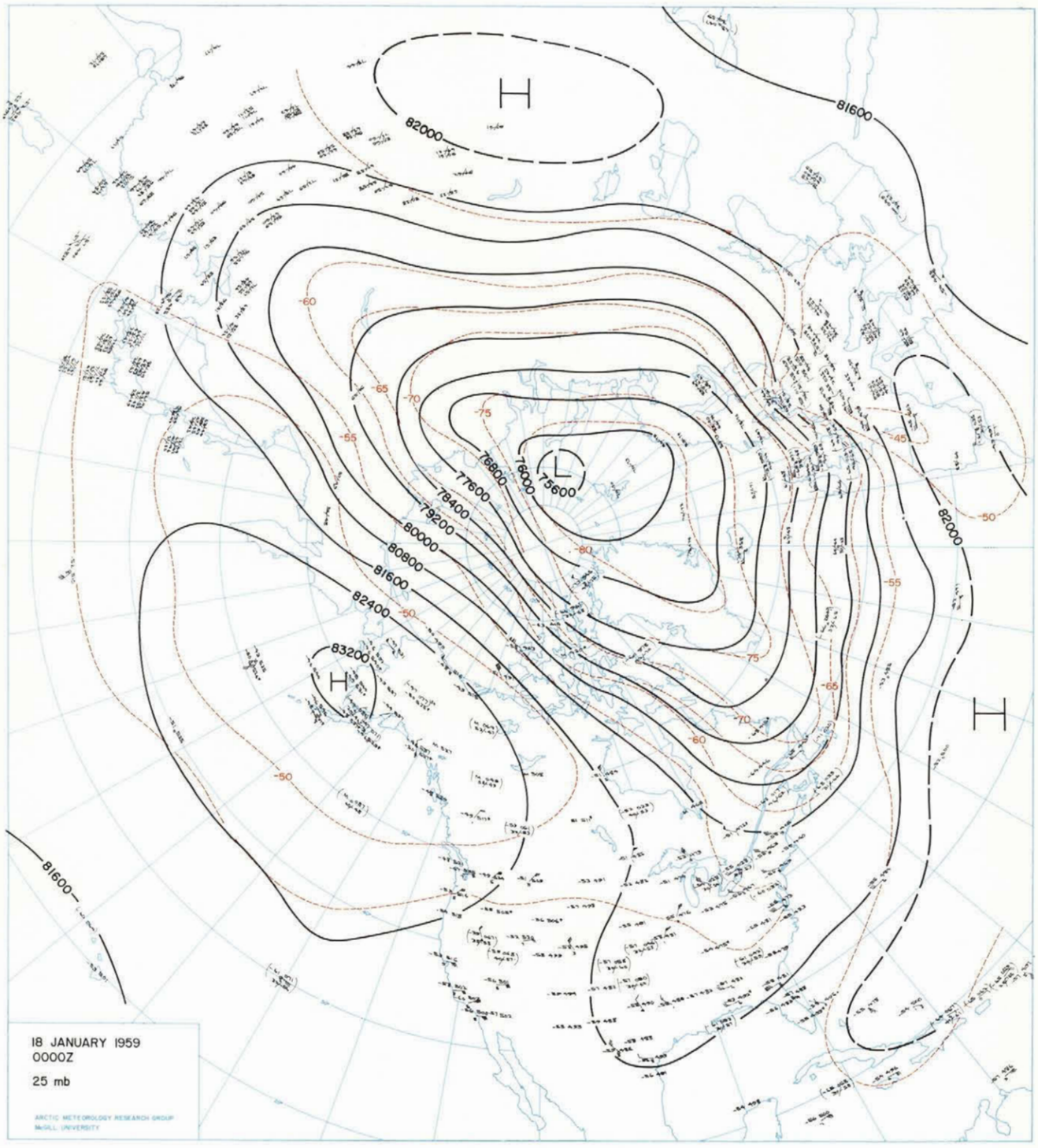
H
82000
81600
-60
-65
-70
-75
-55
L
76800
76000
75600
77600
78400
79200
80000
80800
81600
82400
-80
-50
-45
82000
-50
-55
83200
H
-75
-65
-70
-60
H
-50
81600
18 JANUARY 1959
0000Z
25 mb
ARCTIC METEOROLOGY RESEARCH GROUP
McGILL UNIVERSITY

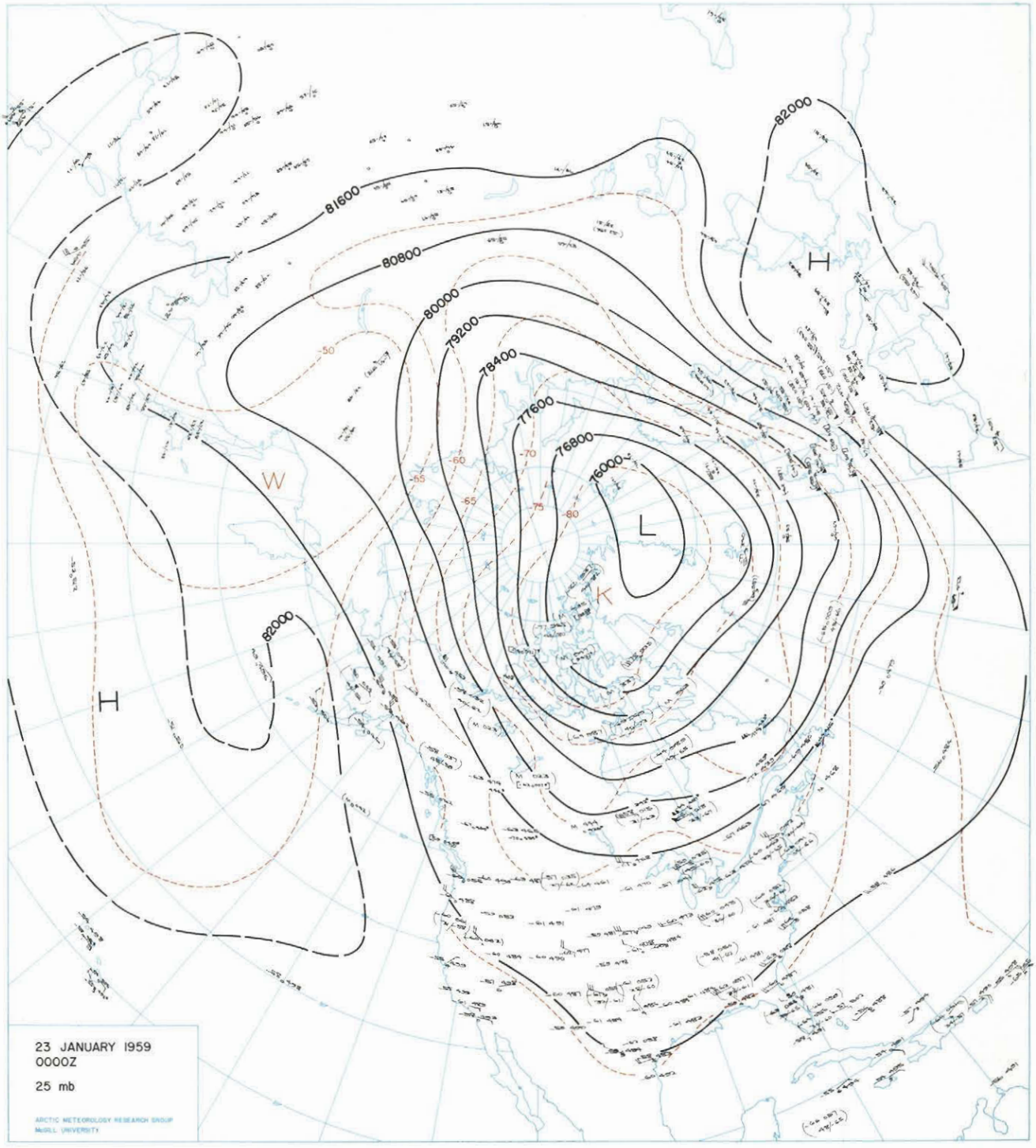
82000
81600
80800
80000
79200
78400
77600
76800
76000
H
L
K
W
H
-50
-60
-65
-55
-75
-70
-80
23 JANUARY 1959
0000Z
25 mb
ARCTIC METEOROLOGY RESEARCH GROUP
McGILL UNIVERSITY

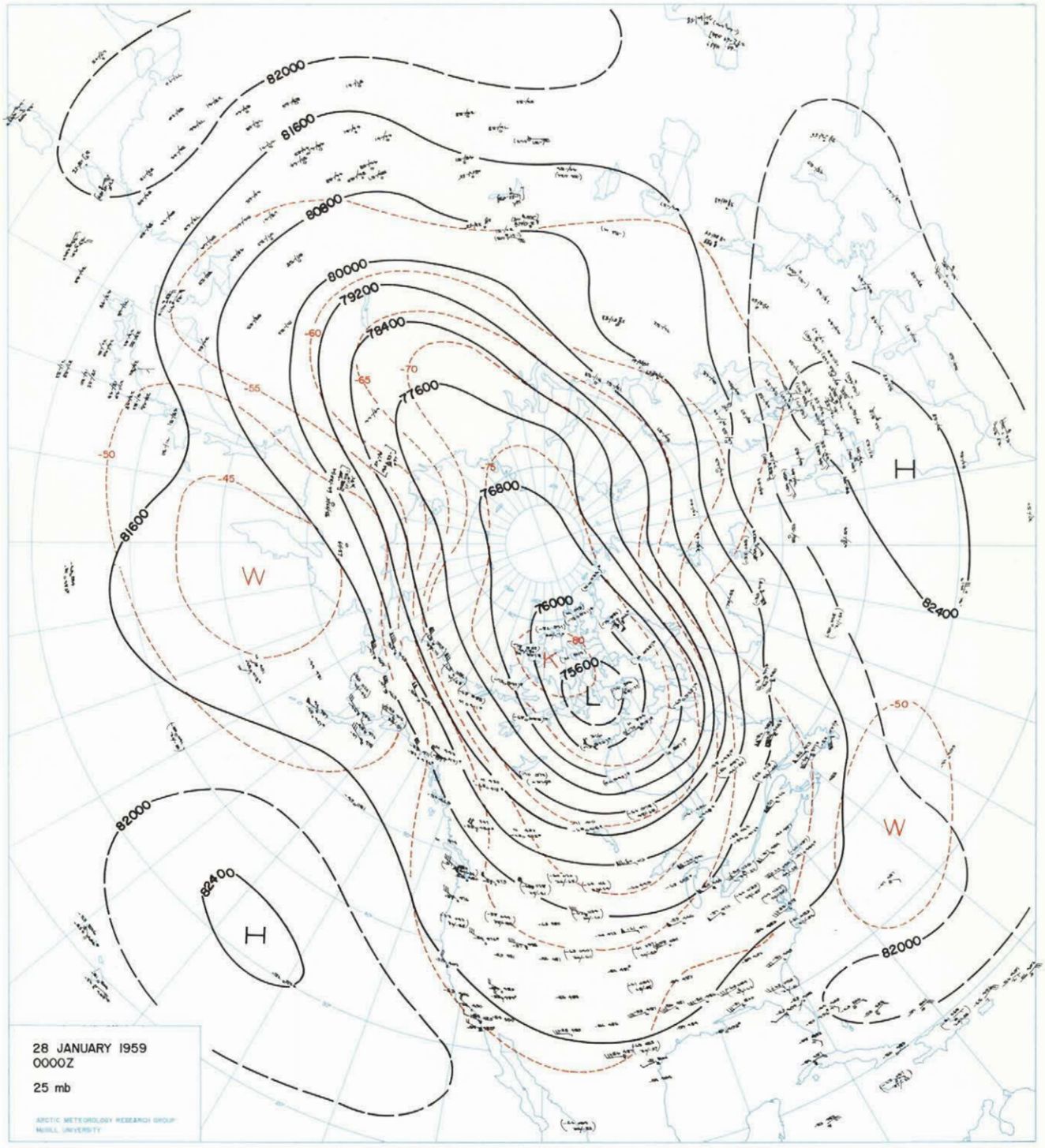
82000
81600
80800
80000
79200
78400
77600
76800
76000
75600
82400
81600
82000
82400
-50
-45
-55
-60
-65
-70
-75
-80
-50
H
W
K
L
H
W
28 JANUARY 1959
0000Z
25 mb
ARCTIC METEOROLOGY RESEARCH GROUP
McGILL UNIVERSITY

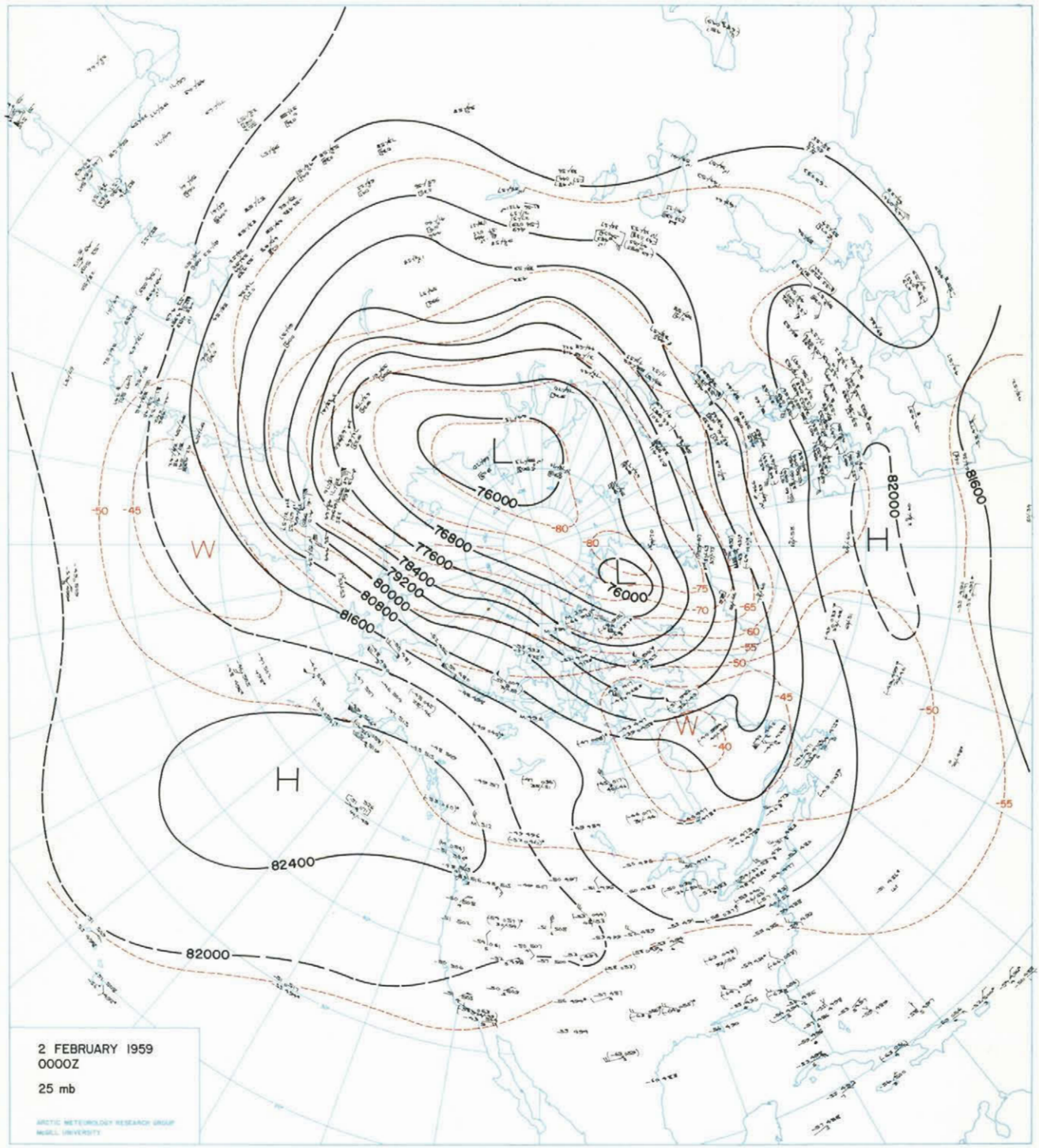
L
76000
76800
77600
78400
79200
80000
80800
81600
82000
L
76000
H
82000
H
82400
82000
W
W
-50
-45
-80
-80
-75
-70
-65
-60
-55
-50
-45
-40
-50
-55
2 FEBRUARY 1959
0000Z
25 mb
ARCTIC METEOROLOGY RESEARCH GROUP
McGILL UNIVERSITY

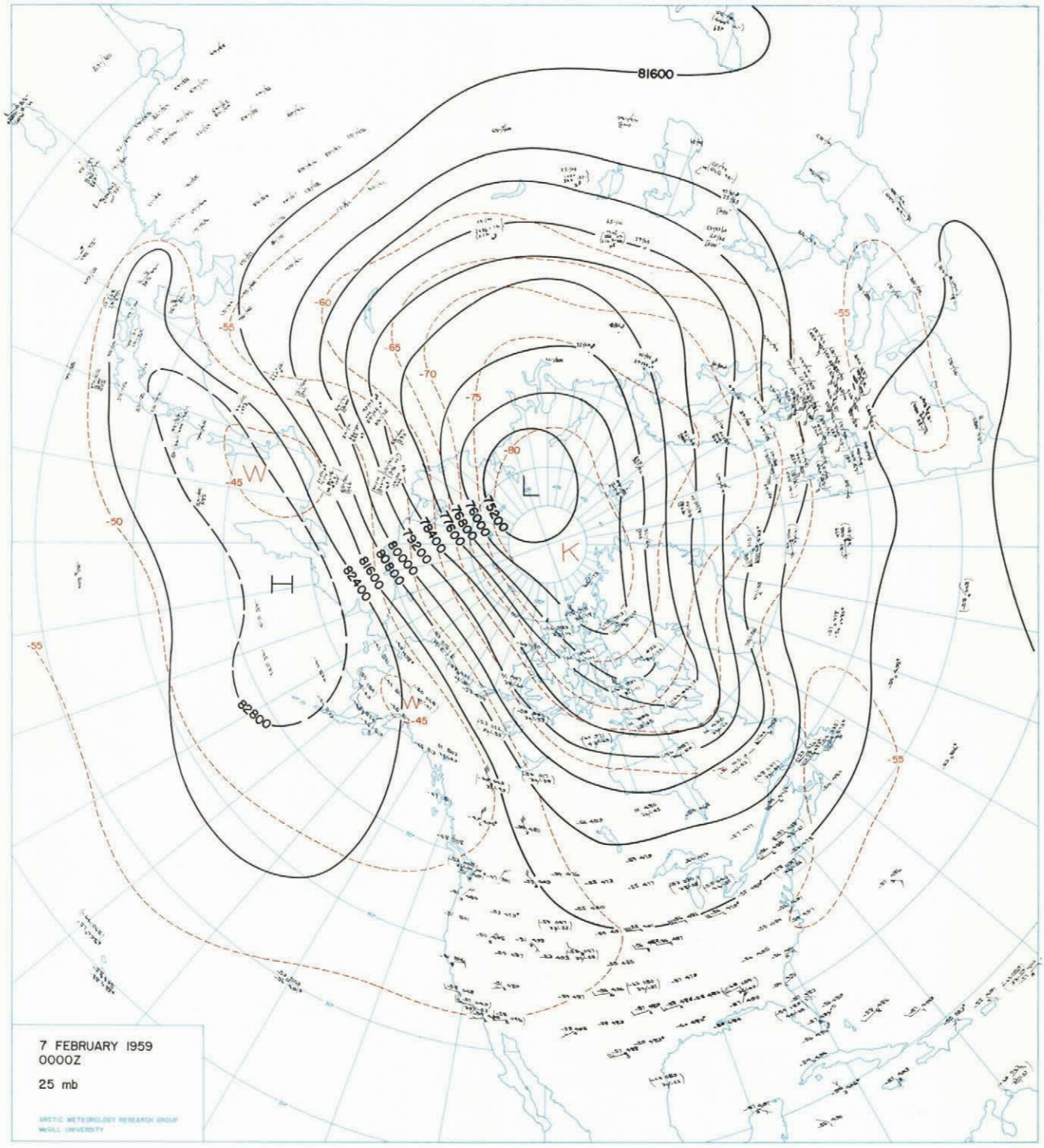
81600
-60
-55
-65
-70
-75
-80
-45
-50
-55
75200
76000
76800
77600
78400
79200
80000
80800
81600
82400
82800
W
H
L
K
-45
-55
7 FEBRUARY 1959
0000Z
25 mb
ARCTIC METEOROLOGY RESEARCH GROUP
McGILL UNIVERSITY

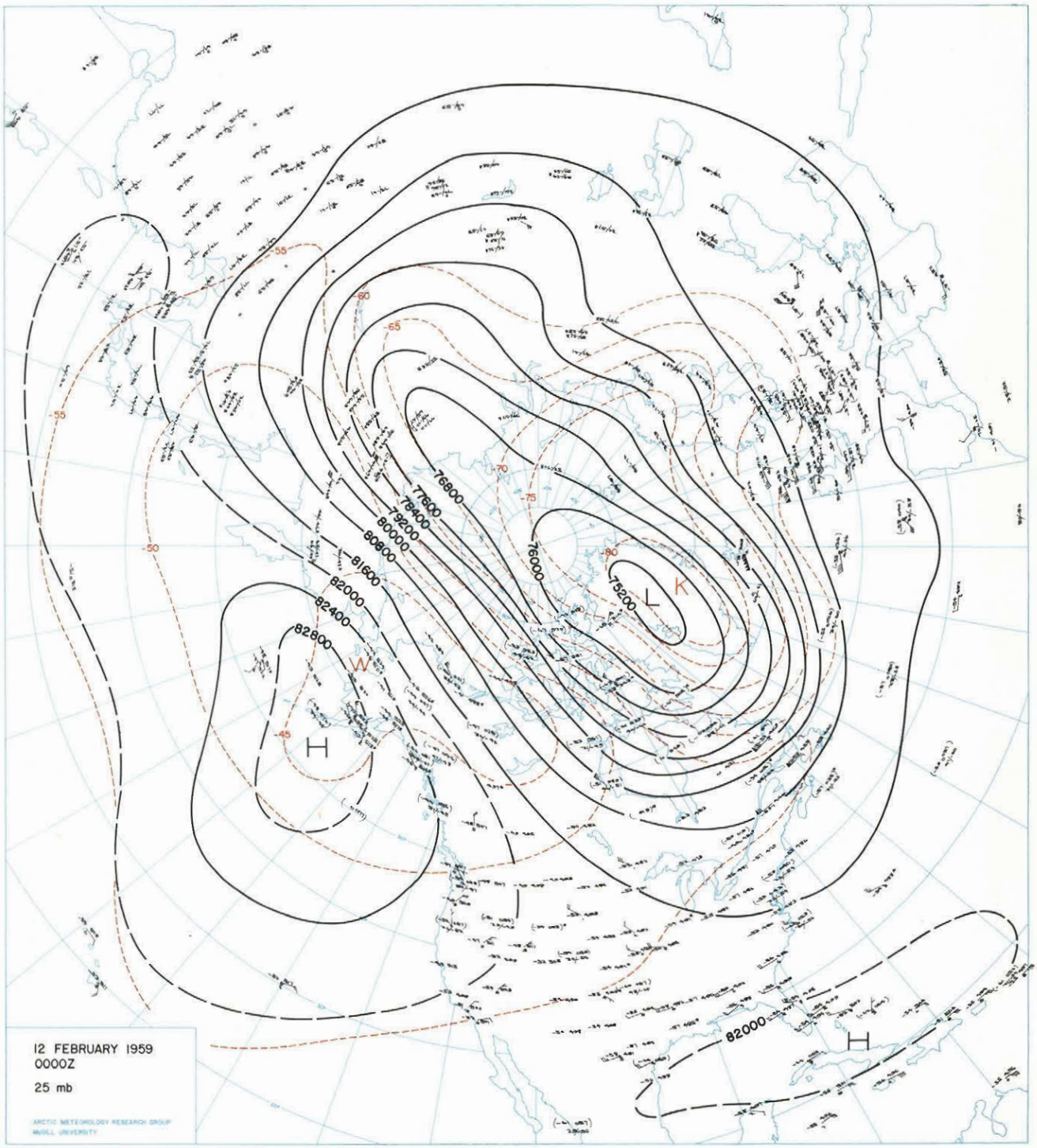
-55
-60
-65
-55
-70
-75
-50
-80
-45
76800
77600
78400
79200
80000
80800
81600
82000
82400
82800
76000
75200
82000
L
K
W
H
H
12 FEBRUARY 1959
0000Z
25 mb
ARCTIC METEOROLOGY RESEARCH GROUP
McGILL UNIVERSITY

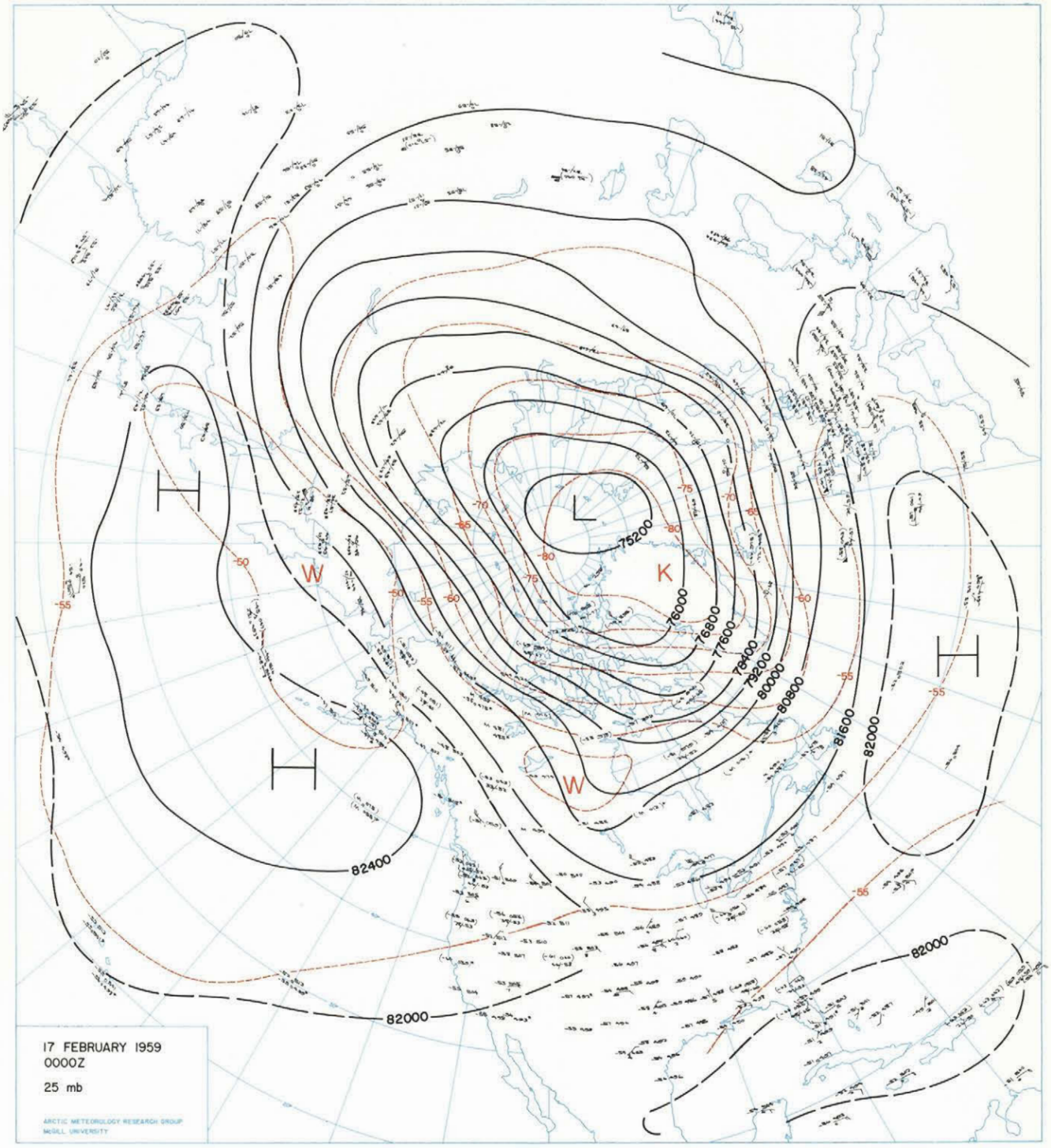
17 FEBRUARY 1959
0000Z
25 mb
ARCTIC METEOROLOGY RESEARCH GROUP
McGILL UNIVERSITY
H
H
H
L
W
W
K
-50
-55
-60
-65
-70
-75
-80
75200
76000
76800
77600
78400
79200
80000
80800
81600
82000
82400

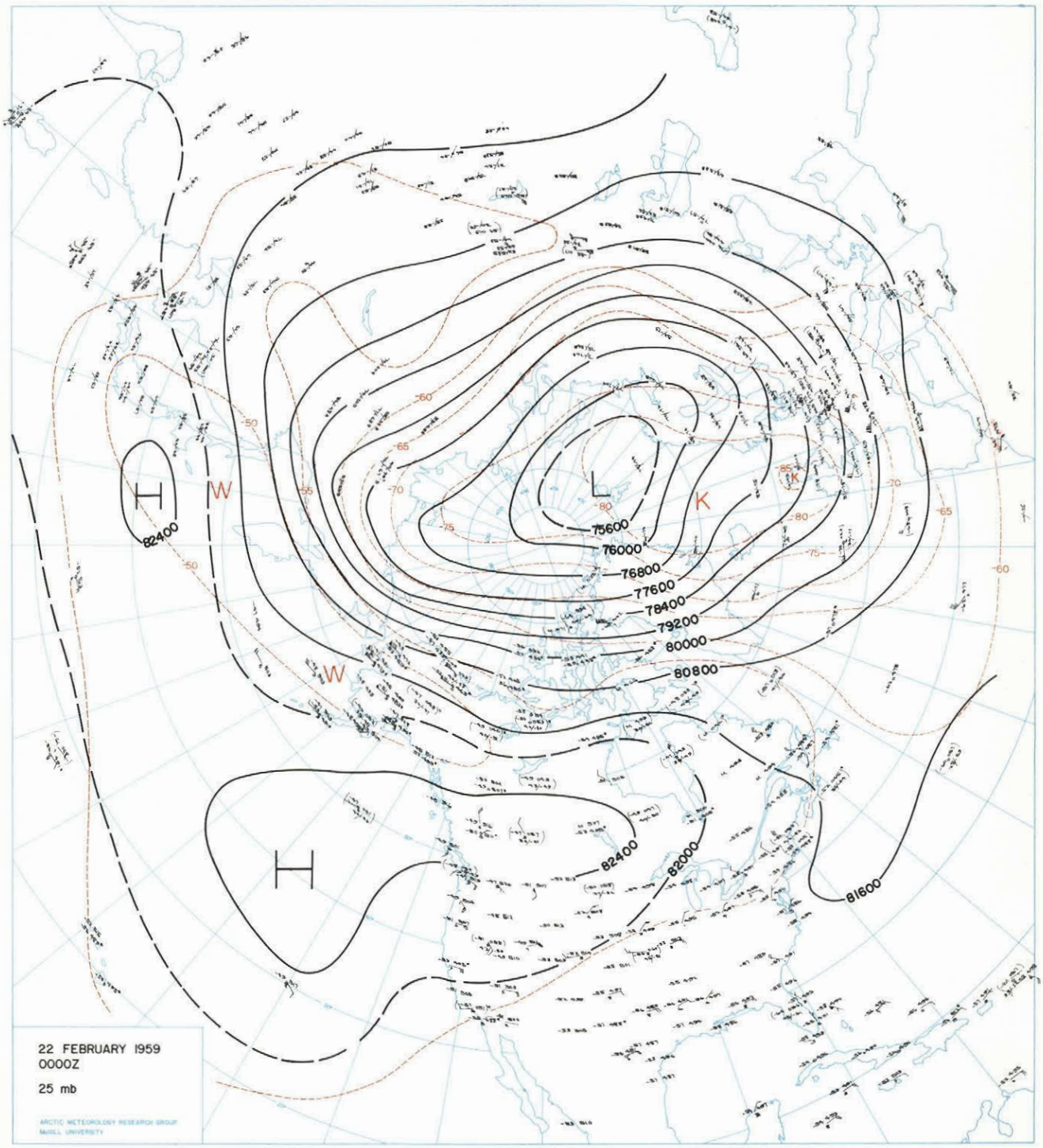
H
W
L
K
W
H
82400
75600
76000
76800
77600
78400
79200
80000
80800
82400
82000
81600
-50
-55
-60
-65
-70
-75
-80
22 FEBRUARY 1959
0000Z
25 mb
ARCTIC METEOROLOGY RESEARCH GROUP
McGILL UNIVERSITY

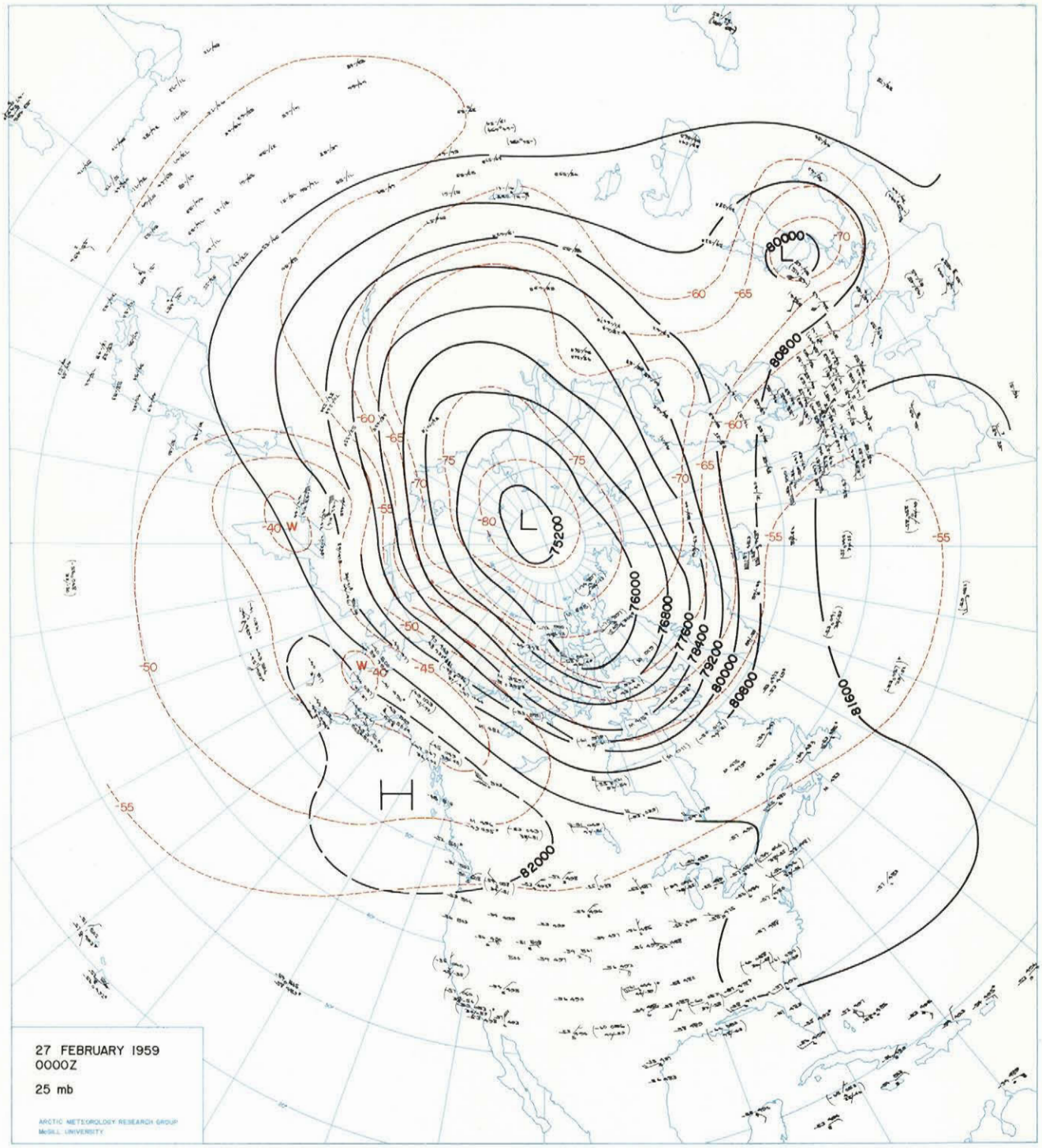
27 FEBRUARY 1959
0000Z
25 mb
ARCTIC METEOROLOGY RESEARCH GROUP
McGILL UNIVERSITY

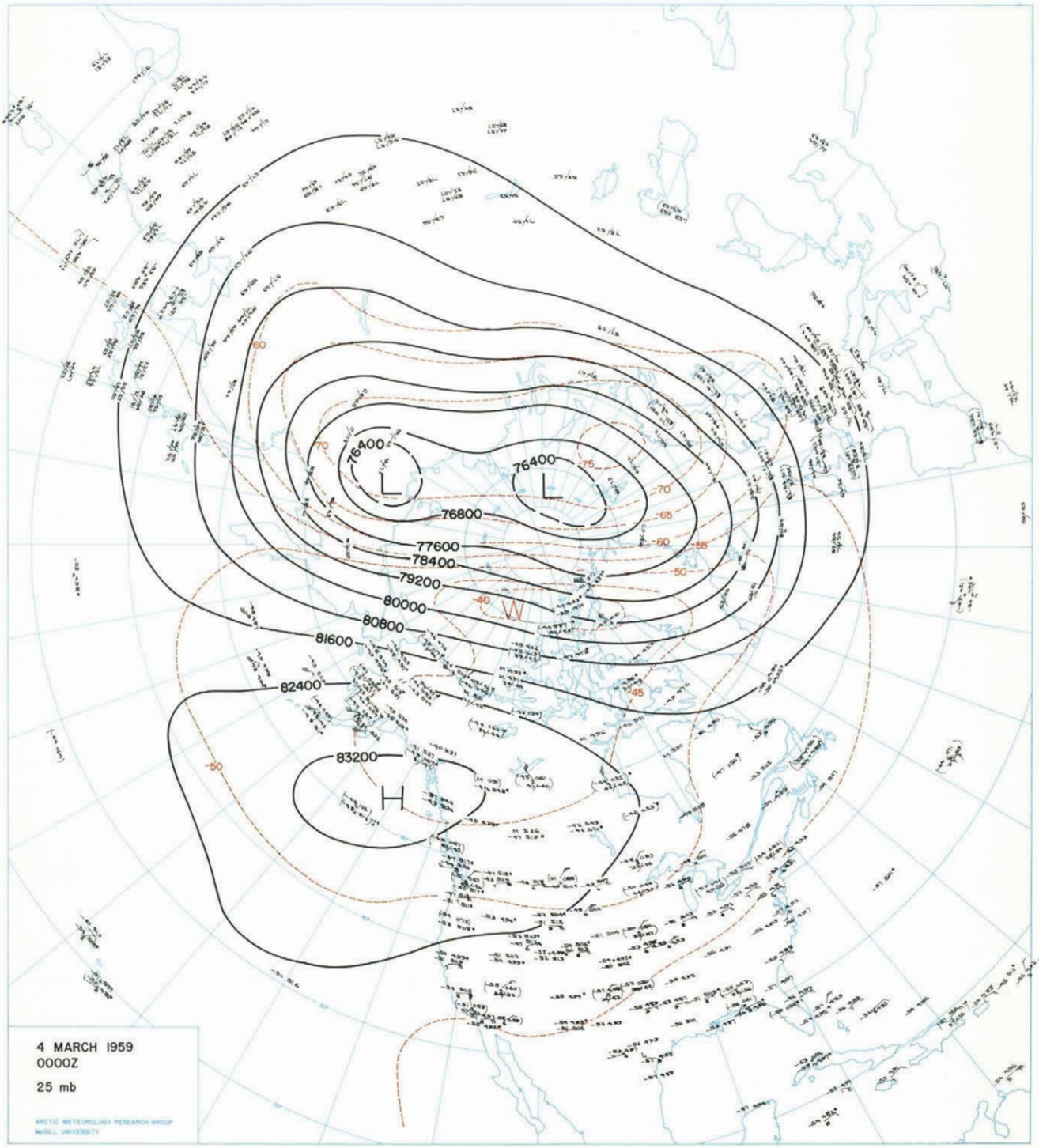
76400
L
76400
L
76800
77600
78400
79200
80000
80600
81600
82400
83200
H
W
60
70
75
70
65
60
55
50
40
45
50
4 MARCH 1959
0000Z
25 mb
ARCTIC METEOROLOGY RESEARCH GROUP
McGILL UNIVERSITY

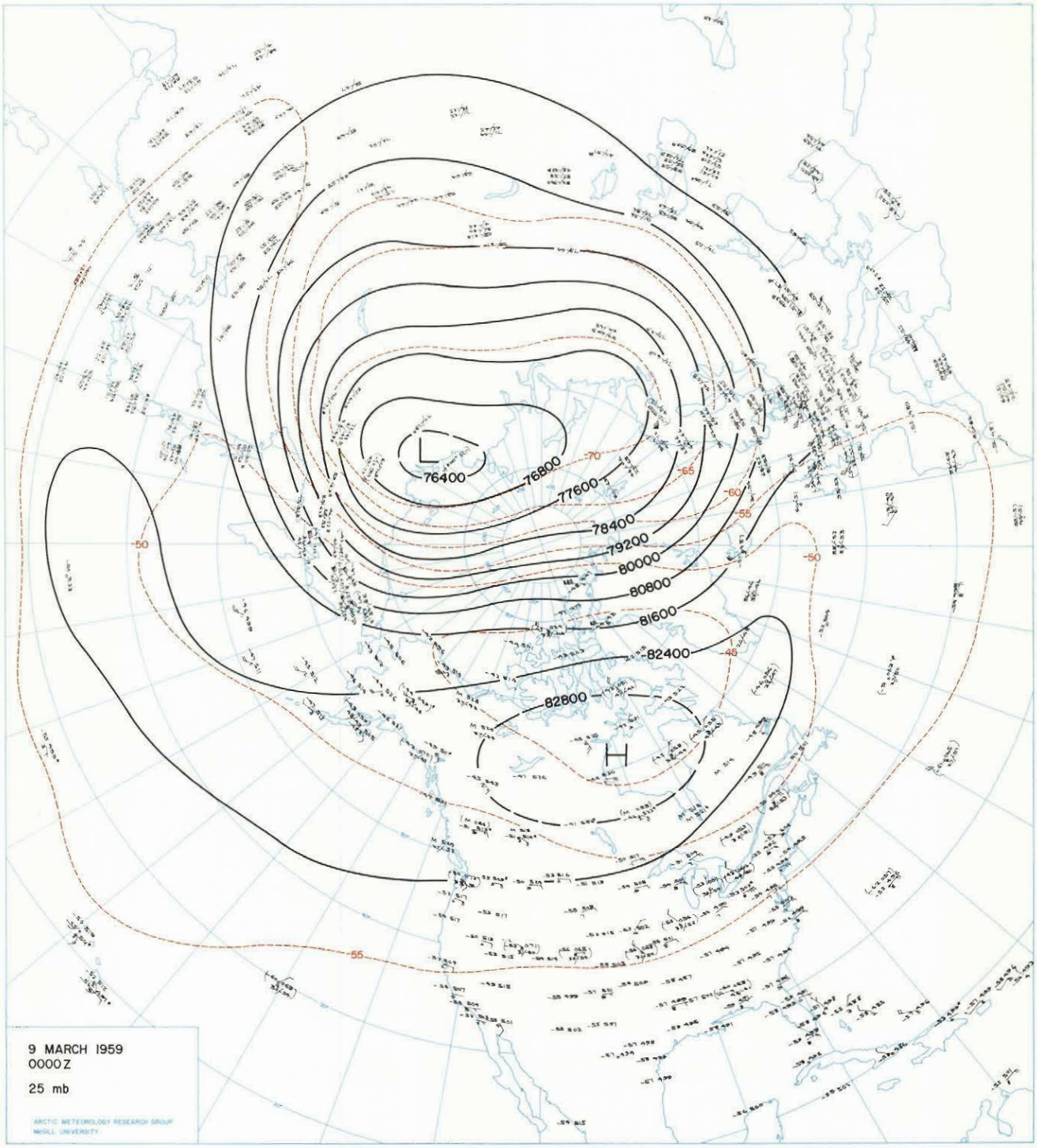
L
H
76400
76800
77600
78400
79200
80000
80800
81600
82400
82800
-70
-65
-60
-55
-50
-45
-50
-55
9 MARCH 1959
0000Z
25 mb
ARCTIC METEOROLOGY RESEARCH GROUP
McGILL UNIVERSITY

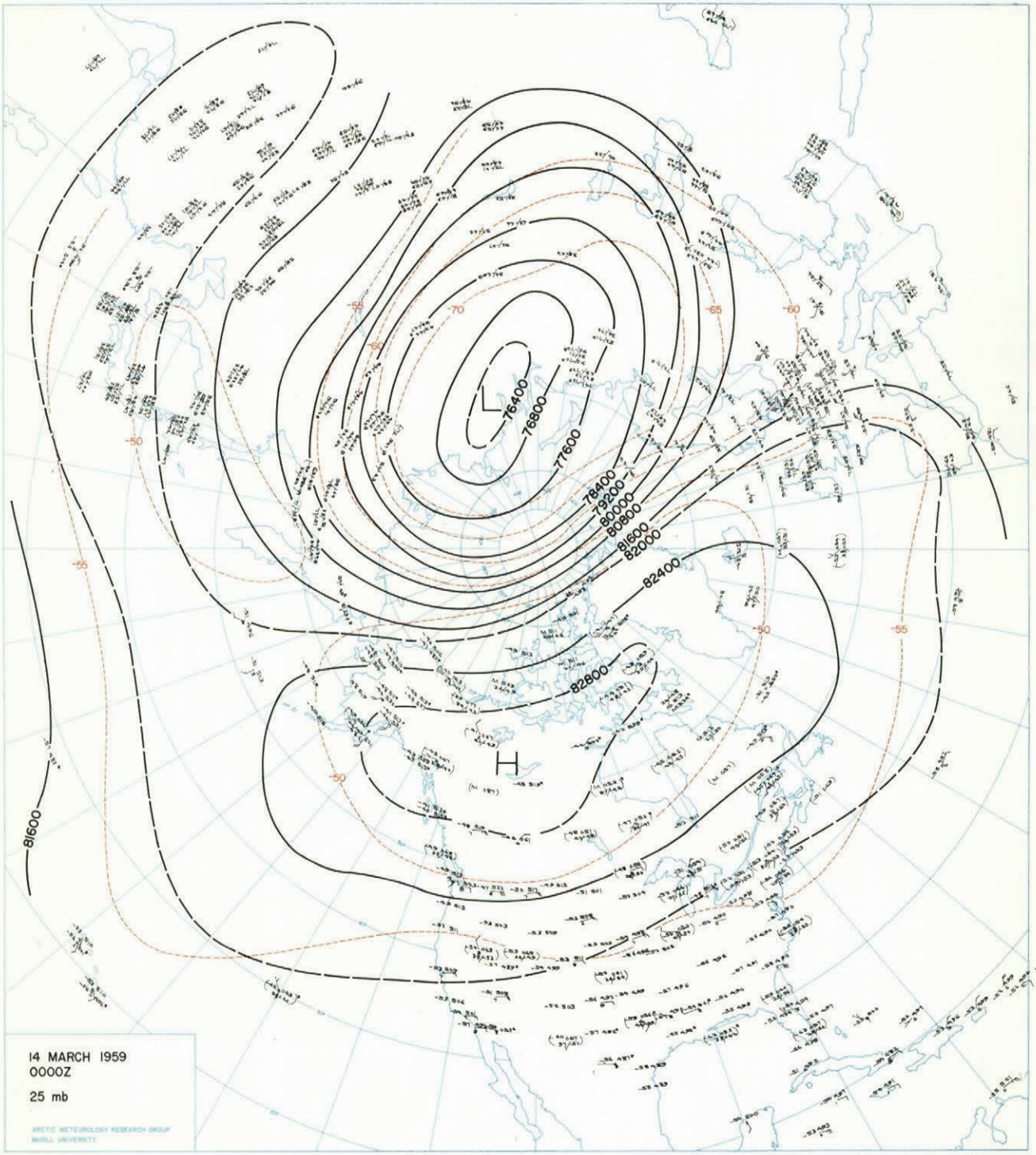
L
H
76400
76800
77600
78400
79200
80000
80800
81600
82000
82400
82800
81600
-70
-65
-60
-55
-50
-55
-50
-55
-50
14 MARCH 1959
0000Z
25 mb
ARCTIC METEOROLOGY RESEARCH GROUP
McGILL UNIVERSITY

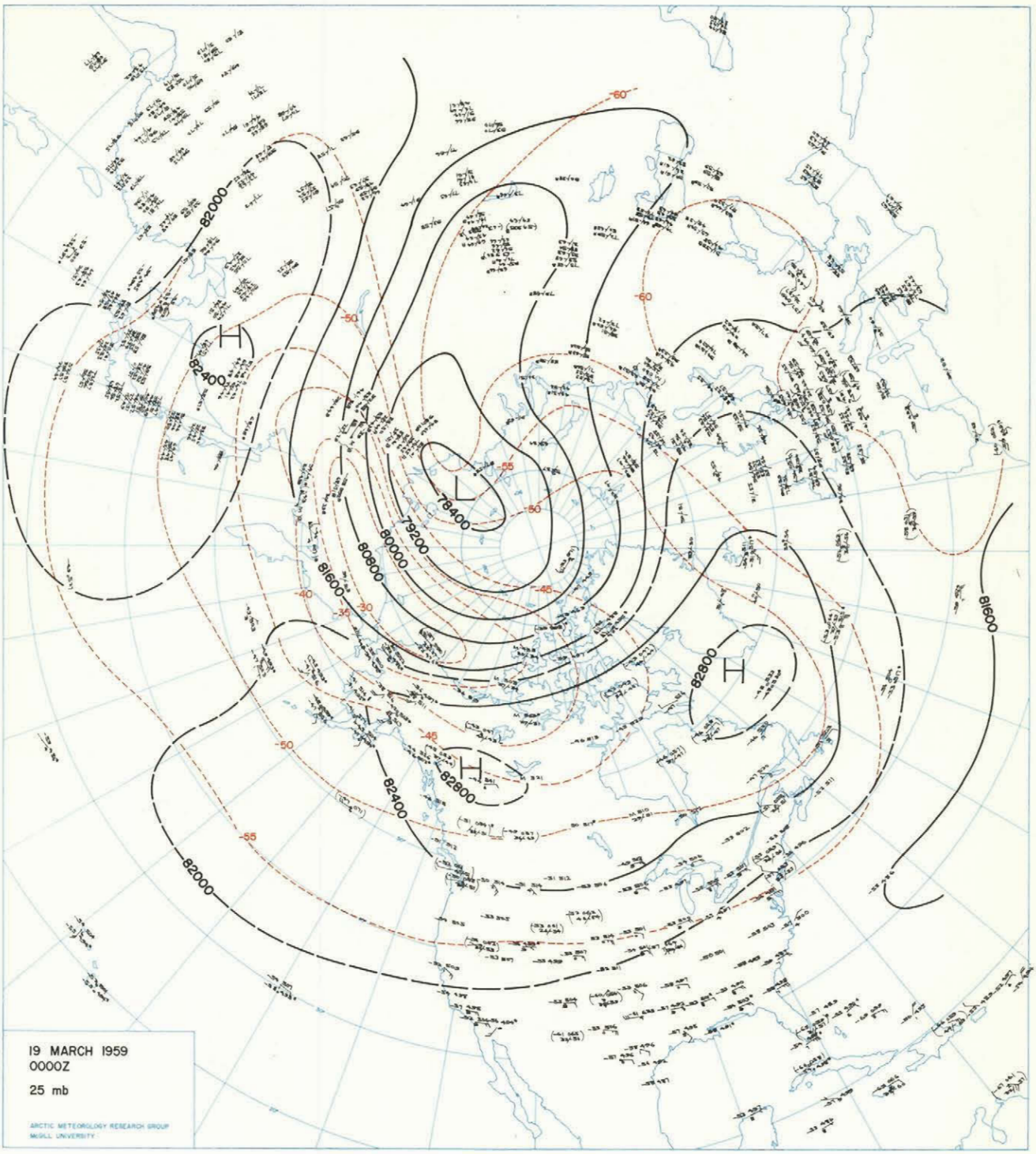
82000
82400
78400
79200
80000
80800
81600
82800
82400
82000
81600
-60
-50
-55
-50
-40
-30
-45
-50
-46
-55
-60
19 MARCH 1959
0000Z
25 mb
ARCTIC METEOROLOGY RESEARCH GROUP
McGILL UNIVERSITY

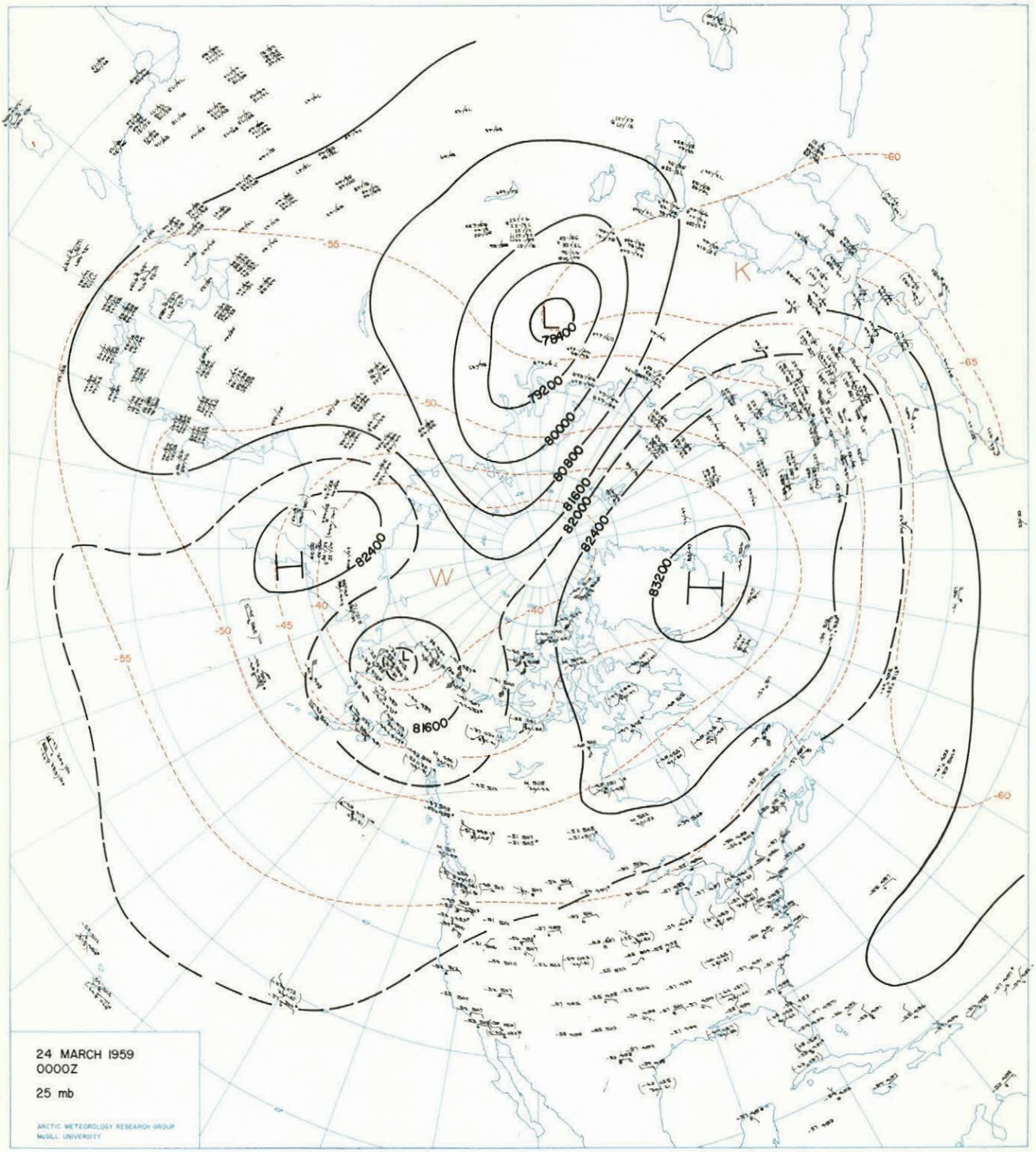
24 MARCH 1959
0000Z
25 mb
ARCTIC METEOROLOGY RESEARCH GROUP
McGILL UNIVERSITY
L
78400
79200
80000
80800
81600
82000
82400
H
82400
W
L
81600
H
83200
K
-60
-55
-50
-45
-40
-65

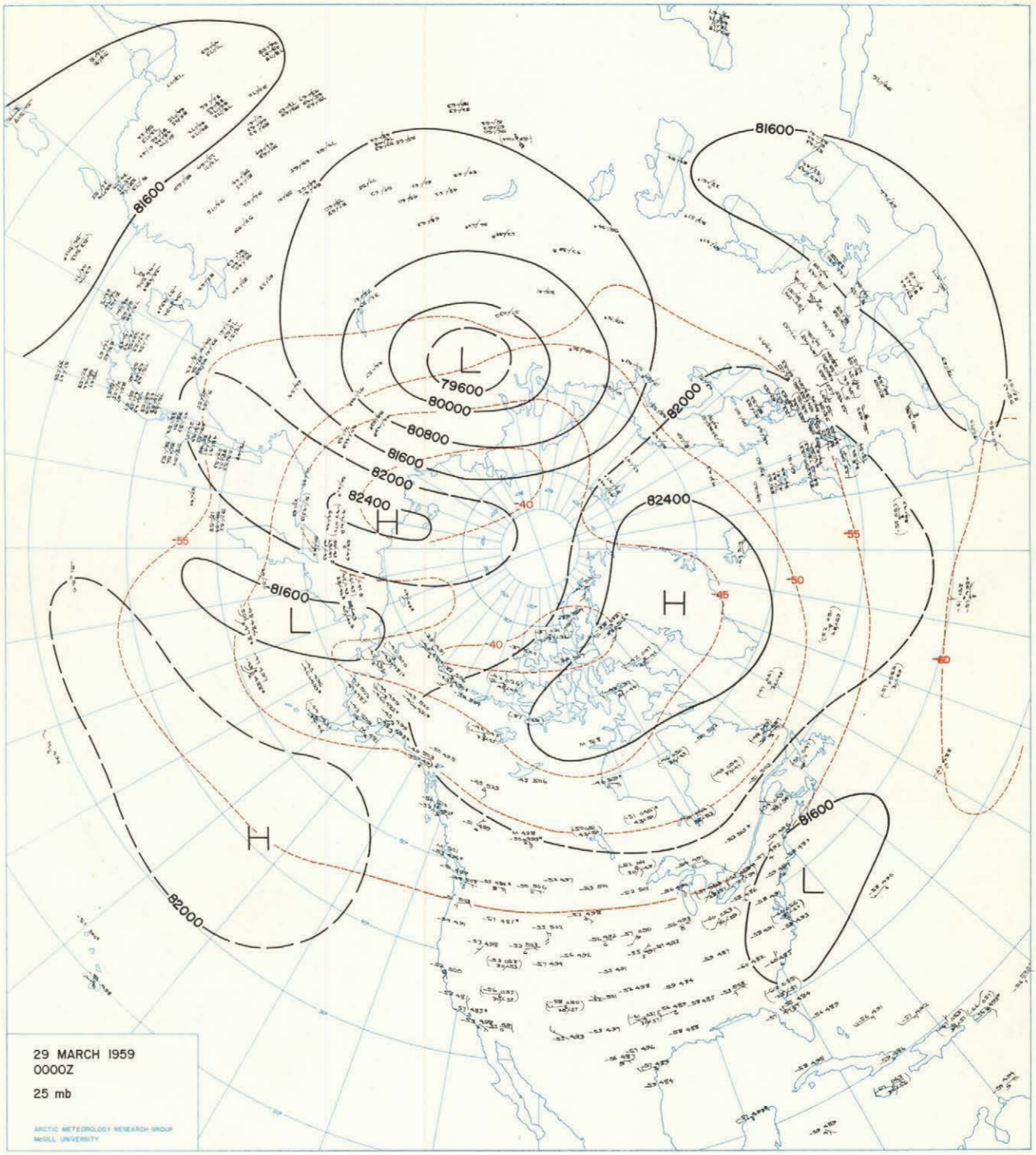
81600
79600
80000
80800
81600
82000
82400
82000
81600
82400
81600
82000
-40
-55
-45
-50
-60
L
H
29 MARCH 1959
0000Z
25 mb
ARCTIC METEOROLOGY RESEARCH GROUP
McGILL UNIVERSITY